The Ultrafast Dynamics of Platinum Based Complexes

Catherine Elizabeth Royle

Doctoral Thesis

The Weinstein Group
Department of Chemistry
University of Sheffield

August 2023

The Ultrafast Dynamics of Platinum Based Complexes

Catherine Elizabeth Royle

PhD Thesis
August 2023

Abstract

Photosynthetic systems can readily convert solar energy into chemical energy. The key process underpinning this mechanism is electron transfer (ET) to form charge separated states (CSS). In order to create an artificial photosynthetic system that could be used as an alternative to non-renewable energy sources, a deeper understanding of how ET works is needed. Transition metal complexes such as Pt(II) donor-bridge-acceptor (DBA) complexes can undergo ET to form a CSS. The excited state dynamics of a series of modified Pt(II) trans-acetylide DBA complexes is interrogated using ultrafast transient absorption (TA) and time-resolved infrared spectroscopy (TRIR). Appending electron rich methoxy (MeO) groups to the PTZ donor increased the rate of formation of the ^{3}CSS by a factor of 8 (TA) and 5 (TRIR), relative to the analogous complex without the MeO groups (unmodified complex). This is attributed to the increased driving force for charge separation. The removal of a CH_2 spacer and the addition of the MeO groups increases the rate of formation of the ^{3}CSS by factor of 16 (TA) and 18 (TRIR), relative to the unmodified complex, while also decreasing the lifetime of the CSS by a factor of 5 (TA) and 4 (TRIR). There is a significant increase in both the formation and decay rates of the ^{3}CSS due to the combined effect of the increased driving force and conjugation of the PTZ donor to the Pt(II)-bridge. The removal of the CH_2 spacer group increases the rate of formation of the ^{3}CSS by a factor of 18 (TA) and 16 (TRIR) and decreases the lifetime of the ^{3}CSS by factor of 8 (TA) and 6 (TRIR), relative to the unmodified complex. The removal of the CH_2 spacer group accelerates both charge separation and charge recombination, due to the increased conjugation between the PTZ donor and the Pt(II)-bridge, ensuring easier reduction of the

oxidised bridge following the charge transfer. The increase in conjugation of the donor reduces the electron donating ability of the donor and molecules containing strongly coupled donors no longer form a ^{3}CSS. The addition of a second PTZ donor donor, yielding the arrangement, Donor$_2$-Donor$_1$-Bridge-Acceptor, extends the lifetime by a factor of 9 with a 1,8-Napthalimide (NAP) acceptor, but by a factor of 5 with an 1,4,5,8-Napthalene diimde (NDI) acceptor. The findings of conducting vibrational control experiments were that the smaller the driving force the more likely that excitation of the acetylide vibration will have an affect on the yield of the ^{3}CSS state. Therefore the molecules with a stronger donor, exhibited less effect with selective IR excitation had on the yield. The ^{3}CSS in complexes which have the biggest energy gap between ^{3}CT and ^{3}CSS, were found to exhibit no manipulation from IR excitation in the excited state. However, complexes with smaller energy gaps between the ^{3}CT and ^{3}CSS, such as NDI-Pt-Ph-PTZ shows a relative 12% change in yield to the ^{3}CSS.

Acknowledgements

First and foremost, I would like to give my thanks to Professor Julia Weinstein for her guidance and enthusiastic support throughout the past four years and the opportunity to carry out this exciting research. I am extremely grateful to both Igor Savonovich and Greg Greetham for their help and guidance at the Rutherford Appleton Laboratory. I would also like to express my gratitude to Weinstein group members past and present. To Tao Cheng for his excellent synthetic ability and without his synthesis of the Complexes the work in this thesis would not be possible. To Heather Carson for her excellent theory work. To James Shipp for helping to teach me transient absorption. To Martin Appleby for not only teaching me how to do Time Resolved Infrared but for also teaching me how to befriend everyone within a square mile and being a great friend and constant support - it has been lovely to share an office and laboratory over the past four years. To David Wu for his assistance in teaching me how to use FLUPS, interesting historical facts and conversations and his consistent disapproval of me wearing acrylic nails whilst performing laser spectroscopy. To Rory Cowin for their assistance at RAL and his excellent cross wording ability. To Ricardo Fernandez-Teran, for his help with experiments and his GUI, especially at RAL and also for his assistance supporting me through my first international conference. To Iona Ivalo for their assistance at RAL, and for making all those late nights bearable and for our netball Thursdays where you doubled up as my driving instructor. I would like to thank Samantha Peralta for help with the more synthetic issues in the lab and also her friendship and support. I would also like to extend my thanks to the rest of the Weinstein group for always being extremely helpful and for the group meetings in which I always felt supported. And to Alexander Auty for teaching me all there is to know

about spectroscopy, data processing and everything in between from how to clean cells to using a paper clip as a magnetic stirrer bar. Es obvio que el doctorado no hubiera sido lo mismo sin tí. Gracias por todo. I would like to thank my friends inside and outside of the university for the all the fun memories and incredible moments we've shared. I would also like to thank my incredible family who have been incredibly supportive throughout the past four years. To my sister, for always being there when I needed someone to talk to. To my dad for helping me proof read my thesis and for always inspiring me to ask questions. To my grandparents for loving me unconditionally and being so proud of their ”little girl”, even if I did have to remind them how to say laser spectroscopist every time I saw them. To my mummy, I couldn't have done this without you. Gracias por siempre estar allí y por todo lo que has hecho por mí, te quiero.

Abbreviations

2DIR **T**wo **D**imensional **I**nfrared **R**ed

CS **C**harge **S**eparation

CSS **C**harge **S**eparated **S**tate

CT **C**harge **T**ransfer

DAS **D**ecay **A**ssociated **S**pectra

DBA **D**onor **B**ridge **A**cceptor

DCM **D**i **C**hloro **M**ethane

DFT **D**ensity **F**unctional **T**heory

DSSC **D**ye **S**ensitized **S**olar **C**ells

ESA **E**xcited **S**tate **A**bsorption

ET **E**lectron **T**ransfer

FLUPS **F**lups **U**pconversion **S**pectroscopy

FWHM **F**ull **W**idth at **H**alf **M**aximum

GLA **G**lobal **L**ifetime **A**nalysis

GUI **G**raphical **U**ser **I**nterface

FTIR **F**ourier **T**ransform **I**nfra **R**ed

IC **I**nternal **C**onversion

IL **I**ntra **L**igand

ISC **I**nter **S**ystem **C**rossing

IVR **I**ntramolecular **V**ibrational **R**elaxation

MeCN Acetonitrile

LLCT **L**igand **L**igand **C**harge **T**ransfer

MLCT **M**etal **L**igand **C**harge **T**ransfer

ML-LCT **M**etal - **L**igand to **L**igand **C**harge **T**ransfer

NAP 1,8-Napthalimide

NDI 1,4,5,8-Napthalene diimde

NOPA **N**on **L**inear **O**ptical **P**arametric **A**mplification

OPA **O**ptical **P**arametric **A**mplification

PTZ **P**henothiazine **I**nterface

SE **s**timulated **E**mission

TA **T**ransient **A**bsorption

TCSPC **T**ime **C**orrelated **S**ingle **P**hoton **C**ounting

T-2DIR **T**ransient **T**wo **D**imensional **I**nfrared **R**ed

TM **T**ransistion **M**etal

TOPAS **T**ravelling **W**ave **O**ptical **P**arametric **A**mplification of **S**uperfluorescence

TRIR **T**ime **R**esolved **I**nfrared **R**ed

VC **V**ibrational **C**ooling

UV-Vis **U**ltra violet - **V**isible

WLC **W**hite **L**ight **C**ontinuum

Contents

Chapter 1

Introduction

1.1 Motivation

The increasing global demand for energy and the imminent threat of anthropogenic climate change are the main motivations for this project. Anthropogenic climate change is driven by our reliance on non-renewable fossil fuel energy sources. The aforementioned referring to a finite energy source that cannot be replenished within a human lifetime. The world consumption of energy is defined as the total energy that is generated and consumed by the entire world population. Current global consumption of energy stands at 113,009 Twh. However, due to the rising population and urbanization of less economically developed countries, global energy demand is predicted to rise by 50% by 2050. Currently there is a strong reliance on non-renewable energy sources to meet the demands of energy consumption. Unsustainable energy sources such as fossil fuels result in carbon emissions, which are partly responsible for climate change.[1–3] Therefore, it is necessary to develop sustainable alternative technologies that take advantage of renewable energy sources. This will allow energy demands to be met in a way that does not negatively impact the environment and does not rely on non-renewable energy sources. The importance of this issue to modern day society is reflected by the large proportion of funding dedicated to the clean energy sector. The UK government promised to invest a total of £2.5 billion between 2015 and 2021 in low carbon solutions, of which, £505 million has been dedicated to the development of novel, clean energy technologies.[4] The incentive to

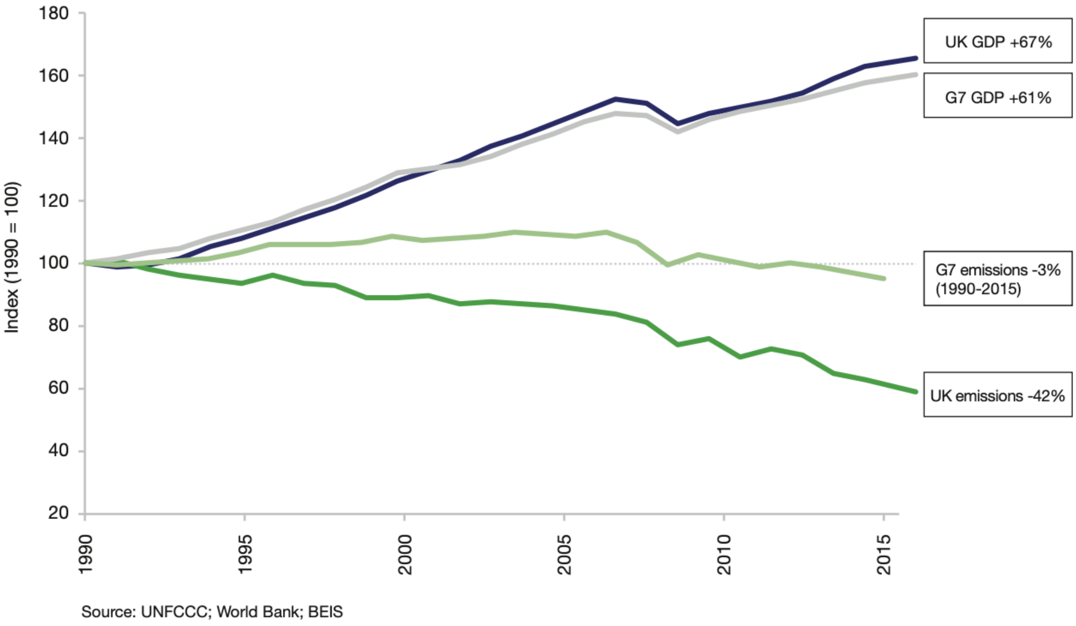

Source: UNFCCC; World Bank; BEIS

Figure 1.1: UK and G7 economic growth and emissions reductions

develop greener, low carbon technologies is not only to ensure the protection of the planet but such green incentives have also been linked to increased economic growth. This is due to the correlation exhibited between the reduction of emissions and the increase in GDP (Figure 1.1).[5]

1.2 Solar energy conversion

The most viable solution to the future global energy demand and the threat of climate change is the use of renewable energy sources such as solar energy. Solar radiation is an abundant source of energy that is both reliable and economical. The power received from the sun by the earth is estimated to be 180,000 TW, which greatly surpasses that of the current global energy demand.[6] Since solar energy has the potential to become the main source of the world's energy supply, much research and investment in recent years has been put into developing light harvesting technologies. There are four main ways of harvesting solar energy. The first, and simplest, way is to use thermal energy from the sun to directly heat objects. This process yields high efficiencies of up to 50% as it requires no conversion of energy. The energy is captured by a black metal sheet which efficiently absorbs the solar energy. Water is then passed through piping that is in thermal contact with the metal sheet and, as a result, the water is heated. These devices can supply up to 40% of annual household hot water demand. The second method is using solar energy to generate electricity directly by means of the photovoltaic effect. Solar photovoltaics employ a semiconductor material which absorbs a photon, forming an electron-hole pair. The separation of the bound electron-hole pair, also known as charge separation, occurs between an n- and p-type junction. This results in the generation of an electric current. The p-type material, which has a surplus of electrons, acts as the electron donor, while the n-type material, which is deficient in electrons, acts as the electron acceptor. The third method involves using solar energy to generate electricity indirectly. Solar energy is absorbed by means of collectors, which then heat a liquid which produces steam. Said steam is then used to drive a turbine or engine. Finally, the fourth way is to harvest light energy to drive chemical reactions.[7] This process occurs in plants and is better known as photosynthesis. The fundamentals of this solar energy conversion process will be the main focus of this thesis.

1.3 Photosynthesis

Photosynthesis is a process that sustains nearly all life on earth, acting as the main food supply to animals through the means of conversion of the sunlight into chemical energy. Photosynthesis is a complex photochemical process, the biological detail of which is beyond the scope of this thesis. Detailed descriptions of the biological architecture and processes involved can be found elsewhere.[8] In brief, oxygenic photosynthesis results in the conversion of CO_2 and H_2O into glucose and O_2, following the absorption of sunlight. The three main excited state processes that underpin photosynthesis are:[9–11]

1. Absorption of light by a chromophore, resulting in population of an excited state of the chromophore (C*)

2. Transfer of electrons from C* to the nearby electron acceptor, forming Acceptor-/Chromophore+, and then from the nearby donor - to the oxidised chromophore,

restoring the chromophore

3. Charge separation, formation of Donor+/Acceptor- state.

The fundamentals of these processes found in nature can be mimicked and optimised in order to use the sun's energy to convert readily available reactants such as water into useful products such as hydrogen. This is known as artificial photosynthesis. One of the main challenges in achieving artificial photosynthesis is finding a way to transfer the energy stored in chemical bonds into useful products. These products can then be used to make high energy fuels. Adopting a modular approach to the artificial photosynthetic problem allows the system to be separated into several components. The light absorbing chromophore is at the centre of the architecture, which is linked covalently to the electron donor and acceptor. These must be capable of transferring charge in the desired direction in order to form a charge-separated state. This direction is controlled by the free energy gradient of the components. The electron donor and acceptor are then connected to the outermost components, the reductive and oxidative catalysts, which can carry out the required chemical reaction. This structure can be seen in Figure 1.2. The design of artificial photosynthetic systems should be influenced by the knowledge gained through a comprehensive study of its natural counterpart. The design of artificial systems can be optimized by considering the fundamental processes that limit its maximum possible efficiency. The efficiency of photosynthesis in plants is partly governed by the fact that the majority of wavelengths of the incident solar radiation are too low in energy to be absorbed by the chlorophyll and that some of the remaining incident light is lost due to reflection. Therefore, at most, only 34% of incident light is absorbed. Not all of the energy that is absorbed

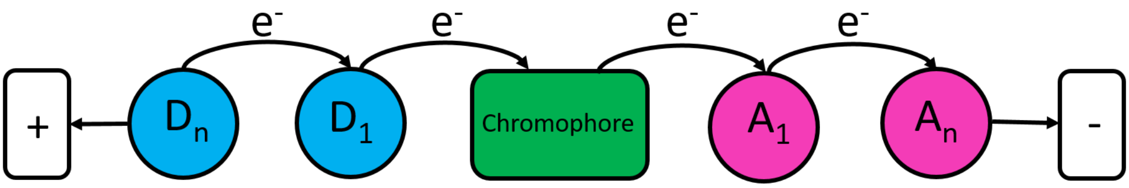

Figure 1.2: Artificial photosynthetic scheme showing the chromophore, which absorbs light and subsequently undergoes charge separation. The chromophore donates electrons to the acceptor, A_1, which is connected to the reductive catalyst. The chromophore is replenished by the donor D_1, which is connected to the oxidative catalyst.[12]

is used to produce useful sugars, as it is not all transferred to the photosynthetic reaction centre. What's more, some of the stored chemical energy is needed to carry out other physiological processes such as aerobic respiration.[13] Hence, the maximum theoretical efficiency of natural photosynthesis under optimal conditions is estimated to be between 8-9%.[14] However, algae, the plant species known for having one of the highest photosynthetic efficiencies can only reach efficiencies of up to 2-3%. The limiting factor here being the energy conversion rate.[15] In its most basic form, artificial photosynthesis can be achieved by the splitting of water to yield oxygen and hydrogen in a photovoltaic cell. These systems can achieve an overall efficiency of up to 11%.[16] Until recently, the research into photovoltaic devices has been mainly based on inorganic solid-state junction devices, such as crystalline solar cells based on silicon. These solar cells make up for over 70% of the photovoltaic devices being currently manufactured. However, due to their high cost and a lack of abundance of silicon based compounds, there has been a paradigm shift towards devices based on dye-sensitized architectures.[17] In this project Dye-Sensitized Solar Cells (DSSCs) will be considered as the structure within which artificial photosynthesis can be carried out in. The components of these structures can be modified in order to achieve maximum efficiency. DSSCs were first fabricated in 1991 by Gratzel in Switzerland, achieving efficiencies of 7.1 %. Further development has allowed efficiencies of over 10% to be achieved.[18,19] In dye-sensitized devices, the light absorption and charge transfer processes occur separately, whereas in solid-state devices both processes occur in the semiconductor. DSSCs operate by photoexcitation of a sensitizer dye which then transfers an electron into the conduction band of the semiconductor. A liquid redox electrolyte, typically I_3^-/ $3I^-$, then reduces the dye back to its initial state by donation of an electron. Back electron transfer (ET) from the semiconductor is counteracted by the electron donation from the iodide electrolyte. The triiodide is reduced back to iodide by electrons supplied from the counter electrode. The advantages of DSSC are owed to their straightforward design and inexpensive components such as the metal oxide semiconductor. TiO_2 is a popular choice for the semiconductor, however other metal oxides can also be used such as ZnO, doped SnO_2 and Nb_2O_5.[20] The structure of the sensitizer dye can be modified or adjusted to have a wide ranging absorption cross-section, corresponding to the peak wavelengths of the solar spectrum.[21] A simplified schematic of a DSSC can be seen in Figure 1.3.

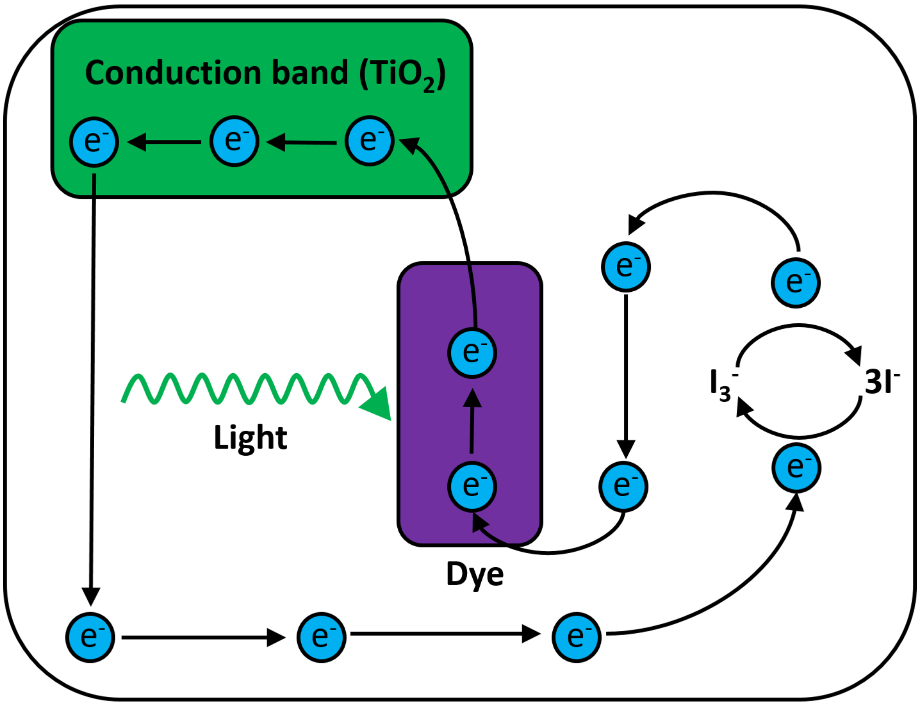

Figure 1.3: A simplified scheme of a general Dye-Sensitized Solar Cell

DSSCs are a promising emerging technology. However, the maximum efficiency of a DSSC is currently 12.3 % which is inadequate and therefore not currently suitable for industrial application.[22]

1.4 Fundamental processes in solar energy conversion and artificial photosynthetic systems

1.4.1 Light absorption

The first process which occurs in an artificial photosynthetic system is the absorption of sunlight. The absorption of a photon of appropriate energy (3.3-1.5 eV) by a molecule leads to the population of an electronic excited state. The molecule will then dissipate this energy via various decay pathways, resulting in the molecule returning to its ground state

(S_0). These decay pathways are illustrated in a Jablonski diagram such as that shown in Figure 1.4.

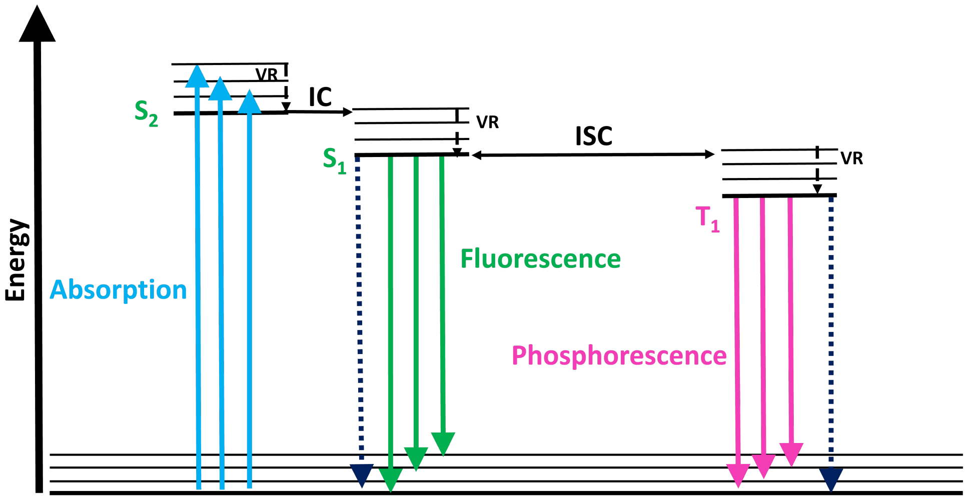

Figure 1.4: Generic Jablonski diagram depicting processes following light absorption

The absorption of a photon by a molecular system can occur when there exists a transition between two states of the system where the energy gap between these two states is equal to the energy of the incident photon. The electronic transition occurs on a femtosecond timescale, and hence much quicker than nuclear coordinate rearrangement (Born-Oppenheimer approximation).[23] Consequently, the transition can be considered to be vertical i.e no changes in the position of the nuclei during absorption. This is known as the Franck-Condon principle,[24] which can be used to rationalise the intensity of vibronic transition, i.e., electronic transitions that occur with an accompanying change in the vibrational energy level. The populated Franck-Condon state is usually a non-equilibrium geometry of the excited state, meaning the molecule is vibrationally excited and therefore will undergo intramolecular vibrational relaxation (IVR) to form a thermally equilibrated excited state S_2. IVR is a fast relaxation process that occurs in large molecules, on a picosecond timescale. The vibrational energy in the excited state molecule can be redistributed from the initially populated vibrational modes to lower frequency modes. The excited state molecule can also can vibrationally relax through interaction with the surrounding environment and in doing so, transfer excess energy to solvent molecules for example. This process is strongly influenced by the solvent environment surrounding the excited state molecule. Internal Conversion (IC) can then occur, which is an isoenergetic, radiationless transition between two electronic states of the same spin multiplicity. IC is then followed by IVR to populate excited state S_1. This state can then either decay via an intersystem crossing (ISC) transition to a triplet state or via fluorescence. Fluorescence is a radiative process whereby a photon of energy equivalent to that of the S_1 to S_0 energy gap is emitted. Emission lifetimes are usually on a timescale of nanoseconds, and therefore occur on slower timescales than processes such as IC and IVR. Therefore, emission typically occurs from the lowest vibrational level of an electronic excited state. Intersystem crossing is a non-radiative, isoenergetic transition between electronic states with different spin multiplicities i.e., from a singlet to triplet state, and is mediated by spin-orbit coupling. ISC is often accelerated in molecules containing heavy atoms such as transition metals like platinum.[25] Triplet states often have longer lifetimes than singlet states due to the triplet to ground state transition being spin forbidden. In contrast singlet states decay via a spin allowed process. The triplet state, T_1 , can decay by phosphorescence, a radiative process similar to fluorescence but occuring between singlet and triplet state. Alternatively T_1 can decay via a ISC pathway..[26–28] Based on the relative rates of the excited state processes introduced above, radiative transitions only occur in appreciable yield from the lowest energy state of a given spin multiplicity. This is known as Kasha's rule.

1.4.2 Electron transfer

Electron transfer is a process which is fundamental to many inorganic and organic reactions. It is often found in nature, in processes such as DNA repair. Self exchange reactions using isotopic labelling were some of the first reactions used to study the electron transfer process.

$$\mathrm{Fe(H_2O)_6}^{2+} + \star\mathrm{Fe(H_2O)_6}^{3+} \longrightarrow \mathrm{Fe(H_2O)_6}^{3+} + \star\mathrm{Fe(H_2O)_6}^{2+} \qquad (1)$$

Initial studies on electron transfer were limited by the lack of spectroscopic methods available at the time. Since then, huge advances have been made in the field of time-resolved spectroscopy, primarily driven by the development of stable, high repetition rate, pulsed lasers.[29,30] This has allowed detailed studies of more complex ET reactions, such as photosynthesis and solar energy conversion. Now, photophysical (and photochemical) processes that occur on sub-picosecond timescales can be routinely studied.[31]

Theoretical models can be used to predict the rate of electron transfer, the most famous of which is the Marcus theory of electron transfer. Rudolph A. Marcus[32,33] developed a theory that can be used describe the rates of electron transfer between molecules. In the Marcus treatment of electron transfer, the transfer occurs once the solvent molecules and the internal nuclear positions (intramolecular displacements) arrange into favourable positions. Such fluctuations in the internal and external environments are driven by the local temperature and therefore Marcus theory assumes that electron transfer is driven by these temperature dependent fluctuations only. The energy required to attain these favourable solvent and intramolecular positions is know as the reorganisation energy.

These assumptions drastically simplify the otherwise complex expressions describing electron transfer..[34] According to Marcus theory, the rate of electron transfer k_{ET} can be expressed as

$$K_{ET} = A\ exp\left[\frac{-(\Delta G_0 + \lambda)^2}{4\lambda k_B T}\right],$$

Where A is a pre exponential factor, Δ G_0 is the overall Gibbs free energy change, λ is the reorganisation energy, k_B is the Boltzmann constant and T, is the temperature. This equation is derived using the expression for the rate of a reaction

$$K_{ET} = A\ exp\left(\frac{-\Delta G^{\ddagger}}{RT}\right)$$

.

Since the free activation energy, Δ $G^{\ddagger}$, is difficult to directly measure, it is expressed in terms of the overall Gibbs free energy change Δ G^0 of the electron transfer reaction and the reorganisation energy λ. The free activation energy is approximated to be the barrier height of the crossing of the potential energy curves of the reactants and products, assuming that these diabatic curves are considered to be parabolas of equivalent curvature.[35] The barrier height, ΔG, and Gibbs free energy, Δ G^0, can be shown more clearly in Figure 1.5.

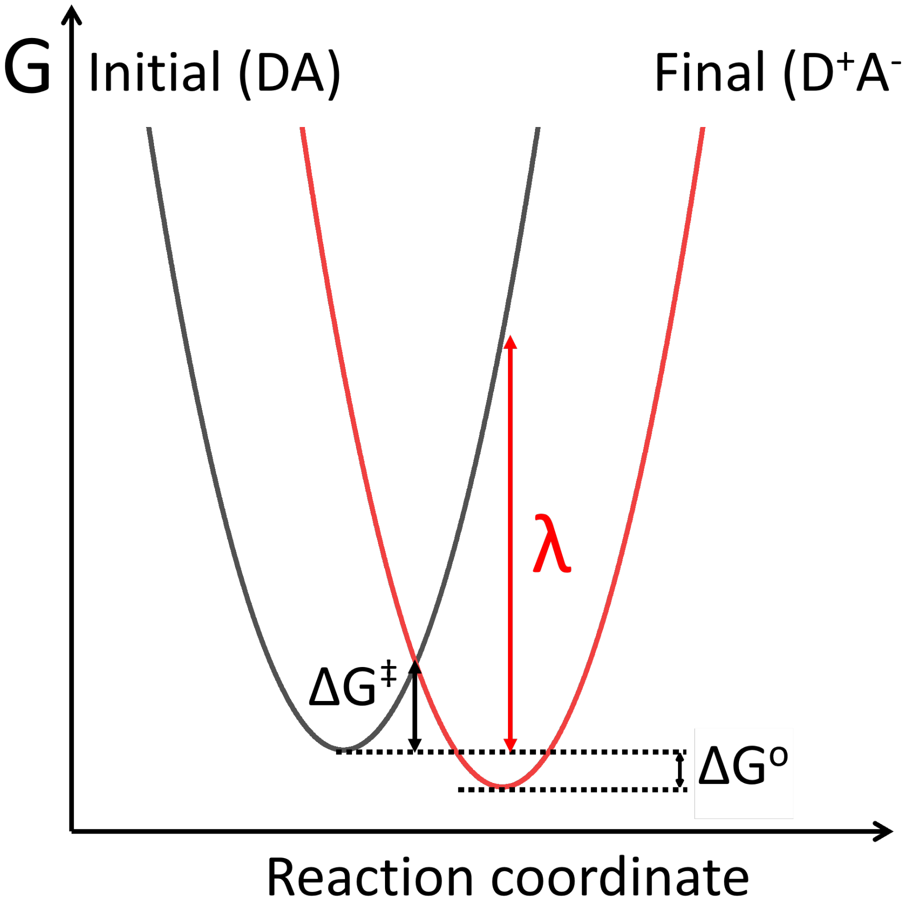

Figure 1.5: The crossing of two diabatic potential energy curves during an unsymmetrical electron transfer reaction. The black free energy curve (DA) shows the initial donor acceptor state and the red free energy curve shows the final donor acceptor state (D^+A^-) in which the donor has donated an electron to the acceptor. The reorganisational energy, λ, the activation energy Δ $G^\ddagger$, and the gibbs free energy, Δ G^0 are shown in the diagram.

In the Marcus model the reactants and products are approximated as spheres. Additionally, the solvent is approximated as a dielectric continuum. Mathematically, this can be described by the following equation:

$$\lambda_s = (\Delta e)^2 \left\{ \frac{1}{2a_1} + \frac{1}{2a_2} - \frac{1}{R} \right\} \left\{ \frac{1}{\varepsilon_\infty} - \frac{1}{\varepsilon_0} \right\}$$

Where λ_s is the solvent reorganisation energy, ΔE is the amount of charge transferred. a_1 is the radius of the donor, a_2 the radius of the acceptor, R is the distance between the centres of said radii and ε_0 is the zero frequency dielectric constant and ε_∞ is the optical frequency dielectric constant.[36] It is important to highlight how the rate dependence of electron transfer on the Gibbs free energy, ΔG_0 can be divided up into three regimes, the normal, the activationless and, perhaps the most remarkable, the inverted regime. In the normal regime as the free energy increases, the rate of electron transfer also increases, the rate then reaches a maximum, where the reaction becomes activationless as the reorganizational energy is equal to the negative of the Gibbs free energy, thus activation energy is equal to zero. Then as the Gibbs free energy continues to increase, the inverted regime is reached, where the rate of electron transfer begins to decrease. This can be demonstrated clearly in Figure 1.6.[37] The inverted region becomes increasingly important with respect to solar energy conversion processes like in photosynthesis. The phenomena of the inverted regime allows for the formation of long lived charge separated states. Although the photoinduced electron transfer occurs in the normal regime, in the inverted regime back electron transfer can take place due to the increased exogercity of this process.

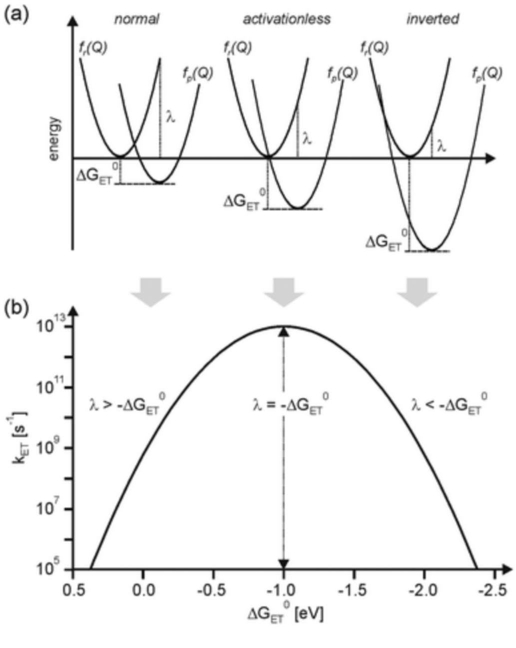

Figure 1.6: Electron transfer rate dependence with changing Gibbs free energy, outlining the normal, activationless and inverted regimes.[38]

1.4.3 Charge Separation

In an artificial photosynthetic system the chromophore absorbs sunlight, resulting in photo-induced electron transfer to the acceptor moiety. Charge recombination can then occur or the donor moiety can sacrifice an electron to replenish the chromophore. The latter results in the formation of a charge-separated state (CSS). The formation of a CSS is a crucial process in the conversion of solar enegry into chemical energy. The energy absorbed by the chromophore is stored in the transient CSS. This CSS must possess a long enough lifetime in order for sufficient charge accumulation to occur at the relevant catalyst; since the main contribution to the decay of ^{3}CSS is back electron transfer, and therefore it is important to have slow back electron transfer (charge recombination).

1.4.4 Transition metal complexes

Transition metal (TM) complexes possess several qualities which make them suitable chromophores for artificial systems. They can exhibit strong metal-to-ligand charge-transfer (MLCT) or ligand-to-ligand charge-transfer (LLCT) transitions which correspond to the absorption in the visible region, making them a suitable contender for a light harvesting complex for solar energy conversion applications.[39,40] Upon light absorption, the CT state is formed, which can easily undergo further charge separation to form the CSS. Furthermore, transition metal complexes are known to have long-lived excited states, often in the nano- or microsecond region and, in particular, long lived CSSs. They also allow for good synthetic tunability meaning a variety of ligands can be attached covalently to the transition metal.[41,42] These ligands can also be modified in order to change the excited state dynamics of the system.[43,44] In this thesis the photophysical properties of a series of donor-bridge-acceptor complexes will be studied. The bridge in these complexes will be made up of a square-planar Pt(II) trans-acetylide moeity. The photophysical properties of Pt(II) trans-acetylide complexes have been extensively studied and it is acknowledged that the general excited state processes that occur following photoexcitation is the formation of the Franck-Condon ^{1}MLCT state, followed by rapid intersystem and internal conversion into a ligand-localised manifold, or a full charge-separated state state.[45,46] In addition to the CT transitions described above, d-d transitions can occur in TM complexes, which are typically forbidden under the Laporte selection rule. The Laporte selection rule states that in centrosymmetric molecules, transitions between states of the same parity i.e., gerade to gerade in the case of d-d transitions, are forbidden However, transient changes in the TM complexes geometry can distort the centre of symmetry, which result in d-d transitions becoming allowable, with molar absorption coefficients ranging between 1 - 1000 mol^{-1} cm^{-1}.

1.4.5 Previous research

Controlling the outcome of chemical reactions has been a long standing goal in the field of chemistry. More specifically and more relevant to this thesis, the idea of controlling the rate of electron transfer within a molecule. One way to do this is to use chemically benign IR light to modulate the ET rate, and therefore the yields of charge separation. Influencing ET using IR light has been previously achieved using narrowband IR pulses and is referred to vibrational control of electron transfer. Perturbing certain vibrational modes (the ”controlling” modes) has been shown to influence excite state yields, rates, and even inhibit the formation of certain excited states.[47–49] One of the main challenges to overcome in these experiments, is the fact that IVR (Intramolecular vibrational redistribution) occurs on very fast timescales. This leads to the vibrational memory of the initial infrared photo-excitation being lost, as the excited vibrational modes are coupled to other vibrational modes within the molecule. Therefore, population of a particular vibration that is deemed to be the controlling mode is quickly depopulated. For vibrational control, it is important to carefully time the IR pulse excitation, following the initial UV excitation. Therefore, for vibrational control experiments, the IR pump is positioned a few picoseconds after the initial UV excitation pulse, where $\tau < \text{T}$. The IR pulse is now positioned within the IVR time frame. The first time that IR light was found to affect the rate of ET transfer in a donor-bridge-acceptor molecule was demonstrated in 2009 by Z. Lin et al.[50] A three pulse sequence (UV$_{pump}$-IR$_{pump}$-IR$_{probe}$) sequence was employed. The first pulse was a 400 nm UV pump which populated an acceptor localised state of the anthracene, followed by a mid-IR pulse (1670 cm^{-1}) which selectively excited bridge localised vibrations in a anthracene (acceptor)-dimethylaniline (donor) molecule. A visible probe was used to then examine the changes in the charge separation rate caused by the IR light. The time delay, τ, remained fixed at 2.7 ps, whilst the time delay T was varied. The structure of the DBA molecule studied is shown in 1.7 along with the pulse sequence used. The effect of utilising Mid-IR pulses in parallel with UV excitation lead to an 60% decrease in the rate of CS (charge separation) which gave rise to a 1.8% decrease in the yield of the^{3}CSS. This showed a clear link between intramolecular ET rate and excitation of vibrational modes in a molecule.[50]

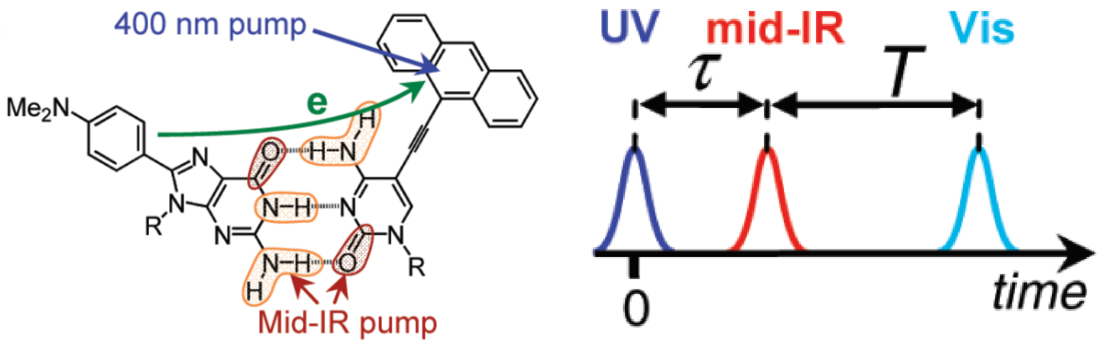

Figure 1.7: DBA molecule with N-H and C=O bonds highlighted which could be selectively excited by Mid-IR pump (left) and three pulse sequence, where τ = 2.7 ps and T = various (right).

More recently, in 2022, the energy transfer mechanism was studied in platinum based molecules containing alkyne bridges of various lengths, employing both experimental and theory techniques including 2DIR and DFT calculations (Figure 1.8). Excitation of the ν(CC) mode lead to energy transfer to various lower frequency modes. It was found that altering both electronic and structural properties could control the energy transfer. For example, decreasing the length of the alkyne bridge lead to shorter waiting times for the formation of cross peaks. The cross peaks correspond to the coupled vibrational transitions. Also different modes had different waiting times, indicating bonding strength plays a role in energy transfer. Theory calculations found that intramolecular energy transfer can occur in the platinum-containing molecules, via high frequency vibrational modes, which is a highly efficient process when the modes on both ligands involved are delocalized. These results give a valuable insight into how structure can affect function and how molecules can be manipulated to create optimised systems for energy conversion and charge separation.[51]

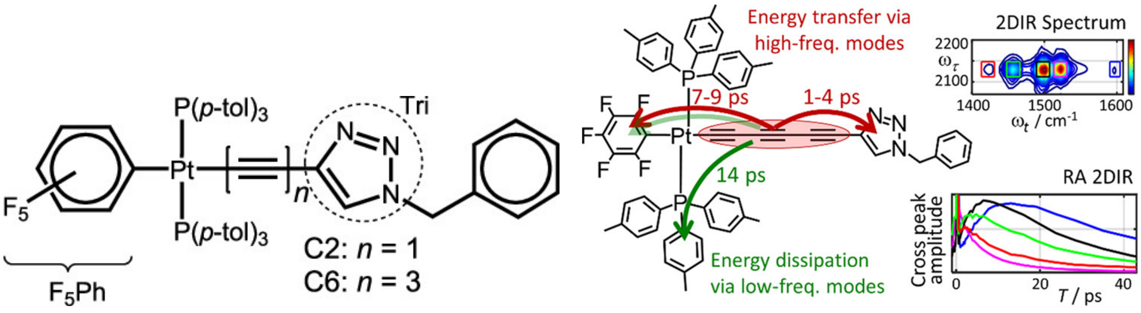

Figure 1.8: Platinum complex bearing ligands with varying bridge length, n (left) and scheme showing energy transfer pathways within the molecule upon excitation of the alkyne bridge mode, ν(CC) (right).

1.5 Aims

The aims of this thesis are to investigate the excited state dynamics of various modified Pt(II) donor-bridge-acceptor trans-acetylide complexes using ultrafast transient absorption and time-resolved infrared spectroscopy, to understand the connection between structure and function with ultimate goal of controlling the electron transfer by vibrationally exciting selected modes. In Chapter Three, the aim is to investigate how structural and electronic modifications, such as the addition of electron donating methoxy groups to the donor moeity and removal of the CH_2 spacer group between the phenyl ring and the donor moiety, affect the formation and decay of the ^{3}CSS. In Chapter Four, the aim is to investigate how the attachment of the donor varies the dynamics of a Donor-Bridge-Acceptor Pt(II) trans-acetylide system with a NAP acceptor. Additionally, the affect of an additional donor is investigated. In Chapter Five, the aim is to investigate how the attachment of the donor varies the dynamics of a Donor-Bridge-Acceptor Pt(II) trans-acetylide system with a NDI acceptor. Additionally, the affect of an additional donor is investigated. In Chapter Six, the aim is to measure the change in the yield of the ^{3}CSS upon selectively exciting the bridge-localised acetylide vibrational mode in the excited state in the Donor-Bridge-Acceptor Pt(II) trans-acetylide complexes studied in Chapters Three and

Five.

Chapter 2

Experimental

The main part of the thesis explores the photophysical properties of an array of Pt(II) based complexes, in the solution phase. A wide range of steady-state and time-resolved spectroscopic techniques are required in order to gain a thorough insight into the excited state dynamics of complex molecules. Time-resolved experiments rely on a femtosecond pulsed laser source for excitation of the sample at the desired wavelength. The sample is then probed over a range of wavelengths at various time delays, achieving both temporal and spectral resolution of the system being studied. Steady-state experiments such as ground state electronic absorption spectroscopy are performed. Steady state measurements can help to gain an understanding into the electronic ground state and the Franck-Condon excited states of the chemical system that is being studied. Furthermore, steady state measurements give an insight into the redox properties of the molecule. The techniques are performed over a broad range of the electromagnetic spectrum, particularly those wavelengths in the UV-visible and infrared ranges. The former provides information on electronic transitions of the system, while latter provides information on vibrational transitions.

2.1 UV-Vis absorption spectroscopy

The energy required to promote an electron from the ground state to an electronic excited state usually lies in the 6 to 1.5 eV (200 nm to 830 nm) region of the electromagnetic spectrum. This correlates to the ultraviolet (UV) and visible regions of the electromagnetic spectrum, hence the name UV-Vis spectroscopy. The absorption spectra generated from UV-Vis spectroscopy allows one to determine the Franck-Condon transitions.[24] The energy at which these transitions occurs allows one to determine the appropriate wavelength with which to excite the sample when conducting excited state absorption measurements. UV-Vis spectra also provide insight into the probability and energy of certain electronic transitions that occur in a complex. Transitions in organic ligands such as π to π^*, generally fall in the region of 200 to 350 nm and have strong oscillator strengths and therefore have a high probability of occurring. Charge transfer transitions such as MLCT transitions in transition metal complexes usually occur at longer wavelengths (350-800 nm), but with a lower absorption probability. Assignment of the MLCT transitions can be difficult due to several overlapping electronic transitions, giving rise to a broad absorption envelopes.[52] For example, in d-metal complexes there could be multiple MLCT transitions close in energy, involving various d-orbitals on the metal. Charge transfer transitions are broad in nature as they are highly polar and so the solvent can have multiple configurations.[53] The polarity of the solvent can have an influence over the absorption spectrum resulting in solvatochromism. For example the energy of charge transfer transitions will be more greatly affected in polar solvents, than in non polar solvents.[53] Thus leading to the distinction between a charge transfer and ligand localised transition, the latter not being as affected by the change in solvent.

UV-Vis spectroscopy uses a light source, typically a xenon lamp to cover a spectral range of 200 to 800 nm. This light is focused on to a diffraction grating and then passes through a monochromator which selects specific wavelengths to be incident on the sample. The transmitted light intensity, I, after passing through a sample is recorded , with respect to the intensity of light transmitted by the blank reference sample, I_0. The logarithm of the ratio between these two intensities is denoted as absorbance, in equation form this can be written as,

$$A = log\left(\frac{I_0}{I}\right).$$

The intensity of this light transmitted by the sample varies with concentration, [C], and path length, L, and therefore so will the absorbance. In order for a direct comparison to be made between complexes of differing concentrations and path lengths, the Beer-Lambert law is introduced.

$$A = log\left(\frac{I_0}{I}\right) = \varepsilon[C]L$$

This law describes the relationship between absorbance, concentration, path length, and also allows for the calculation of ε, the molar absorption coefficient.

2.2 Fourier-Transform Infrared spectroscopy (FTIR)

Vibrational transitions in molecules usually lie within the energy range of 0.1-0.45 eV and therefore fall in the infrared region of the electromagnetic spectrum. Infrared spectra contain more structural information compared to electronic absorption spectra, owing to the fact that the vibrational frequencies of bonds are sensitive to the atoms that constitute the bond and the local electronic environment. In the field of chemistry IR spectra are commonly presented along wavenumber axis, $\tilde{\nu}$. IR spectra are often highly structured compared to the broad absorption bands observed in UV-Vis spectra, due to the narrow spectral linewidths of vibrational absorption bands. Bonds contained with functional groups often have characteristic vibrational frequencies, facilitating their assignment. The intensity of an IR band is proportional to the oscillator strength of the vibration that gives rise to the band.

In a Michelson interferometer (Figure 2.1, a broadband IR light source (typically a silicon carbide element) is split into two different beams travelling along separate paths, using a beamsplitter. One of the beams directed onto a stationary mirror, whilst the other beam is directed onto a movable mirror, which introduces a controllable optical path difference between the two beams. The beams are then reflected back onto the beam splitter, where they recombine and interfere constructively and destructively. When the optical path difference introduced is an integer multiple of the wavelength, then constructive interference occurs. When the optical path difference introduced is $(n+\frac{1}{2})$ multiple of the wavelength destructive interference occurs. As the path difference is scanned by moving the mirror, different frequency components of the broadband IR light will fall in and out of phase. This will result in a modulation of the intensity recorded by the detector. The plot of intensity vs path difference is referred to as an interferogram. The interferogram is converted from a function of path difference (spatial domain) into the reciprocal domain (i.e., wavenumber, cm^{-1}) using a Fourier transform. The resulting transform is the vibrational spectrum. The intensity recorded by the the detector can be written as,

$$I(p,\tilde{v}) = I(\tilde{v})[1+cos(2\pi\tilde{v}p)],$$

where p is the difference in path length, $\tilde{v}$ is wavenumber. The total intensity measured is therefore defined as,

$$I(p) = \int_0^\infty I(p,\tilde{v}) = \int_0^\infty [1+cos(2\pi\tilde{v}p)]\cdot d\tilde{v},$$

as I(p) ans I($\tilde{v}$) have a cosine Fourier transform relationship, the inverse of the previous equation, gives the desired spectrum I($\tilde{v}$) in terms of I(p), which is the measured intensity.

$$I(\tilde{v}) = 4\int_0^\infty [I(p) - \frac{1}{2}I(p=0)]cos(2\pi\tilde{v}p)]\cdot dp$$

FTIR has numerous advantages over previously used dispersive methods, including improved signal to noise ratio and quicker performance time. This is due to the fact that all the light is detected simultaneously, instead of single wavelength interval at a time.[54]

2.3 Steady-State Emission Spectroscopy

In order for a molecule to return to the ground state the excess energy must be dissipated. One possibility is via the emission of a photon, where the energy of emitted photon is equal to the energy difference between the initial and final states. This process is known as spontaneous emission and can be studied using a variety of techniques. In this thesis, steady-state emission experiments will be conducted. Steady state refers to the fact that all the emission from the sample is collected in a given detector exposure time. Any time

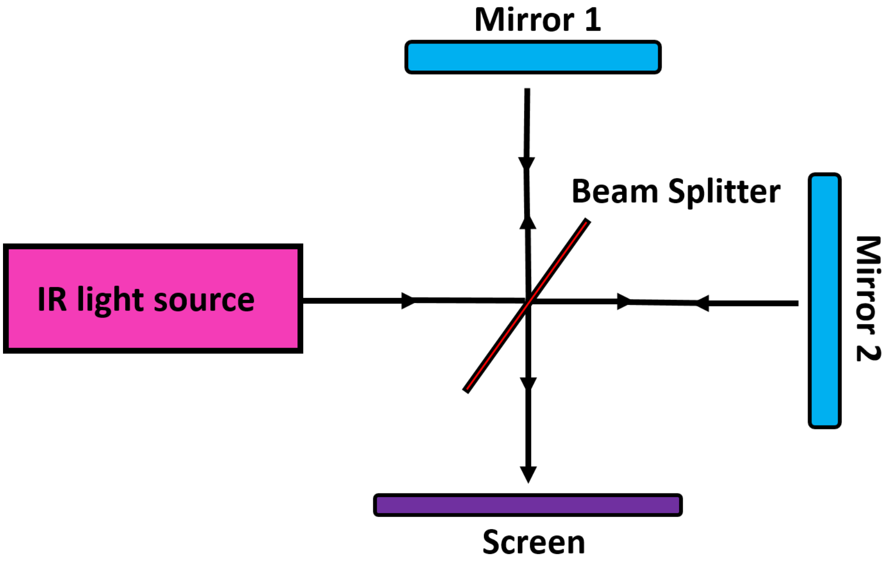

Figure 2.1: Schematic of a Michelson Interferometer

dependence of the fluorescence intensity is lost. Generally, the energy emitted is less than that absorbed by the Franck-Condon transition. This phenomenon is called Stokes shift. The shape of the emission spectrum aids in identifying the nature of the emitting state. Structured emission spectra which demonstrate vibrational structure are often associated with π-π^* emitting states. Whereas broad featureless emission bands often arise from CT excited states and emission decay measurements can assist in determining excited state lifetimes.[55]

2.4 Pump-Probe Spectroscopy

The first pump-probe technique was invented by Abraham and Lemoine in 1899.[56] Where an optical delay line was introduced for the first time. The technique employs two light pulses: a pump pulse and a time-delayed probe pulse. The former excites the sample, the latter then measures the change in transmission of the sample due to the initial excitation pulse. Later flash photolysis was achieved in 1949 by G. Porter and R. Norrish. They won the Noble Prize in chemistry in 1967 for their work.[57,58] Since its inception, the pump-probe method has evolved into a highly sophisticated experimental technique, incorporating the latest ultrafast laser systems. For example, in 1999 Ahmed Zewail won the Nobel

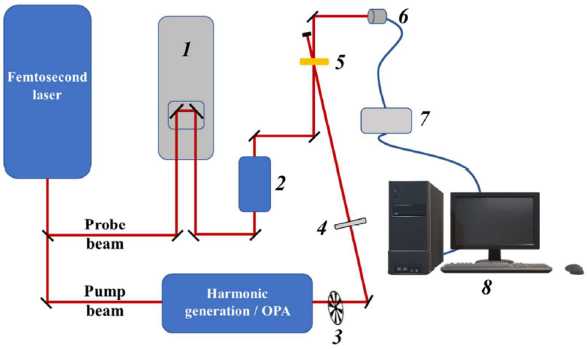

Figure 2.2: Schematic of Pump-Probe experimental set-up, 1. Optical delay stage 2. White light continuum generation 3. Mechanical or optical chopper 4. Half waveplate 5. Sample 6. Fibre optic cable 7. Spectrograph and detector 8. Computer. Courtesy of Alex Auty

Prize for his work on the study of chemical reactions on a femtosecond timescale.[59] The development of the pump-probe technique is owed to the ability of modern laser systems to: (1) produce pulses, the temporal full-width-half-max of which, range from the atto to nanosecond domain (2) excellent shot-to-shot stability (3) the capability to tune pulses to a desired frequency. The general set-up of a pump-probe experiment incorporating a femtosecond laser source can be seen in Figure 2.2. The laser beam is commonly produced by a Ti-Sapphire amplifier, from which the output is split into the pump and probe beams using a beam splitter. The pump pulse wavelength can be altered as desired in order to excite the appropriate transitions of the the system. The fundamental emission wavelength of the Ti:Sapphire laser is 800 nm; too low an energy for the excitation of most electronic transitions. Therefore, the most commonly used excitation wavelengths for exciting electronic transitions are those of 400 nm and 267 nm, the 2nd and 3rd harmonics of the Ti:Sapphire fundamental (800 nm). The 2nd and 3rd harmonics are generated via a process known as sum frequency generation. This is a specific case called frequency doubling where the beam produced is twice the frequency of the original beam, but half the wavelength. To obtain other excitation wavelengths, optical parametric amplification (OPA) is used to tune the frequency of the pump. Further information on OPA can be found elsewhere.[60–62] A portion of the 800 nm Ti:Sapphire fundamental is used to seed optical parametric amplifiers, which, through nonlinear optical processes, can generate different frequencies of light. In order for a wide spectral range to be covered, the probe pulse needs to be a spectrally broad pulse. An optical crystal, such as CaF_2 or Sapphire crystal is used to generate a while light continuum (WLC), which serves as this broad pulse. The pump pulse excites the sample at the chosen wavelength, this could be either a vibrational transistion of the sample or an electronic transition. The sample is then probed over a broad spectral range (UV-Vis or IR) by the probe pulse, which arrives at the sample at various time delays after the excitation pulse. The time delay is controlled by an optical delay line. The differential absorption spectrum is obtained through modulation of the pump repetition rate, such that the repetition rate of the pump pulse is half that of probe pulse. This allows the transmission of the probe, through the sample, to be measured with and without the initial excitation pulse. The change in transmission of the sample, as a result of excitation is then defined by the equation below,

$$\Delta T = \frac{T^* - T}{T},$$

where T^* and T are the transmission of the probe through the sample with and without excitation respectively. ΔA is then calculated from ΔT using the following equation,

$$\Delta A = -log(\Delta T + 1). \tag{2.4.1}$$

For each time delay, t,a spectrally resolved ΔA is recorded. Therefore ΔA is measured as a function of both t and wavelength, λ. When probing wavelengths in the UV-Vis spectral range, this is known as transient absorption (TA), whereas probing in wavelengths in the infrared region is known as Time-resolved Infrared Spectroscopy (TRIR).[29,30]

2.5 Transient Absorption

Transient Absorption is a useful technique for studying the ultra-fast electronic excited state dynamics of chemical systems. The ΔA spectrum produced is made of several contributions from different processes, these include ground state bleach, transient absorption and stimulated emission. The ground state bleach contribution originates from a small portion of the molecules being promoted from the ground state to the excited state from the excitation pump pulse. Therefore the number of molecules in the ground state decreases. This gives rise to a negative signal at wavelengths where the ground state absorption spectrum occurs. Following excitation from the pump pulse, stimulated emission can happen when the probe pulses transverses through the sample. The probe pulse triggers the emission of a photon from molecules in the excited state, these molecules then return to the ground state. The photon which is emitted, travels in the same direction as the probe and so therefore will be detected, resulting in an increase in intensity of the transmitted probe light. This means there is an apparent decrease in absorption and so creates a negative ΔA signal. Stimulated emission is governed by selection rules and so only optically allowed radiative transitions can occur. This signal will have a similar spectral shape to that of the ground state bleach if the stimulated emission occurs from the same excited state that is initially populated. Dynamic shifting of the SE maximum can be observed in early time TA measurements as a result of SE emanating from a vibrationally hot excited state. As the excited state dissipates the excess vibrational energy, a redshift of the SE maximum is observed. Excited State Absorption (ESA) is the final contribution the ΔA spectrum. After the pump pulse has excited some of the molecules from the ground state to an excited state, new transitions from this excited state to other excited states can occur, for example from S_1 to S_2. This results in positive signal in the ΔA spectra.[30] TA absorption spectrum are often combinations of multiple absorbances overlapping, and so it is difficult to deconvolute spectra. Combining TA with TRIR can be advantageous in assigning certain excited state absorption bands to certain excited states. For example, if a spectral feature in TA and TRIR spectra both share the same dynamics it is likely that they are they correspond to the same electronic excited state.

2.6 Time-resolved Infrared

Time-resolved infrared spectroscopy is a similar technique to that of TA, in that a pump pulse is used to electronically excite the sample. However, in TRIR the sample is probed in wavelengths corresponding to the IR region. Probing in the IR-region allows for vibrational transitions in the newly formed excited state to be studied. When a molecule is excited, there is a shift in electronic density in comparison to the ground state. As vibrational transitions are heavily dependent on the strength of the bond, which in turn depends on the electron density on the vibrating fragment, their frequency can change from the ground state to the excited state. Therefore they can be useful indicators of shifts in charge distribution/electron density. Bonds with high IR oscillator strengths such as carbonyl (C=O) and acetylide (C≡C) bonds are especially sensitive to such changes. For example, in transition metal complex with CO ligands, the CO IR frequency would increase in an MLCT state compared to the ground state. This is due to the decrease in back-bonding, which is donation of electron density from the orbitals of the metal to those of the ligands. Due to the decreased back-bonding, the CO bond is stronger and therefore the frequency is higher.

2.7 Fluorescence Upconversion Spectroscopy

Fluorescence Up-conversion Spectroscopy (FLUPS) is a pump-probe technique used to measure time- resolved emission on a femtosecond timescale. Owing to advancements in recent decades, broadband time-gated fluorescence spectra can be recorded in a single measurement. (previously multiple scan experiments probing 10-15 nm). A femtosecond laser pulse (FWHM 40 fs) is used to excite a sample. The sample then produces fluorescence, at a frequency V_F, which then passes through a β

-barium borate (BBO) crystal, which when it is overlapped in time with a second gate pulse, which has a frequency V_G, the gate pulse upconverts the fluorescence via a process known as sum frequency generation to give V_U, where V_U is the frequency of the upconverted emission. Obeying conservation of momentum, V_U is calculated from V_F and V_G using the following equation,

$$V_U = V_F + V_G.$$

The gate pulse provides the time resolution by only allowing the fluorescence to be up converted when it is overlapped in time. The pump pulse travels via a delay stage which controls the time at which the pump reaches the sample.

2.8 2DIR

2DIR (Two-Dimensional Infrared) spectroscopy is an experimental technique that employs an IR pump and probe. There are two methods for carrying out 2DIR measurements, it can be either time or frequency domain. In this thesis time domain 2DIR will be discussed. In time domain 2DIR, two IR pump pulses creates a vibrational coherence i.e a superposition of vibrational states in the sample, while the IR probe measures the shift in vibrational frequency of the modes due to IR excitation. 2DIR can be used in order to study chemical exchange, structure and vibrational coupling in molecules. In this thesis the focus will be on vibrational coupling. The aforementioned occurs through space when two molecules feel the electrostatic potential of the other. This can cause a change in electronic structure i.e the molecular orbitals of a molecule and therefore causing a shift in the vibrational frequencies of a molecule. This is due to the direct link between electronic structure, bond length and vibrational frequency.[63,64] Vibrational coupling can also occur through bonds. When one vibration is coupled to another, this takes longer for the signal to appear as the energy has to travel through the molecule.[65,66] Figure 2.3 shows the experimental set-up where two broadband IR pumps are scanned at various time delays, τ_1 for every time delay τ_2, known as the waiting or coherence time.

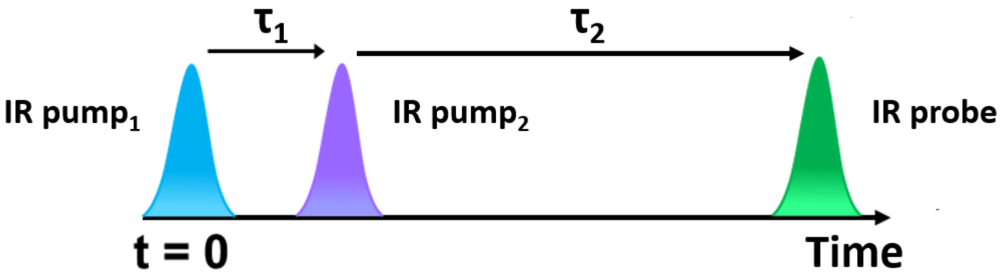

Figure 2.3: Three pulse sequence for 2DIR

2.9 Three-pulse experiments

Three pulse experiments are an extension of the 2DIR experiment, by means of the addition of a UV pulse, creating a three pulse sequence (UV$_{pump}$-IR$_{pump}$-IR$_{probe}$). The time delay, τ, between the UV pump and the narrowband IR pump can be altered to achieve two sub types of 3 pulse experiments, as shown in Figure 2.4. The first of which is called vibrational control, which was previously introduced in Chapter 1. Here, τ is fixed at either 1 or 2 ps and T is varied. For T, two time delays are used. One being at a time just after IR excitation and then the other at a longer time delay when all vibrational memory is lost so changes being measured, are changes in electronic excited state population i.e 200 ps. In other words, if there are two pathways a state can decay into, the vibrational excitation can influence the ET in a such a way that one pathway is switched off. The second type of 3 pulse experiments is called Transient-Two Dimensional Infrared (T-2DIR), the UV pulse and the broadband IR probe are a fixed time delay, T, from each other. The IR excitation pulse is now varied from $\tau < \text{T}$ to $\tau > \text{T}$. This allows for the vibrational modes in a molecule in the excited state to be probed. Changes to excited state yield due to IR excitation in three pulse experiments will produce either positive or negative peaks. Positive peaks present at the corresponding transient peak position in the TRIR represent an increase in excited state yield. Negatives peaks at the corresponding transient peak position in the TRIR indicate a decrease in excited state yield. This is the reverse for positive and negative peaks present at the positions of ground state bleaches in the corresponding TRIR experiments i.e a positive peak at a bleach position would indicate increased bleach recovery. The percentage change in excited state yield can be calculated by dividing the magnitude of the peak relevant the three-pulse experiment by that of the relevant TRIR peak. This percentage change is normalised with respect to the number of IR photons absorbed.

The pulsed repetition rates of the lasers as follows; IR probe is 10 KHz, the UV-Vis is 5 KHz, and the IR pump is 2.5 KHz. This allows for TRIR signal (UV$_{pump}$-IR$_{probe}$) and 2DIR signal (IR$_{pump}$-IR$_{probe}$) to be recorded at the same time as the T-2DIR signal. The calculation of the signal due to changes from both UV and IR photo-excitation is done in

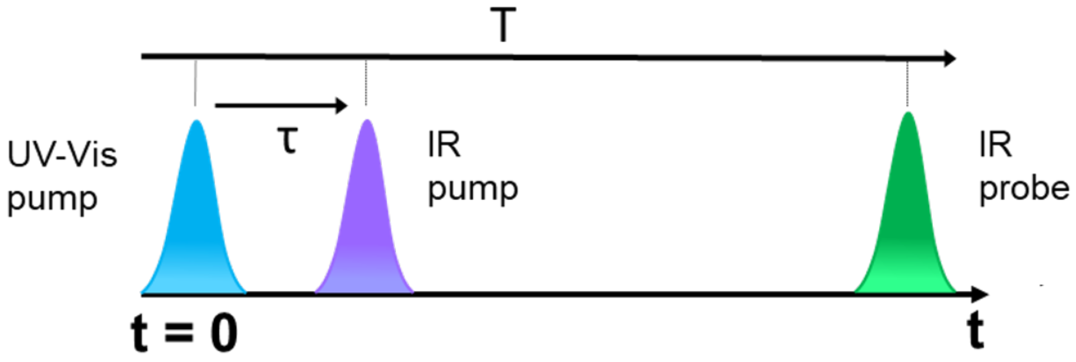

Figure 2.4: Three pulse sequence for T-2DIR and Vibrational Control experiments

the subsequent way,

$$\Delta T = \frac{probe_{11} - probe_{01} - probe_{10} + probe_{00}}{probe_{00}},$$

where probe denotes the IR probe signal and the subscript numbers denotes if the probe signal was recorded with the UV/IR pump is on or off. For example, probe$_{01}$ means UV pump is off, IR pump on. The data is recorded in transmission, ΔT, which is then converted into absorbance, ΔA, using the previsuosly mentioned Equation 2.4.1.

2.10 Cyclic Voltammetry and Spectroelectrochemistry

Cyclic voltammetry is an electrochemical method which is used to estimate the reduction and oxidation potentials of chemical complexes. This is achieved by the addition or removal of electrons and measuring the change in current. An estimation of the energy of the ^{3}CSS can be calculated from the difference between the redox potentials. The driving force of electron transfer, ΔG$_{et}$, can also be calculated using the Weller equation,

$$\Delta G_{et} = e\left[E_{ox}\left(donor\right) - E_{red}\left(acceptor\right)\right] - E^{*} + - \frac{e^2}{4\pi\varepsilon_0\varepsilon_S r_{DA}},$$

where E* is the energy of the initial excited state before charge separation. Spectroelectrochemistry produces a UV-Vis and FTIR spectrum for the anion/cation of a molecule, this allows for assignment of these species in excited state spectroscopy.[67]

2.11 Specific apparatus used

2.11.1 UV-Vis absorption spectroscopy

All ground state electronic absorption spectra were recorded using a Cary 50 Bio spectrometer, the samples were measured in quartz cuvettes.

2.11.2 Emission spectrosocpy

All ground state emission spectra were recorded using a Fluromax-4 Spectrofluorometer.

2.11.3 Time resolved luminescence

The Mini Tau fluorescence spectrometer (Edinburgh instruments) was used to record time resolved luminescence. The sample is excited at either 405 (FWHM 60 ps) or 445 nm (FWHM 100 ps), using one of the two picosecond pulsed laser diodes. TCSPC (Time-Correlated Single Photon Counting) is used in combination with a PMT detector to measure the luminescence. Samples with low optical densities were prepared in 1 cm quartz cells and were either aerated or degassed. The emission is detected by selecting the appropriate bandpass filter.

2.11.4 FTIR

All ground state infrared spectra were recorded using a PerkinElmer One FTIR spectrometer, the samples were measured in FTIR solutions cells with CaF_2 windows with a path length 0.25mm.

2.11.5 Time-resolved Infrared Spectroscopy (TRIR)

All TRIR experiments were performed at the STFC ULTRA facility in the Rutherford Appleton Laboratory, an outline of the experimental scheme can be seen in Figure 2.5. A Ti-Sapphire laser generates 800 nm pulses 10 kHz, 40 fs, 1mJ, a part of which is used to generate tuneable 400 cm^{-1} mid-IR probe light, some of which used to pump fs-NOPA

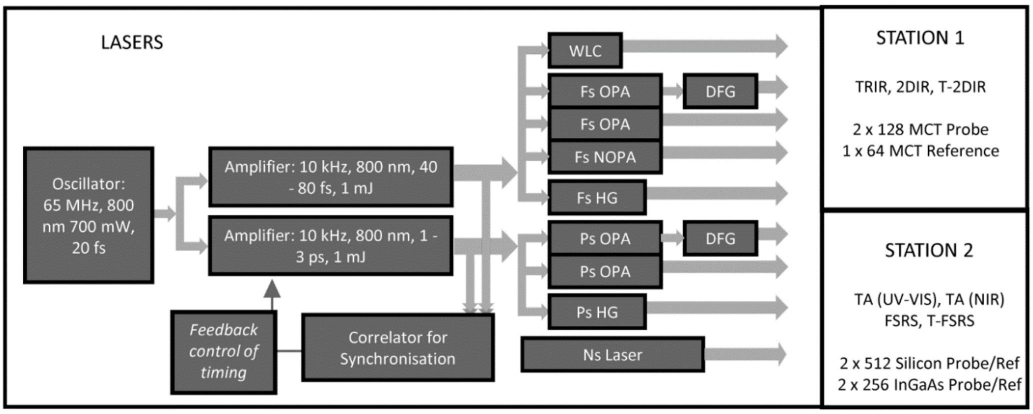

Figure 2.5: An outline of the experimental set-up in the Rutherford Appleton Laboratory at the STFC ULTRA facility.[68]

TOPAS which was used to generate visible pump pulses between 500 and 520 nm. The experiments were performed in solution in a Harrick cell. A peristaltic pump was used to flow and raster the solution in order to prevent degradation of the sample.

2.11.6 Two-Dimensional Infrared Spectroscopy (2DIR)

All 2DIR experiments were performed at the STFC ULTRA facility in the Rutherford Appleton Laboratory, an outline of the experimental scheme can be seen in Figure 2.5.

2.11.7 Transient Two-Dimensional Infrared Spectroscopy (T-2DIR)

All T-2DIR experiments were performed at the STFC ULTRA facility in the Rutherford Appleton Laboratory, an outline of the experimental scheme can be seen in Figure 2.5. The experiments were performed in solution in a Harrick cell. A peristaltic pump was used to flow and raster the solution in order to prevent degradation of the sample.

2.11.8 Transient Absorption

All TA experiments were performed at the Ultrafast Lord Porter Laboratory, at the University of Sheffield (ULS), an outline of the experiemntal set-up can be seen in Figure. Two Nd:YLF lasers pump the Mai Tai Ti:Sapphire oscillator. The later pumps the Ti:Sapphire Spitfire Ace amplifier, which generates 800 nm pulses (10 KHz, 40 fs, 12W). Travelling-

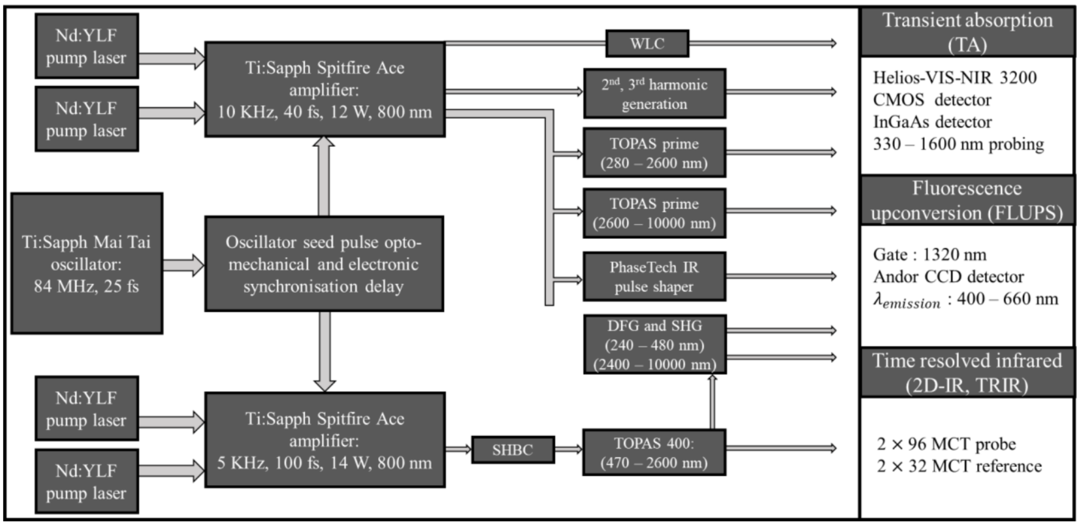

Figure 2.6: An outline of the experimental set-up in the Ultrafast Lord Porter Laboratory, at the Univerisity of Sheffield

wave optical parametric amplifier of superfluoresence (TOPAS) was used to create tunable pulses.

2.11.9 Fluorescence Upconversion Spectroscopy

All FLUPS experiments were carried out at the Ultrafast Lord Porter Laboratory, at the University of Sheffield (ULS), an outline of the experimental set-up can be seen in Figure 2.6. Two Nd:YLF lasers pump the Mai Tai Ti:Sapphire oscillator. The later pumps the Ti:Sapphire Spitfire Ace amplifier, which generates 800 nm pulses (10 KHz, 40 fs, 12W). The 800 nm is split into two beams using a beam splitter. The first beam is used to generate a 400 nm beam (10 KHz, 40 fs) by frequency doubling within a BBO crystal. The second beam is used to pump the TOPAS, which generates the 1320 nm (10 KHz, 80 fs FWHM) gate pulse. An Andor CCD camera is used for ultrafast detection of the upconverted signal.

2.12 Data Analysis

A range of software packages were used to to fully analyse the data. The graphing software OriginPro 9.7 was used to plot the data and perform simple analysis. Surface Xplorer was used to chirp correct the data and perform basic data analysis. Glotaran v1.5.1, in conjunction with the R package TIMP, was used to perform more complex data analysis, such as global lifetime analysis (GLA) in order to extract kinetic information from the data.[69,70] The decay associated spectra (DAS) and the solid trace kinetic fittings for all data were realised using a sequential kinetic model. Errors extracted from global analysis software are too small to be accurate. Errors extracted from single kinetic analysis are given. The use of a MATLAB GUI designed by Ricardo Fernández-Terán was also used to process the 2DIR data.[71]

Chapter 3

Photophysics of a series of modified Pt(II) donor-bridge-acceptor trans-acetylide complexes, which have modifications on the donor by addition of methoxy groups and/or removal of a CH_2 spacer

3.1 Introduction

The excited state dynamics of a Pt(II) donor-bridge-acceptor trans-acetylide complex have been extensively studied, where the acceptor ligand is 1,4,5,8-naphthalene diimide (NDI) and the donor ligand is phenothiazine (PTZ). A range of techniques were utilised including transient absorption (TA) and time-resolved infrared spectroscopy (TRIR). This complex will be referred to as the unmodified 'original' complex or Complex 1 in the results section, for the ease of comparison to the other complexes studied in this thesis. In Figure 3.1 the energy diagram for Complex 1 is shown. In Complex 1, the Frank-Condon state is populated on a sub 500 fs timescale. This state then decays on a sub 500 fs timescale, which is concomitant with the formation of the ^{3}IL state localised on the CC-NDI moeity, this state then decays with a lifetime of 4.5 ps to form the ^{3}IL(CT) state. There is then a direct population from the ^{3}IL(CT), which decays with a lifetime of 793 ps to form the final ^{3}CSS state. The decay of the final ^{3}CSS state occurs with a lifetime of 5.8 ns. A small driving force of 0.1 eV was found for the formation of the ^{3}CSS, which could be responsible for its long lifetime of 5.8 ns. The results of this complex have inspired the modification of three further complexes with the aim of gaining a greater understanding in how structure can affect the excited state dynamics of a complex. It is possible to change the driving force for the formation of the ^{3}CSS by modifying the strength of the donor. The energy level diagram for the excited state processes following excitation at 500 nm can be seen in Figure 3.1. The results found are that the acceptor group played

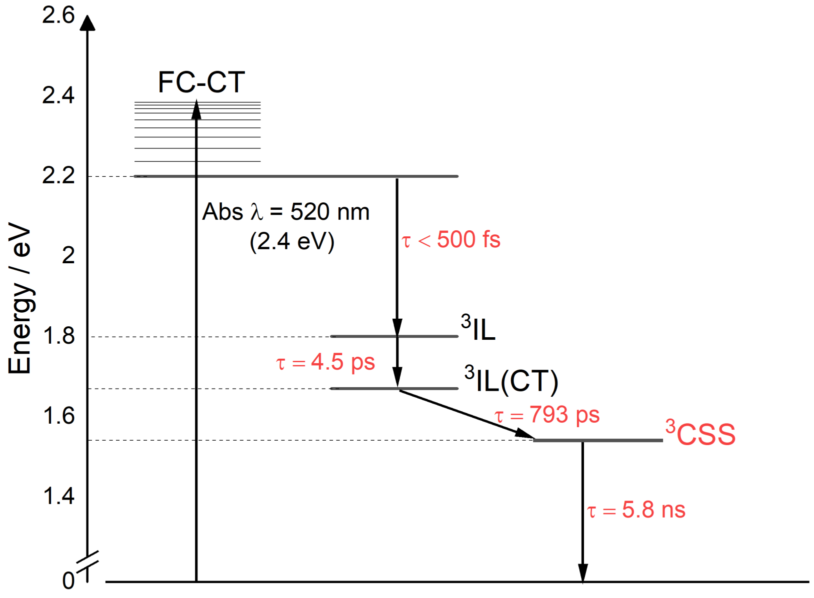

Figure 3.1: Energy diagram for the excited state processes following excitation at 500 nm

little role in altering the rate of formation and decay lifetime of the ^{3}CSS state. Therefore the modifications to the complexes in this chapter are on the donor group. The ultrafast dynamics of three Pt(II) donor-bridge-acceptor trans-acetylide complexes have been studied and compared to the original 'unmodified' complex (Complex 1), employing a variety of techniques including steady-state measurements, ultrafast TA spectroscopy and TRIR spectroscopy. All complexes have the same acceptor ligand, 1,4,5,8-naphthalene diimide (NDI), but have various modifications to the donor ligand, phenothiazine (PTZ).[46] The use of DFT (Density Functional Theory) calculations have been used to aid the characterisation and energies of excited states. NDI-Pt-Ph-CH_2-PTZ will be known as Complex 1 and is the original unmodified complex. NDI-Pt-Ph-CH_2-PTZ-$(OMe)_2$ will be known as Complex 2, which is identical to Complex 1 but has the addition of methoxy groups to the donor. NDI-Pt-Ph-PTZ-$(OMe)_2$ will be known as Complex 3 and also has the addition of methoxy groups but with removal of the CH_2 spacer between the phenyl ring and the donor ligand. NDI-Pt-Ph-PTZ will be known as Complex 4 and is identical to Complex 1 with the removal of the CH_2 spacer.

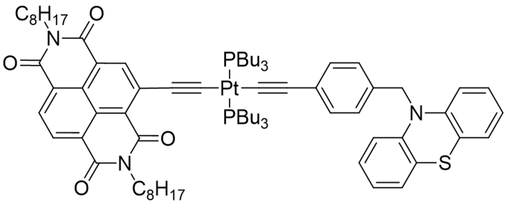

(a) Complex 1

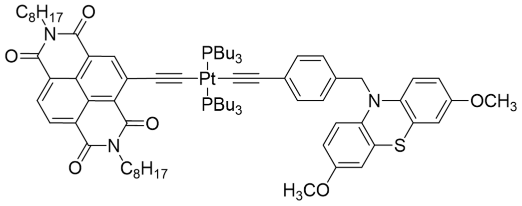

(b) Complex 2

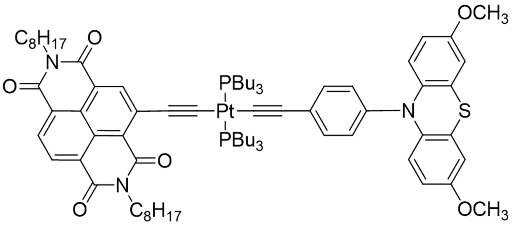

(c) Complex 3

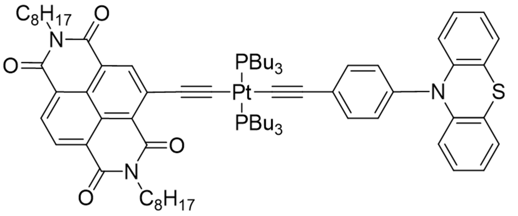

(d) Complex 4

3.2 UV-Vis spectroscopy

The steady state absorption spectra of Complexes 1-4 are shown in Figure 1. The spectra were recorded at room temperature in CH_2Cl_2 (DCM), covering a spectral range between 225 and 700 nm. All of the complexes display a well-structured spectrum from 240 to 370 nm, with the various absorption bands assigned to π-π* electronic transitions localised on the NDI, PTZ and Ph fragments. The intraligand π-π* transition centred on the PTZ occurs at 255 nm for Complexes 1, 2 and 4, but is slightly red shifted to 260 nm in Complex 3. The absorption bands centred at 285 and 330 nm are assigned to (π-π^*) electronic transitions centred on the phenyl-acetylide fragment. The shoulder present at 360 nm and the sharp peak centred at 380 nm are both assigned to (π-π^*) electronic transitions of the NDI ligand. The low energy mixed-metal-ligand to ligand charge transfer (ML-LCT) transition is responsible for the broad absorption band with maxima at 496, 504, 505 and 501 nm for complexes 1, 2, 3 and 4 respectively. This ML-LCT transition involves charge transfer from the Pt-acetylide bridge to the NDI acceptor ligand.

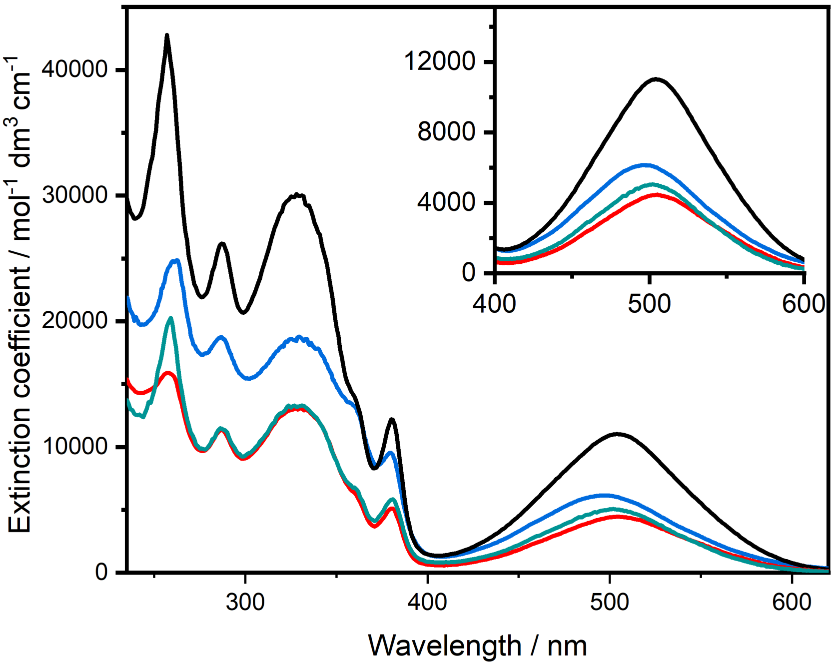

Figure 3.3: UV/VIS absorption spectra for Complexes 1 (Black), 2 (Red), 3 (Blue) and 4 (Green) recorded in DCM, at room temperature. (Normalized to the absorption band at ca. 500nm.)

3.3 Emission spectroscopy

Figure 3.4 shows the steady state emission spectra of Complexes 1 – 4, in aerated DCM, following excitation at 510 nm (ML-LCT absorption band). The emission maxima for complexes 1 – 4 appear at 558, 575, 564 and 556 nm, respectively. These emission bands are not sensitive to the presence molecular oxygen and are likely to arise from the radiative decay of the initially populated ML-LCT state. When dissolved in hexane, all four complexes display an additional, broad NIR emission band centred at ca. 680 nm. Such behaviour suggests that an excited state is present in DCM which can efficiently quench the excited state responsible for the NIR emission. However, formation of this quenching state in hexane is inhibited, suggesting this state is highly sensitive to solvent polarity. Additionally, in Complexes 2 – 4, the higher energy emission band blue shifts in hexane. Solvatochromic behaviour is indicative of emission from an excited state with charge transfer character, therefore the high energy emission is likely to emanate from the initially populated ML-LCT state.

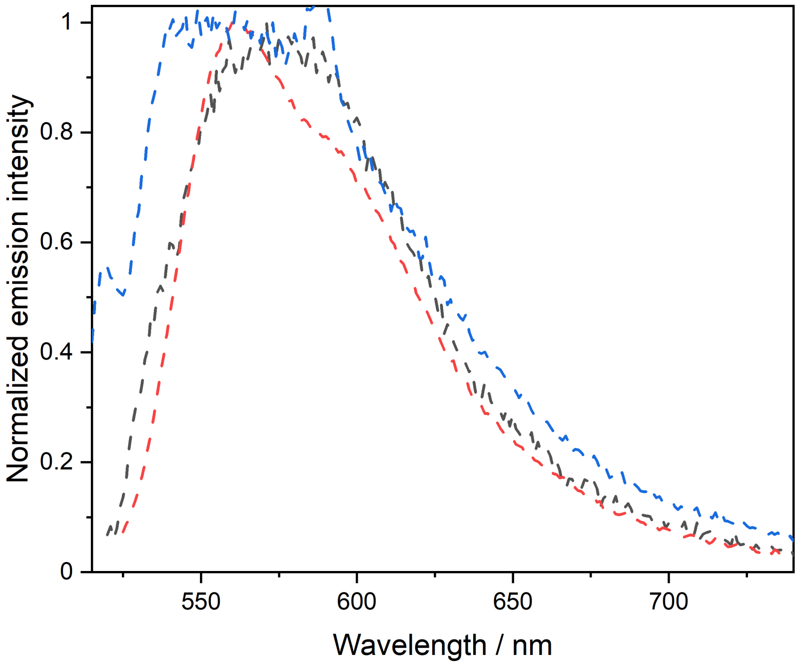

Figure 3.4: Normalized emission spectra for aerated solutions of Complexes 2, 3, and 4 (blue) in DCM Insert legend.)

3.4 Cyclic Voltammetry

Cyclic voltammetry of Complexes 2 and 3 were recorded in dry DCM with a solution of 0.4 mol dm^{-3} $[NBu_4][PF_6]$. The first and second one-electron reversible oxidation process of the PTZ donor ligand with the appended MeO groups in Complex 2, was found to be $E_{\frac{1}{2}}$: 0.1 and 0.75 V respectively versus Fc/Fc^+. The first and second one electron reduction process of the NDI acceptor ligand in Complex 2 was found to be $E_{\frac{1}{2}}$: -1.2 and 1.63 V respectively versus Fc/Fc^+. The first and second one-electron reversible oxidation process of the PTZ donor ligand with the removal of CH_2 spacer group and the appended MeO groups in Complex 3, was found to be $E_{\frac{1}{2}}$: 0.1 and 0.76 V respectively versus Fc/Fc^+. The first and second one-electron reversible reduction process of the NDI acceptor ligand in Complex 2 was found to be $E_{\frac{1}{2}}$: -1.2 and -1.63 V respectively versus Fc/Fc^+. There is a cathodic shift of around 20 mV for Complex 2 and 3 compared to Complex 1. This means that the reduction and oxidation processes can occur more easily in Complexes 2 and 3 than in Complex 1. This could be due to the addition of the electron donating methoxy groups which increases the driving force for the oxidation of the bridge by lowering the oxidation potential. The removal of the CH_2 spacer creates a more conjugated PTZ donor ligand, meaning it can be more easily reduced. The difference in oxidation and reduction potentials for complex 2 and 3 is 1.3 V, which is estimated to be the energy of the charge separated state. The cyclic voltammograms for Complexes 2 and 3 can be seen in Figure 3.5. The oxidation and reduction potentials of Complex 4 have been estimated based on previous complexes. The difference in oxidation and reduction potentials for Complex 4 is 1.46 V, which is estimated to be the energy of the charge separated state. A summary of the absorption and emission maxima, along with the first and second oxidation and reduction potentials for all complexes can be seen in Table 3.1.

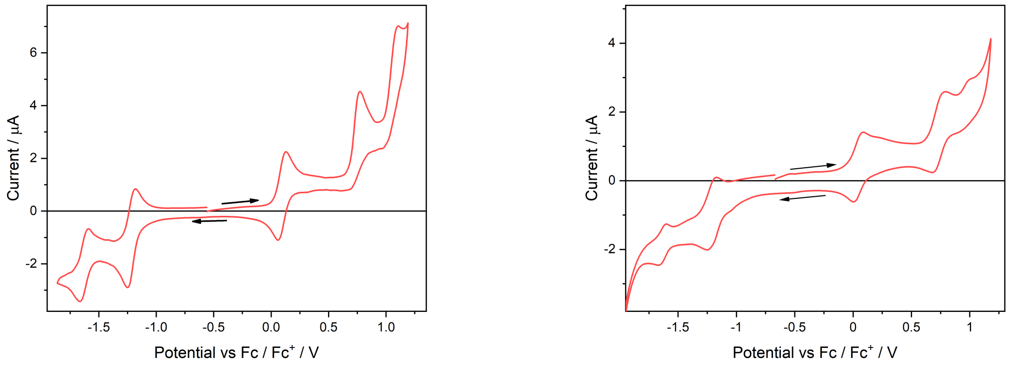

Figure 3.5: Full range cyclic voltammogram scans recorded in DCM of Complexes 2 and 3 versus Fc/Fc$^+$.

	Abs max / nm	Em max / nm	$E_{\frac{1}{2}}$Red. / V	$E_{\frac{1}{2}}$ Red. / V	$E_{\frac{1}{2}}$ Ox. / V	$E_{\frac{1}{2}}$ Ox. / V
Complex						
1	505	558	-1.44	-1.04	+0.33	+0.85
2	505	575	-1.2	-1.63	+0.1	+0.75
3	495	575	-1.2	-1.63	+0.1	+0.76
4	505	558	-1.2	-1.63	+0.26	+1.07

Table 3.1: A table showing the absorption and emission maxima for Complexes 1-3 recorded in DCM. The first and second reduction and oxidation potentials vs Fc/Fc$^+$ for Complex 1,2 and 3 recorded in DCM. Complex 4 is predicted from previous complexes.

3.5 Transient Absorption (DCM)

The TA spectra of Complex 2, 3 and 4 have been recorded in DCM, upon excitation at 500 nm. The excited state dynamics, following excitation, were probed for the three complexes between 340 and 740 nm. All spectra are dominated by coherent artefact signal before approximately 300 fs and have therefore been trimmed accordingly. The lifetimes were obtained from global analysis of the time resolved datasets. All decay trace colours increase in chronological order from black to red to blue to green to purple to yellow to cyan to brown.

3.5.1 NDI-Pt-Ph-Ch$_2$-PTZ-(OMe)$_2$ (Complex 2)

In complex 2, 0.27 ps after excitation, there is a ESA band centred at 430 nm. There is also featureless ESA between 600 and 680 nm. In between the two ESA bands bleaching of the ML-LCT absorption band is clearly visible, with a peak at 510 nm. Over the following 350 ps there is a significant change in spectral shape in the ESA features. There is a redshift of the signal from 430 nm to 475 nm, and the growth of a ESA signal at 640 nm. There is also apparent partial loss of the bleach signal at 510 nm. This is possibly due to the growth of overlapped ESA band at 475 nm. Between 350 and 6000 ps (maximum delay) the shape of the spectra remains constant while there is uniform decay of the signal.

3.5.2 NDI-Pt-Ph-PTZ-(OMe)$_2$ (Complex 3)

In complex 3, 0.3 ps after excitation there is an ESA band centered at 430 nm, along with broad/featureless ESA between 600 and 680 nm. In between the two ESA bands, bleaching of the ML-LCT absorption band is visible with a peak at 510 nm. Unlike complex 2 there is some degree of pump scatter round this region, which somewhat obscures the true ΔA signal. Between 0.3 and 10 ps there is a redshift of the ESA signal at 430 nm to 455 nm. Similar to Complex 2, there is a rise of ESA signal, with a peak at 625 nm. Between 10 and 30 ps, there is further decay of the ESA centred around 430 nm, resulting in further redshifting of the new ESA peak to 470 nm. Likewise there is also marginal decay, from 550 to 700 nm. Between 30 and 200 ps, there is partial decay of bleaching and ESA signal across the full spectral window, resulting in slight shifting of the signal at 470 nm to 480 nm. The ESA band at 625 nm does not shift. Between 200 and 5000 ps there is complete loss of the ESA signals at 480 and 625 nm. However, this reveals a small amount of residual signal at 430 nm and between 550 to 700 nm. The spectral shape of this residual signal is similar to that observed at early time.

3.5.3 NDI-Pt-Ph-PTZ (Complex 4)

In complex 4, 0.27 ps after excitation there is an ESA band centered at 430 nm. There is also featureless ESA between 580 and 700 nm. In between the two ESA bands, bleaching of the ML-LCT absorption band is visible with a peak at 510 nm. However, this is partly obscured due to pump scatter in this region. Therefore the spectra has been removed between 500 and 525 nm. Between 1 and 350 ps there is a redshift of signal from 430 to 480 nm, which is concomitant with the growth of a broad ESA band at 630 nm. Between 350 and 6000 ps (maximum delay) the shape of the spectra remains constant while there is uniform decay of the signal.

3.6 Transient Absorption (Hexane)

3.6.1 NDI-Pt-Ph-Ch_2-PTZ-$(OMe)_2$ (Complex 2)

In complex 2, 1 ps after excitation there is an ESA signal centered at 430 nm. There is also featureless ESA between 570 and 680nm. The spectra displays very little change from 1 ps to 5 ns and there are no new electronic bands formed on the timescale of this experiment, unlike in DCM.

3.6.2 NDI-Pt-Ph-PTZ-$(OMe)_2$ (Complex 3)

In complex 3, 0.4 ps after excitation there is an ESA signal centered at 430, 569 and 618 nm. Over the next few ps the band at 618 nm decays to reveal broad absorption between 585 and 7000 nm. The spectra displays very little change from 776 ps to 7 ns and there is only small decay of the signal, the signal does not decay on the timescale of the experiment, like in DCM.

3.6.3 NDI-Pt-Ph-PTZ (Complex 4)

In complex 4, 1 ps after excitation there is an ESA signal centered at 430 nm along with featureless ESA between 560 and 780 nm, similar to that which is observed in DCM at early time. Between 1 ps and 5 ns the TA absorption spectrum displays very little change in spectral shape and there are no new electronic bands formed on the timescale of this experiment.

3.7 FTIR

The ground state infrared absorption spectra of complexes 2, 3, and 4, recorded in DCM between 1450 and 2150 cm-1, are shown in Figure 2. Complexes 2 and 3 have absorption bands at 1660 and 1701 cm^{-1}, with a shoulder at 1708 cm^{-1}. Complex 4 has absorption bands at 1660 and 1708 cm^{-1}, with a shoulder at 1725 cm^{-1}. These absorption bands are assigned to the asymmetric/symmetric NDI-localised carbonyl ν(C=O) vibrations, however, the origin of the band at 1725 cm^{-1} remains unknown. The absorption band present in Complexes 2, 3 and 4 at 2073 cm^{-1}, with a shoulder at 2108 cm^{-1}, are assigned to the bridge-localised acetylide ν(CC) vibration. The absorption bands between 1450 and 1650 cm^{-1} are assigned vibrations localised on the aromatic rings of the ligands, ν(Ar). This region is noticeably different for Complexes 2 and 3, which have been appended with MeO groups on the PTZ donor. Unlike Complexes 1, 2 and 4, Complex 3 contains an additional absorption band centred at 1920 cm^{-1}. Interestingly, Complex 3 also displays minor differences in the acetylide region. When the spectra are normalised to the 1660 cm^{-1} ν(CO) stretch, the ν(CC) stretch of Complex 3 clearly has less intensity. Additionally, the shoulder at ca. 2108 cm^{-1} is less defined, suggesting the relative peak positions of the main band and shoulder are different in Complex 3 relative to the others. It is unclear if these differences are a coincidence or are the part of the reason why there's an extra band at 1920 cm^{-1}. There could potentially beam Fermi resonance in Complex 3 which is providing more intensity to a combination or overtone mode, with the intensity being borrowed from the acetylide vibration, hence the subtle changes in the acetylide bands.

3.8 TRIR data

3.8.1 NDI-Pt-Ph-Ch$_2$-PTZ-(OMe)$_2$ (Complex 2)

The TRIR spectra of Complex 2 are shown in Figure 3.11. The low frequency region has been trimmed spectrally from 1450 to 1750 cm^{-1} and has been trimmed temporally to 0.37 ps. Before 0.37 ps the spectra are dominated by coherent artefact signals. After excitation at 520 nm, there are bands at 1613 (with a shoulder at 1625) and 1645 cm^{-1} which are assigned to carbonyl vibrations in the initially populated excited state. Bleaching signals at 1665 and 1705 cm^{-1} are also observed which are assigned to the ν(CO) ground state vibrations at 1660 and 1701 cm^{-1}. The shift in peak position of the ν(CO) bleach at 1660 cm^{-1} (to 1665 cm^{-1}), is likely due to the overlap with the ESA at 1645 cm^{-1}. Accompanying the transient carbonyl bands are two more transients at 1480 and 1526 cm^{-1}, which are assigned to ν(Ar) signals in the initially populated excited state. Over the following 400 ps there is decay of the ν(CO) transient signals at 1613 and 1645 cm^{-1} and the the transient ν(Ar) signals at 1480 and 1526 cm^{-1}. Concomitant with this decay is the growth of new transient bands at 1515, 1588 and 1630 cm^{-1}, the latter two bands are assigned to transient ν(CO) vibrations.

The high frequency region has been trimmed spectrally from 1680 to 2175 cm^{-1} and the data has been trimmed temporally to 0.3 ps. Before 0.3 ps the spectra are dominated by coherent artefact signals. After excitation at 505 nm, there is a band at 1870 cm^{-1} which is assigned to the transient ν(CC) vibration in the initially populated excited state. There is also a bleaching signal at 2070 cm^{-1} which is assigned to the ν(CC) ground state vibration at 2070 cm^{-1}. There is a bleaching signal present at 1700 cm^{-1} (which has a shoulder at 1715 cm^{-1}) which is assigned to the ν(CO) ground state vibrations and is also present in the low frequency TRIR spectrum. Between 0.3 and 2.2 ps there is a shift in peak position of the transient ν(CC) band from 1870 to 1962 cm^{-1}. Over the following 15 ps the ν(CC) transient band at 1962 cm^{-1} decays concomitantly with the growth a new red shifted band at 1924 cm^{-1}. The new transient at 1924 cm^{-1} then decays fully over the full experimental window (1500 ps). Concomitant with this decay, is the formation of a new transient ν(CC) vibration at 2090 cm^{-1}. This ν(CC) transient at 2090 cm^{-1} partially decays within experimental time window along with partial recovery of both bleaches.

3.8.2 NDI-Pt-Ph-PTZ-(OMe)$_2$ (Complex 3)

The TRIR spectra of Complex 3 are shown in Figure 3.11. The low frequency region has been trimmed spectrally from 1450 to 1750 cm^{-1} and has been trimmed temporally to 0.26 ps. Before 0.26 ps the spectra are dominated by coherent artefact signals. After excitation at 510 nm, there are bands at 1492 and 1510 cm^{-1} (with a shoulder at 1525 cm^{-1}), which are assigned to the transient ν(Ar) vibrations in the initially populated excited state. There are also bands at 1589 and 1630 cm^{-1}, which are assigned to transient ν(CO) vibrations. There are bleach signals at 1661 and 1706 cm^{-1}, which are the ν(CO) ground state vibrations at 1660 and 1701 cm^{-1}, respectively. Between 2.2 and 310 ps there is partial decay of all transient and bleach signals. Between 210 and 2600 ps there is uniform decay of the signal and there is almost full recovery of bleach and transient signals. The high frequency region has been trimmed spectrally from 1715 to 2125 cm^{-1} and the data has been trimmed temporally to 0.37 ps. Before 0.37 ps the spectra are dominated by coherent artefact signals. Upon excitation at 510 nm there is a band at 2072 cm^{-1} which corresponds to the ν(CC) ground state vibration at 2070 cm^{-1}. There is also a band at 2089 cm^{-1} which is assigned to a transient ν(CC) vibration. Between 0.37 and 2.2 ps there is a shift in peak position of the transient ν(CC) band from 1875 to 1962 cm^{-1} and then to 2015 cm^{-1}. Between 2.2 and 210 ps there is significant decay of the transient ν(CC) peaks at 1962, 2015, 2089 cm^{-1}. By 2.6 ns (full experimental window) there is almost full recovery of the bleach and transient signals.

3.8.3 NDI-Pt-Ph-PTZ (Complex 4)

The TRIR spectra of Complex 4 are shown in Figure 3.11. The low frequency region has been trimmed spectrally from 1450 to 1750 cm^{-1} and the data have been trimmed temporally to 0.37 ps. Before 0.37 ps the spectra are dominated by coherent artefact signal. After excitation at 510 nm, bleaching signals are observed at 1701 and 1665 cm^{-1} which correspond to the ground state ν(CO) vibrations. There are also bands at 1493 and 1528 cm^{-1} which are assigned to the transient ν(Ar) vibrations. There are bands at 1649 and 1612 cm^{-1} (with a shoulder at 1628cm^{-1}) corresponding to ν(CO) vibrations in the initially populated excited state. Between 2.2 and 100 ps the ν(CO) bands at 1649 and 1612 both shift to lower frequencies at 1590 and 1630 cm^{-1}. Concomitant with the growth of these carbonyl signals, is the shift/ decay of the transient peak at 1528 cm^{-1} to a lower frequency.

The high frequency region has been trimmed spectrally from 1675 to 2150 cm^{-1} and the data has been trimmed temporally to 0.37 ps. Before 0.37 ps the spectra are dominated by coherent artefact signal. Upon excitation at 510 nm, there is a bleaching signal observed at 1701 cm^{-1} which corresponds to the ground state ν(CO) vibration also seen in the low frequency region. There is also a bleaching signal at 2064 cm^{-1} corresponding to the ground state ν(CC) vibration. What is more there is a band at 2095 cm^{-1} corresponding to a transient ν(CC) signal. Over the first 1 ps, the band at 1891 cm^{-1} shifts to 1964 cm^{-1}. Between 2.2 and 100 ps there is decay of the transient ν(CC) signal. There is almost full recovery of the bleach and decay of the transient signals by 3 ns (full experimental time window). A summary of the carbonyl and acetylide vibrations for both FTIR and TRIR can be found in Table 6.1.

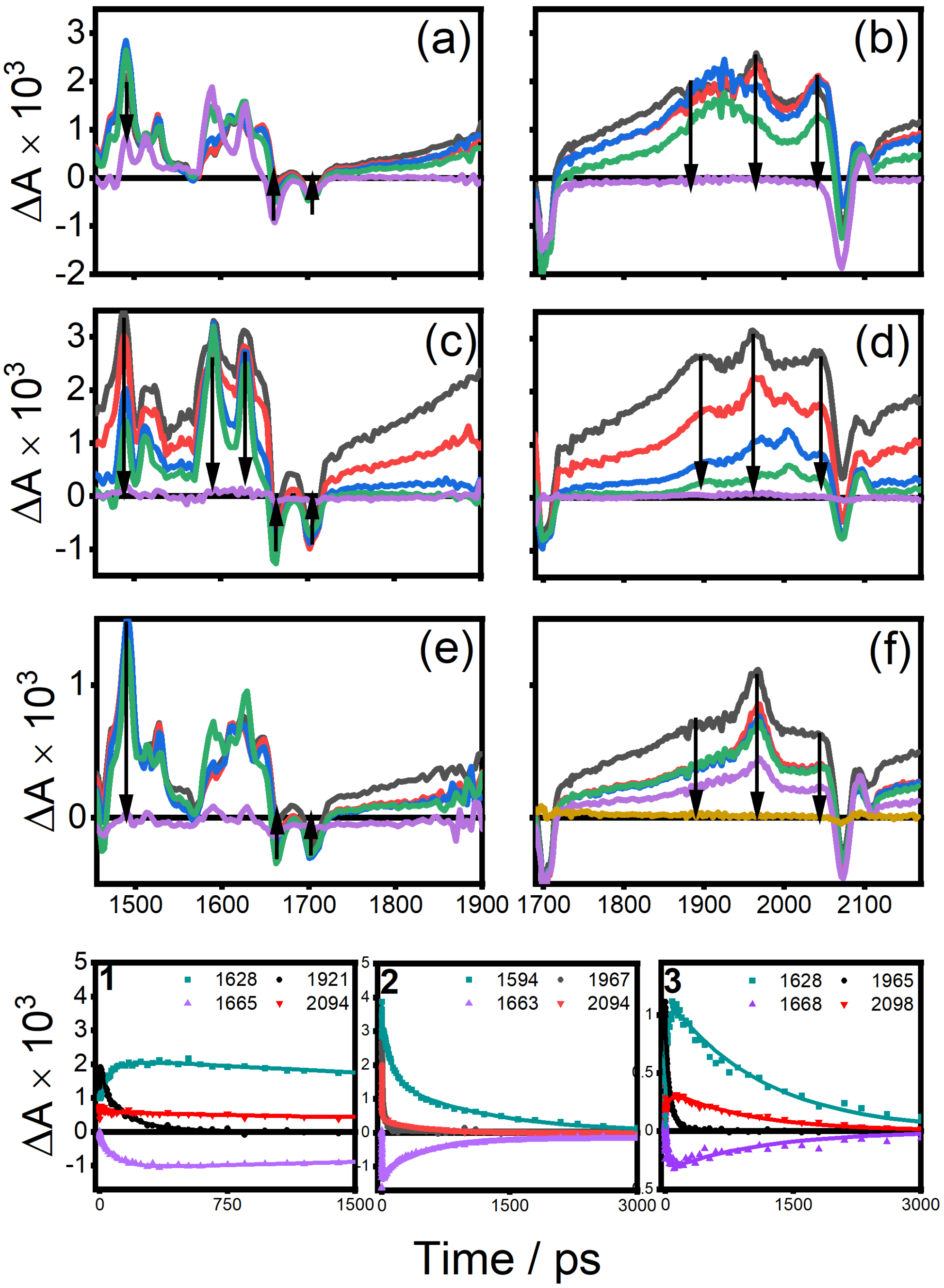

Figure 3.11: TRIR spectra for Complexes 2,3,4 (top to bottom), following excitation at 500 nm of the ML-LCT band in DCM. The time delays for Graphs a, c, d, e and f are 0.6, 2.2, 10, 37 and 3000 ps. The time delays for Graphs b are 0.6, 2.2, 10, 37 and 1500 ps. Single point kinetics for the TRIR spectra are shown in Graphs 1, 2 and 3 with the corresponding the solid lines which represent the residual fittings.

	FTIR / cm^{-1}		**TRIR / cm^{-1}**	
Complex	carbonyl region	acetylide region	carbonyl region	acetylide region
1	1659, 1699, 1708	2072, 2107	1612, 1647 / 1592, 1626	1885 / 1963 / 1928 / 2097
2	1660,1701, 1708	2070, 2110	1613, 1645 / 1588, 1630	1870 / 1962 / 1924 / 2090
3	1660, 1701, 1708	2070, 2110	1589, 1630	1875 / 1962 / 2015 / 2089
4	1660, 1701, 1708, 1725	2070, 2110	1612, 1649 / 1590, 1630	1891 / 1964 / 2095

Table 3.2: A table of the carbonyl and acetylide vibrational frequencies present in Complexes 1-4, for both FTIR and TRIR experiments. The forward slashes indicate the peak frequency at different times during the TRIR experiment

3.9 Discussion

3.10 Transient Absorption

3.10.1 NDI-Pt-Ph-Ch$_2$-PTZ-(OMe)$_2$ (Complex 2)

In complex 2 in DCM, the featureless ESA between 600 and 680 nm, is characteristic of the spectra of the ^{3}IL excited state localised on the [NDI-CC] moiety. This spectroscopic behaviour was also observed in Complex 1. The signal redshifts from 430 nm to 475 nm, which is concomitant with the growth of broad ESA signal at 640nm. Two DAS lifetimes of 44 and 142 ps were needed in order to describe this change in spectral shape. The need for two DAS lifetimes could be to account for the change in spectral shape and the other for the decay of the signal. This change in spectral shape indicates a change of electronic state, said excited state is formed after 350 ps. The new bands at 475 and 640 nm are consistent with those previously reported in the spectroelectrochemistry of the NDI radical ion. Therefore, it is likely that the new excited state has an electron density distribution on the NDI ligand consistent with that of the previously studied NDI radical anion.[46,72] This suggests that the new excited state formed is a ^{3}CSS state, whereby the NDI is formally reduced and is presumed to be the ^{3}CSS state. The bands at 475 and 640 nm associated with the ^{3}CSS state state decay with a lifetime of 3.8 ns. The spectral shape remains the same from 350 to 6000 ps apart from the decay in the signal. This suggests that all relaxation processes have occurred as there is no change in vibrational structure and therefore the decay from the final populated state, presumed to be the charge separated state, all occurs from the same state to the ground state. The PTZ donor in Complex 2 has the addition of the electron donating MeO groups. The addition of these groups increases the strength of the donor and therefore increases the driving force for the reduction of the transiently oxidised bridge, subsequently forming the ^{3}CSS state. Therefore the appended MeO groups decrease the DAS lifetime for the formation of the ^{3}CSS by a factor of 8, due to the increased oxidation ability of the donor.

In Complex 2 in hexane, the featureless ESA at 640nm, is characteristic of the ^{3}IL excited state localised on the [NDI-CC] moiety. The spectral shape remains the same from 1 ps to 5 ns i.e the spectra is quasi-stationary, so there is no decay of the signal and therefore a constant of 146 ns is needed to fit the data. There is no population of a sequential state from the ^{3}IL state in hexane, unlike in DCM. This gives the idea that the excited state formed in DCM from the ^{3}IL state is likely to be the ^{3}CSS state, as it does not form in hexane. This could be due to the difference in solvent polarity. DCM is more polar than hexane. Therefore the ^{3}CSS state could be too high in energy to form in hexane, i.e the solvent cannot stabilise the highly charged ^{3}CSS state. The kinetic traces shows that there is no growth or decay of any excited states.

3.10.2 NDI-Pt-Ph-PTZ-(OMe)$_2$ (Complex 3)

In complex 3, in DCM, the broad ESA between 600 and 680 nm is assigned to the ^{3}IL state localised on the [NDI-CC] moiety. The signal redshifts from 430 nm to 475 nm, which is concomitant with the growth of the electronic band at 630 nm. This change in spectral shape indicates the formation of a new excited electronic state, this excited state is fully formed by 10 ps. The new bands at 475 and 630 nm are consistent with those previously reported in the spectroelectrochemistry of the NDI radical ion.[46,72] Therefore, it is likely that the new excited state has an electron density distribution on the NDI ligand consistent with that of the NDI radical anion. This suggests that the new excited state formed is a ^{3}CSS state, whereby the NDI is formally reduced and is presumed to be the ^{3}CSS state. Two DAS lifetimes of 6.4 and 126 ps were needed in order to describe this change in spectral shape (Figure 3.12. The need for two DAS lifetimes could be to account for the change in spectral shape and the other for the decay of the signal. This state is formed 340 ps earlier than in Complex 2. The removal of the CH_2 spacer group could be responsible for the quicker formation of the ^{3}CSS as the PTZ donor is more conjugated than in Complex 2. Between 200 and 5000 ps there is no change in spectral shape, indicating the decay from the ^{3}CSS state occurs directly to the ground state. Two lifetimes of 94 and 695 ns were needed in order to model the decay of the ^{3}CSS state. A constant was need need in order to fit the data set. The removal of the CH_2 spacer and addition of the MeO groups creates an electron rich highly conjugated PTZ donor which results in the formation of the ^{3}CSS state being decreased by a factor of 16, and decreases the lifetime of the decay by a factor of 5.

3.10.3 NDI-Pt-Ph-PTZ (Complex 4)

In complex 4, in DCM, the featureless ESA between 580 and 700 nm is assigned to the ^{3}IL state. The signal redshifts from 430 to 480 nm, which is concomitant with the growth of a broad ESA band at 630 nm. This change in spectral shape indicates the formation of a new excited electronic state, this excited state is fully formed by 10 ps. The new bands at 480 and 630 nm are consistent with those previously reported in the spectroelectrochemistry of the NDI radical ion. Therefore, it is likely that the new excited state has an electron density distribution on the NDI ligand consistent with that of the NDI radical anion.[46,72] This suggests that the new excited state formed is a ^{3}CSS state, whereby the NDI is formally reduced and is presumed to be the ^{3}CSS state. One lifetime of 51 ps is assigned to the formation the ^{3}CSS state, which shows good agreement to the lifetime for the formation of the ^{3}CSS state in TRIR. The rates of decay of the initial excited state signal and the growth of new excited state signal are the same, which suggests that their is a direct population from the original state to the new excited state. Two lifetimes of 207 and 1491 ps were needed in order to describe the decay of the ^{3}CSS state. The ^{3}CSS state in Complex 4 has both the shortest lifetime for its formation and decay of all the complexes. The removal of the CH_2 spacer group is thought to be responsible for the acceleration of both the formation of the charge separated state and the charge recombination. The removal of this group means that the PTZ donor is more conjugated than in Complex 1 and so can reduce the oxidised bridge more easily after excitation. The removal of the CH_2 spacer decreases the formation lifetime of the ^{3}CSS state by factor of 18 and decrease the decay lifetime by a factor of 8.

In complex 4, in hexane the featureless ESA between 560 and 780 nm is assigned to the ^{3}IL excited state localised on the [NDI-CC] moiety. There is no change in spectral shape from 1 ps to 5 ns and so the spectra is quasi-stationary for the timescale of this experiment. This indicates that any other excited states such as the ^{3}CSS state are too high in energy to be populated in hexane. As hexane is not as polar as DCM, and so cannot stabilise a highly charged state such as a charge separated state.

3.11 TRIR

3.11.1 NDI-Pt-Ph-Ch$_2$-PTZ-(OMe)$_2$ (Complex 2)

In Complex 2 in Figure 3.14 in the high frequency region there is a shift from the frequency at 1975 cm^{-1} to 1924 cm^{-1}, which is hypothesised as a change from an ^{3}IL state to an ^{3}IL(CT) state. In Complex 2 there is a blueshift of the transient ν(CO) signals from 1613 and 1645, to 1588 and 1630 cm^{-1}. The shift in the transient ν(CO) signals indicates a significant change in the electronic environment around the NDI-localised vibrations, suggesting a change in the electronic state. These new ν(CO) bands are consistent with those previously reported in the FTIR spectrum of the one-electron reduced NDI-Pt-Cl complex.[72] Therefore, it is likely that the new excited state has an electron density distribution on the NDI ligand consistent with that of the NDI radical anion. This suggests that the new excited state formed is a ^{3}CSS state, whereby the NDI is formerly reduced. Two lifetimes of 32 and 107 ps are required to fit the grow-in of signals associated with the ^{3}CSS state in the low frequency region. This is corroborated by the TA experimental data, from which two lifetimes of 44 and 142 ps were obtained for the grow-in of ^{3}CSS state signals. One lifetime of 7 ns was extracted to fit the decay of the ν(CO) transients at 1588 and 1630 cm^{-1}; longer than the ^{3}CSS decay lifetime extracted from the TA data. The large shift in signal frequency of the transient ν(C≡C) band, from 1924 cm^{-1} to 2090 cm^{-1}, over a comparable timescale to the formation of the ν(CO) transients at 1588 and 1630 cm^{-1}, implies a large change in electron density on the Pt-acetylide bridge moiety. This could be indicative of electron transfer from the PTZ donor to the electron deficient bridge and therefore, formation of the ^{3}CSS state, where the NDI is reduced and PTZ oxidised. The formation of the ν(C≡C) transient at 2097 cm^{-1} is concomitant with the growth of the transient ν(CO), further confirming that the new electronic excited state is the ^{3}CSS state, which is fully formed after 300 ps. Two lifetimes of 27 and 148 ps were needed to fit the formation of the ^{3}CSS in the high frequency region, consistent with that of both the low frequency and TA experimental data. One lifetime of 4.5 ns was obtained to fit the decay of the ^{3}CSS state. This is quicker than the lifetime extracted from the low frequency data, but more consistent with the TA data, which extracted a lifetime of 3.8 ns. Appending the MeO groups to PTZ donor reduced the lifetime for the formation of the ^{3}CSS by a factor of 8 (TA) and 5 (TRIR), there is a significant reduction of the lifetime which is owed to the increased oxidation ability of the donor. The decay lifetime for the ^{3}CSS state is decreased by a factor of 1.6 (TA) and 1.3 (TRIR), therefore the modification of the donor has no significant effect on the decay lifetime of ^{3}CSS state. The DAS associated with all the lifetimes above are shown in Figure 3.14.

3.11.2 NDI-Pt-Ph-PTZ-(OMe)$_2$ (Complex 3)

In Complex 3 in Figure 3.14 the high frequency region the peak at 1975 cm^{-1} is assigned to an ^{3}IL state, which then shifts to an ^{3}IL(CT) state with the growth of the peak at 2010 cm^{-1}. In the FTIR of Complex 3 there is an additional band present at 1920 cm^{-1}, this could be responsible for the bleaching signal overlapped with ESA, which may give the appearance of another band at 1924 cm^{-1} in the TRIR spectrum.The transient ν(CO) bands at 1589 and 1630 cm^{-1} are consistent with those previously reported in the FTIR spectrum of the one-electron reduced NDI-Pt-Cl complex. Therefore, it is likely that the new excited state has an electron density distribution on the NDI ligand consistent with that of the NDI radical anion. This suggests that the new excited state formed is a ^{3}CSS state, whereby the NDI is formerly reduced. One lifetime of 4 ps is required in order to fit the formation the ^{3}CSS state. The transient ν(CO) bands at 1589 and 1630 cm^{-1} which are present in the ^{3}CSS are populated within a much faster timescale, within instrument response, compared to Complexes 1, 2 and 4. One lifetime of 856 ps is required to fit the decay of the ^{3}CSS state, which is consistent with the corresponding lifetime extracted from the experimental TA data. Appearance of ν(C≡C) transient at 1962 cm^{-1} and 2015 and 2090 cm^{-1}, over a comparable timescale to the formation of the ν(CO) transients at 1589 and 1630 cm^{-1}, implies a large change in electron density on the Pt-acetylide bridge moiety. This could be indicative of electron transfer from the PTZ donor to the electron deficient bridge and therefore, formation of the ^{3}CSS state, where the NDI is reduced and PTZ oxidised. The formation of the ν(C≡C) transient at 2089 cm^{-1} is concomitant with the growth of the transient ν(CO), further confirming that the new electronic excited state is the ^{3}CSS state, which is fully formed after 3 ps. One lifetime of 5 ps was extracted in order to fit the formation of the ^{3}CSS state, which is the same as that found for the low frequency region. One DAS lifetime of 513 ps was required to fit the decay of the ^{3}CSS state, which is considerably shorter than that of the lifetimes extracted in experimental TA data and the low frequency region. The removal of the CH_2 spacer group and the addition of the MeO groups decreases the lifetime of the formation of the ^{3}CSS state by a factor of 18 and decreases the lifetime of the decay of the ^{3}CSS by a factor of 4. The removal of CH_2 spacer group accelerates both formation of the ^{3}CSS and the subsequent charge recombination. This is due to the increased conjugation between the PTZ donor and the bridge compared to that in Complex 1. As a result the donor can reduce the oxidised bridge more easily following charge transfer.

3.11.3 NDI-Pt-Ph-PTZ (Complex 4)

In Complex 4 there is a blueshift of the transient ν(CO) signals from 1612 and 1649, bands consistent with previously reported NDI-localised excited state carbonyl vibrations i.e an ^{3}IL state, to 1529 and 1630 cm^{-1}. The shift in the transient ν(CO) signals indicates a significant change in the electronic environment around the NDI-localised vibrations, suggesting a change in the electronic state. These new ν(CO) bands are consistent with those previously reported in the FTIR spectrum of the one-electron reduced NDI-Pt-Cl complex. Therefore, it is likely that the new excited state has an electron density distribution on the NDI ligand consistent with that of the NDI radical anion. This suggests that the new excited state formed is a ^{3}CSS state, whereby the NDI is formerly reduced. One lifetime of 50 ps was extracted in order to fit the formation of the ^{3}CSS state. One lifetime of 1 ns was obtained in order to fit the decay of the ν(CO) transients at 1588 and 1630 cm^{-1}. The recovery of the bleaching ν(CO) signals at 1460, 1590 and 1630 cm^{-1} occurs with the same time constant as the decay of the ^{3}CSS bands. This suggests that the ^{3}CSS is undergoing charge recombination to reform the ground state. In the high frequency region, the transient acetylide band at 1964 cm^{-1} is assigned to the initial NDI-localised excited state. This band shares the same temporal dynamics as the transient carbonyl bands at 1612 and 1649 cm^{-1}.The rate of decay of band at 1964 cm^{-1} is commensurate with the rate of decay of the broad absorption, suggesting that these excited state signals originate from the same excited state. Decay of these excited states signals occurs concomitantly with the formation of a new band at 2095 cm^{-1}, which corresponds to a transient ν(CC) signal. There is a large shift in frequency of the acetylide transient, suggesting that there is a large change of electron density on the Pt-acetylide bridge. This indicates the formation of a new electronic state is being formed. This new state is assigned to a charge separated state, where the NDI ligand has been reduced and the PTZ ligand has been oxidised. One lifetime of 56 ps was extracted in order to fit the formation of the ^{3}CSS state. This is very similar to the lifetime of 51 ps extracted in experimental TA data and 50 ps extracted for the low frequency region. One lifetime of 0.96 ns was obtained in order to fit the decay of the ^{3}CSS state. This lifetime is very similar to that acquired for the low frequency region. However, in the experimental TA data two lifetimes of 200 and 1500 ps were necessary in order to fit the decay of the ^{3}CSS state, but averaging these lifetimes give a lifetime of 850 ps, which is consistent with the TRIR lifetimes extracted. The removal of the CH_2 spacer decreases the formation lifetime of the ^{3}CSS state by a factor of 16 and decreases the lifetime of decay of the ^{3}CSS state by factor of 6. The removal of the CH_2 spacer group has a significant effect on both the formation and decay of the ^{3}CSS state due to combination of the increased conjugation of the PTZ donor. An energy level diagram of the excited state processes following excitation at around 500 nm in DCM for Complexes 2-4 can be seen in Figure 3.15. The first oxidation (-1.2 V) and reduction (0.1 V) potentials of Complexes 2 and 3 have been used to estimate the energy of the ^{3}CSS state. Said energy is 1.3 V, which is 26 mV lower than that of the energy of the ^{3}CSS state in Complex 1. When comparing these DBA complexes to similar complexes (NDI-Pt-Ph-CH_2-PTZ, NDI-Pt-Cl, NDI-Pt-Ph and NAP-Pt-Ph-CH_2-PTZ) found in the literature[73] it is clear that the ^{3}CSS states are not as long lived and the rate of formation has significantly been increased. Therefore, there still remains a gap in the research to make DBA complexes with long lived ^{3}CSS states whose meaning their yield could potentially be increased via IR perturbation. A summary of the lifetimes for both the formation and decay of the ^{3}CSS state of all complexes can be seen in Table 3.3 along with the energy level diagrams in Figure 3.15.

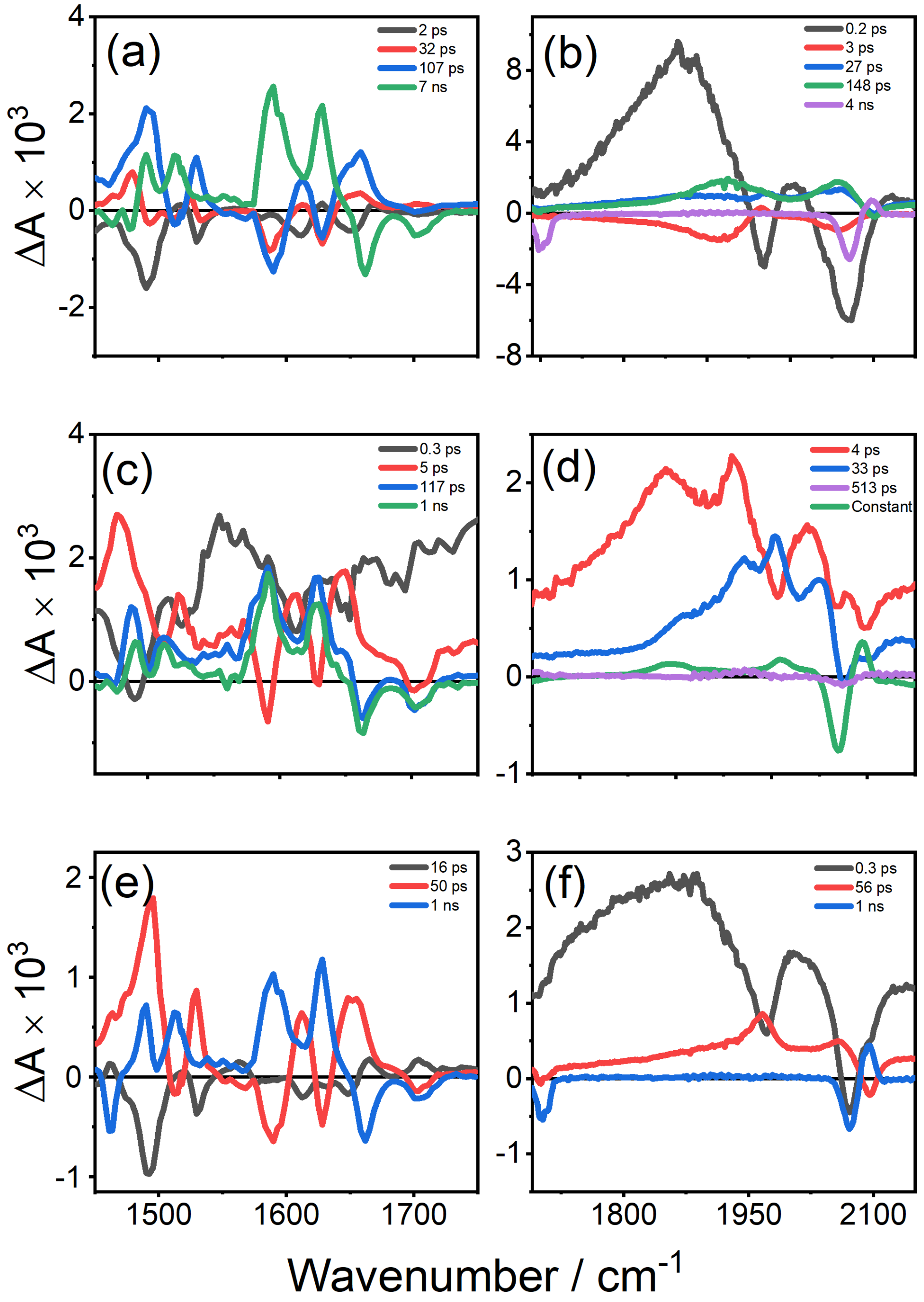

Figure 3.14: Decay associated spectra for Complexes 2, 3 and 4 in DCM for the low and high frequency regions. The lifetimes are given as in insets in the graphs.

Complex	Formation lifetime of ^{3}CSS / ps		Decay lifetime of ^{3}CSS / ps	
	TA	TRIR	TA	TRIR
1	929	793	6200	5805
2	44, 142	27, 148	3800	4480
3	6	5	695	1000
4	51	50	201, 1491	957

Table 3.3: Table showing the lifetimes required to fit the formation and decay of the ^{3}CSS state extracted from TA and TRIR (either low or high frequency).

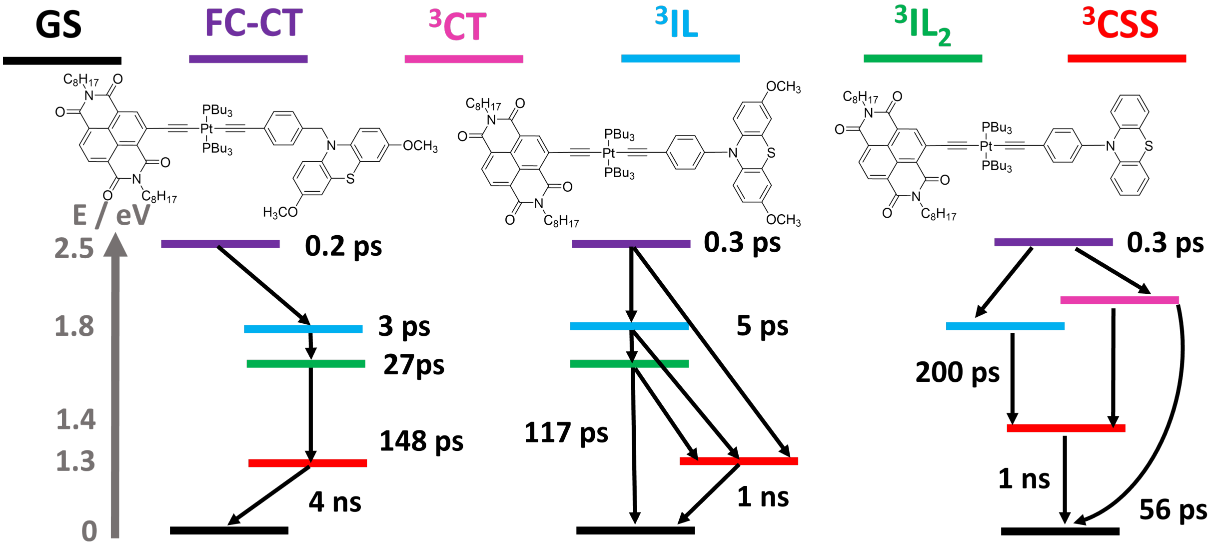

Figure 3.15: An energy level diagram showing the excited state processes following excitation at around 500 nm, in DCM, for Complexes 2 , 3 and 4 (left to right). The energies of the states have been estimated using emission and cyclic voltammetry experimental data.

3.12 DFT Calculations

Electron density difference diagrams have been calculated by Heather Carson in the Meijer group at The University of Sheffield. They predict both the nature and the energy difference between the singlet ground state, S_0, and the lowest calculated triplet states using DFT. In Complex 2, the DFT calculations estimated that the lowest energy triplet state, T_1, is a ^{3}CSS, with an energy of 1.502 eV. This is roughly 0.2 eV lower than the predicted energy for T_1 in Complex 1, suggesting that addition of the methoxy groups on the donor stabilise the ^{3}CSS. T_2, the second lowest triplet state is predicted to be a ^{3}MLCT state with an energy of 1.640 eV, which is also 0.2 eV lower than T_2 in Complex 1. There are also two higher triplet states, T3 and T4, which are also ^{3}MLCT states. From spectroscopic experiments I characterised T2 and T3 as ^{3}NDI states in DCM, due to the ^{3}NDI band being present in both DCM and hexane at the same spectral position, indicating that it is non solvatochromic and therefore does not exhibit strong CT character.

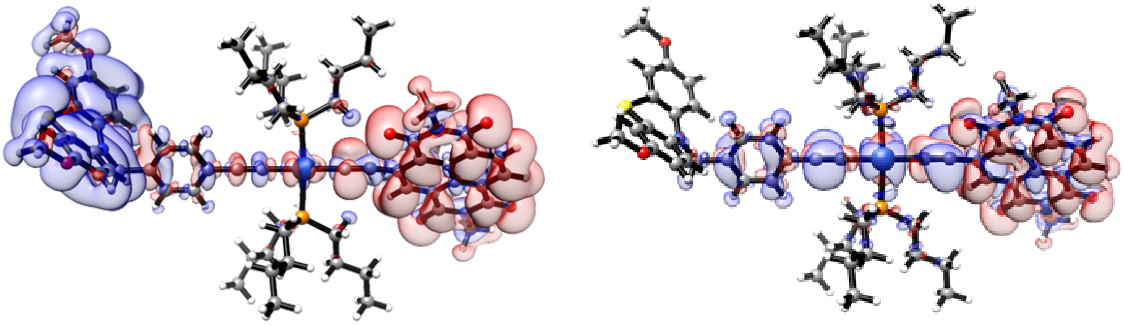

(a) T_1 (b) T_2

Figure 3.16: T_1 and T_2 electron density difference diagrams for Complex 2. Blue indicates loss of electron density, whereas red indicates gain in electron density.

In Complex 3, the DFT calculations predict that, T_1, the lowest energy triplet state is a ^{3}CSS with an energy of 1.530 eV and that T_2, the second lowest triplet state is a ^{3}MLCT state with an energy of 1.692 eV. There are also two higher triplet states, T3 and T4, which are also ^{3}MLCT states. There are also two higher triplet states, T3 and T4, which are also ^{3}MLCT states. From spectroscopic experiments I characterised T2 and T3 as ^{3}NDI states in DCM, due to the ^{3}NDI band not exhibiting strong CT character like in Complex 2. The energies of T_1 and T_2 are similar to that seen in Complex 2, reaffirming that the addition of the methoxy groups stabilises the energies of the triplet excited states.

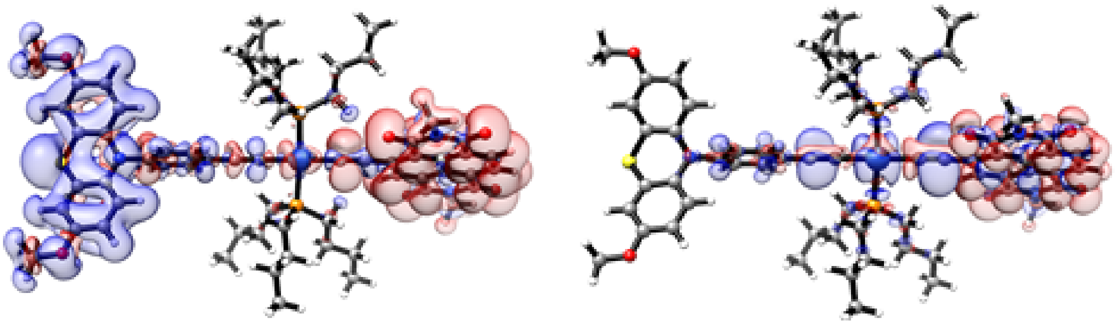

(a) T_1 (b) T_2

Figure 3.17: T_1 and T_2 electron density difference diagrams for Complex 3. Blue indicates loss of electron density, whereas red indicates gain in electron density.

In Complex 4, the DFT calculations predict that, T_1 is a ^{3}LA-MLCT state with an energy of 1.711 eV and that T_2 is a ^{3}CSS with an energy of 1.842 eV. From the DFT calculations it appears that the ^{3}CSS is not the lowest in energy, unlike in Complexes 1-3. However, from the spectroscopic experiments conducted in DCM, the ^{3}CSS is in fact the lowest energy state. However, as the formation of the excited states is heavily dependent on geometry of nuclei and the DFT calculations predict that the two lowest energy triplet states, the ^{3}CSS and the ^{3}NDI, are very close in energy, only differing by 0.13 eV, the order of these could be heavily dependent on the solvent used. This was in fact seen when Complex 4 was studied in hexane and the ^{3}NDI state was the lowest triplet state in energy. As DCM is a more polar solvent than hexane, the ^{3}CSS is therefore stabilised in DCM and is the lowest in energy.

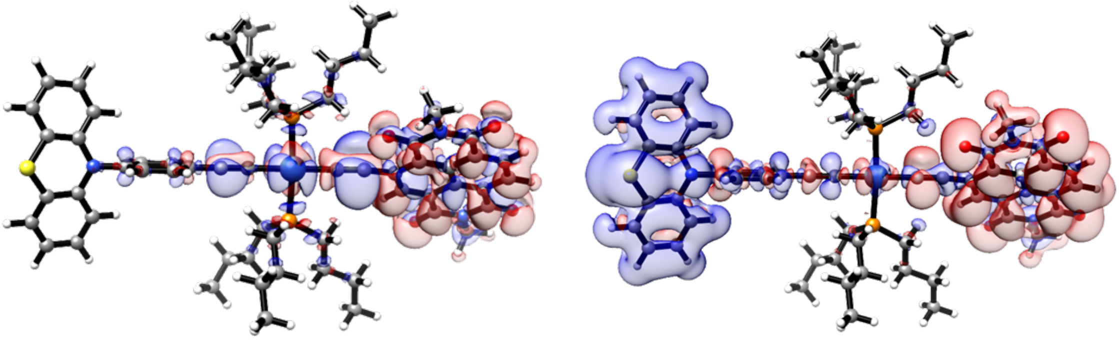

(a) T_1 (b) T_2

Figure 3.18: T_1 and T_2 electron density difference diagrams for Complex 4. Blue indicates loss of electron density, whereas red indicates gain in electron density.

There is also good agreement between time resolved experimental and the calculated

TRIR spectrum for Complexes 2-4. The calculated TRIR spectrum was estimated by taking the difference between the vibrational singlet ground state spectrum (S_0) and a vibrational excited triplet state spectrum (T_n). This confirms that the lowest lying state is a triplet state.

3.13 Conclusions

A series of novel Pt(II) donor-bridge-acceptor trans-acetylide complexes have been studied using TA and TRIR. They have been chemically modified to change the PTZ donor. All complexes after excitation at around 500 nm display excited state dynamics. The Frank-Condon CT state is populated on a sub 500 fs timescale and is therefore difficult to identify due to coherent artefact signals being present at this time. All complexes studied in DCM directly populate the NDI-localised state from the FC-CT state following electron-transfer from the bridge and then is sequentially reductively quenched by the donor to populate the ^{3}CSS before undergoing charge recombination to return to the ground state. In the TA experiments conducted in hexane, the spectra are quasi stationary within the experimental time window and the ^{3}CSS state is not populated. Appending the MeO groups to the PTZ donor reduced the rate of the formation of the ^{3}CSS by a factor of 8 (TA) and 5 (TRIR), there is a significant reduction of the lifetime which is due to the increased oxidation ability of the donor. The decay lifetime for the the ^{3}CSS state is decreased by a factor of 1.6 (TA) and 1.3 (TRIR), therefore the modification of the donor has no significant effect on the lifetime of ^{3}CSS state. The removal of the CH_2 spacer and addition of the MeO groups decreases lifetime of the formation of the ^{3}CSS state by factor of 16 (TA) and 18 (TRIR) and decreases the lifetime of the decay of the ^{3}CSS by a factor of 5 (TA) and 4 (TRIR). This is due to the increased conjugation between the PTZ donor and the bridge compared to that in Complex 1 and so therefore can reduce the oxidised bridge more easily following charge transfer. Here there is a acceleration on both the formation state due to combination of the increased driving force and conjugation of the PTZ donor and accelerated decay of the ^{3}CSS due to the more conjugated donor. The removal of the CH_2 spacer decreases the formation lifetime of the ^{3}CSS state by a factor of 18 (TA) and 16 (TRIR) and decreases the lifetime of decay of the ^{3}CSS state by factor of 8 (TA) and 6 (TRIR). The removal of the CH_2 spacer group has significant effect on both formation and of ^{3}CSS and the subsequent charge recombination. The removal of the spacer has the same factor of acceleration, a factor of 17 (averaged from TA and TRIR) in both Complexes 3 and 4. Complex 4 does however have greater acceleration of the ^{3}CSS when compared to its methoxy analogue. It is apparent that the removal of the spacer has a greater impact on increasing driving force leading to an increase in rate of charge separation and recombination.

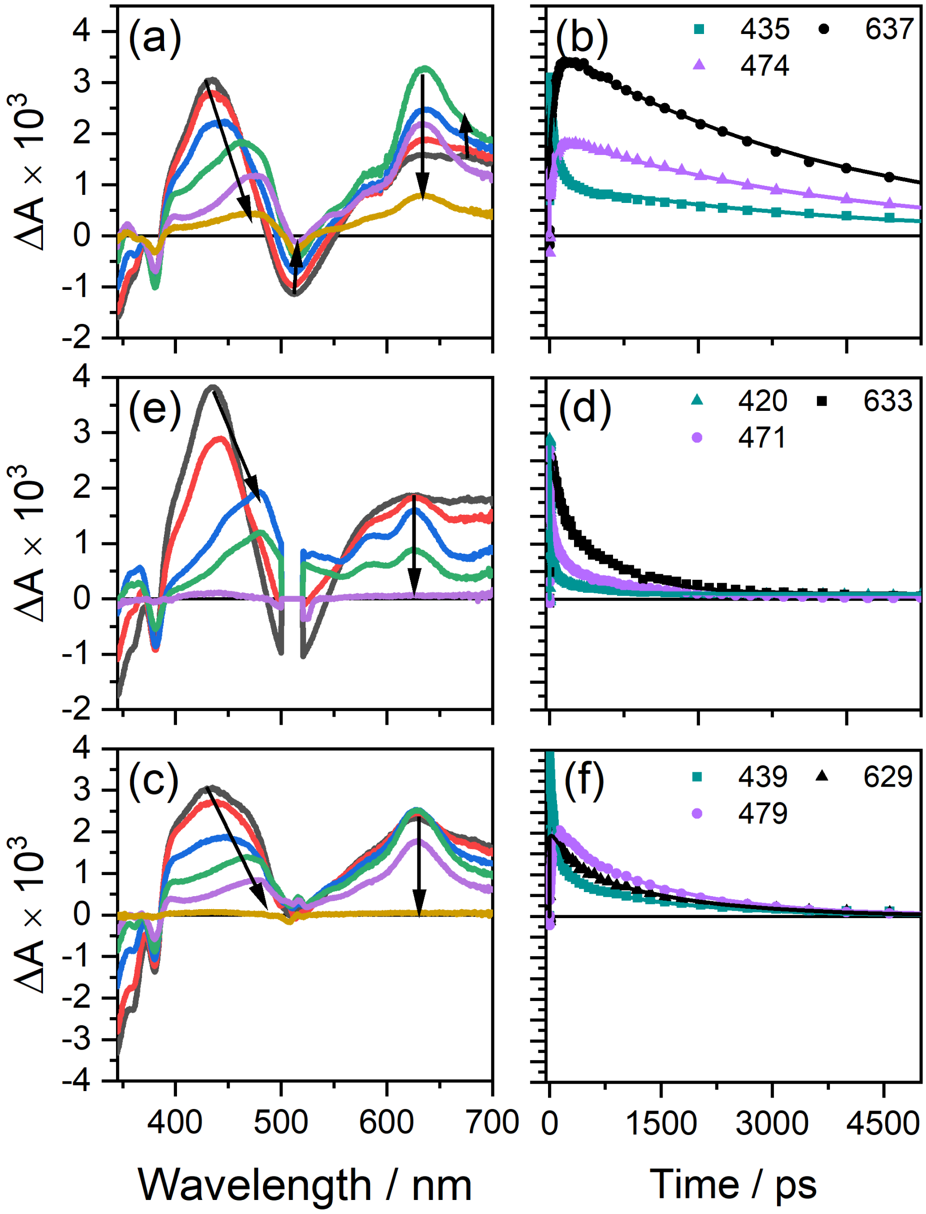

Figure 3.6: TA spectra for Complexes 2,3 and 4 following excitation at 500 nm of the ML-LCT transition in DCM are shown in Graphs a, e and c. The given time delays for a, e and c are 0.5 , 7, 35, 136, 2000 and 6000 ps, 0.5, 22, 178, 690 and 6000 ps, and , 0.5, 2, 8, 31, 146 and 5000 ps respectively. Single point kinetics at chosen wavelengths are shown in Graphs, b, d and f for the corresponding TA spectra. The wavelengths are given as insets. The fittings are overlaid which have been extracted from global lifetime analysis.)

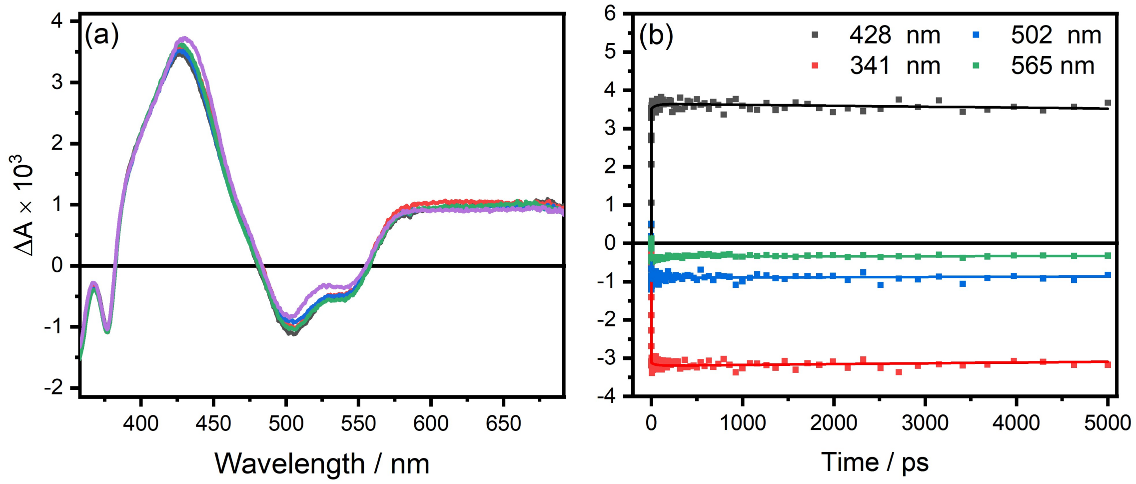

Figure 3.7: Transient absorption spectra of Complex 2 following excitation at 500 nm, in Hexane. Single point kinetics traces are shown at select wavelengths, which are given as insets. The solid line kinetic traces are obtained from global analysis fitting of the data.)

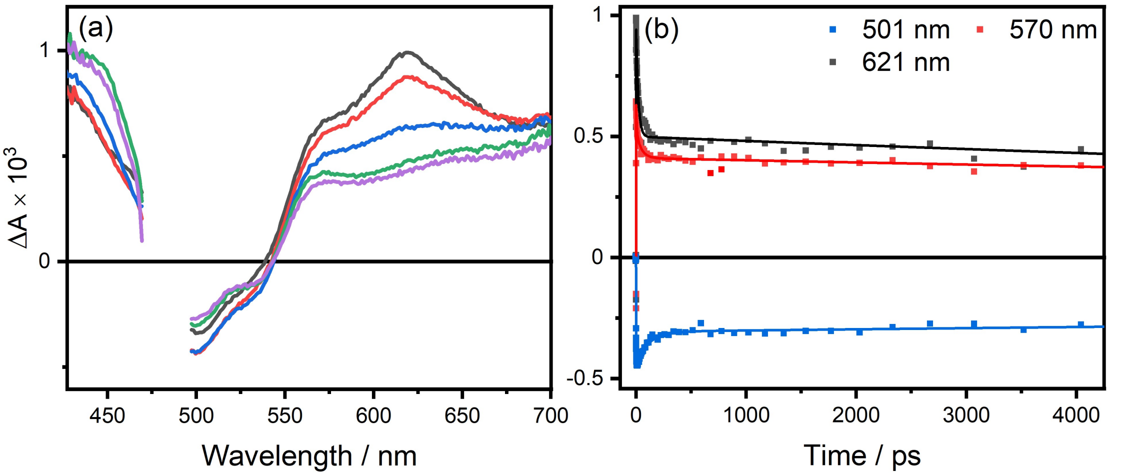

Figure 3.8: The transient absorption spectrum for Complex 3 following excitation of the ML-LCT transition at 500 nm in Hexane is shown in Graph a. The given time delays for a are 0.44 ps (black) , 3.66 ps (red), 31.9 ps (blue), 776 ps (green) and 6990 ps (purple). Single point kinetics at chosen wavelengths are shown in Graph b for the corresponding TA spectrum. The wavelengths are given as insets. The fittings are overlaid which have been extracted from single point kinetic analysis.)

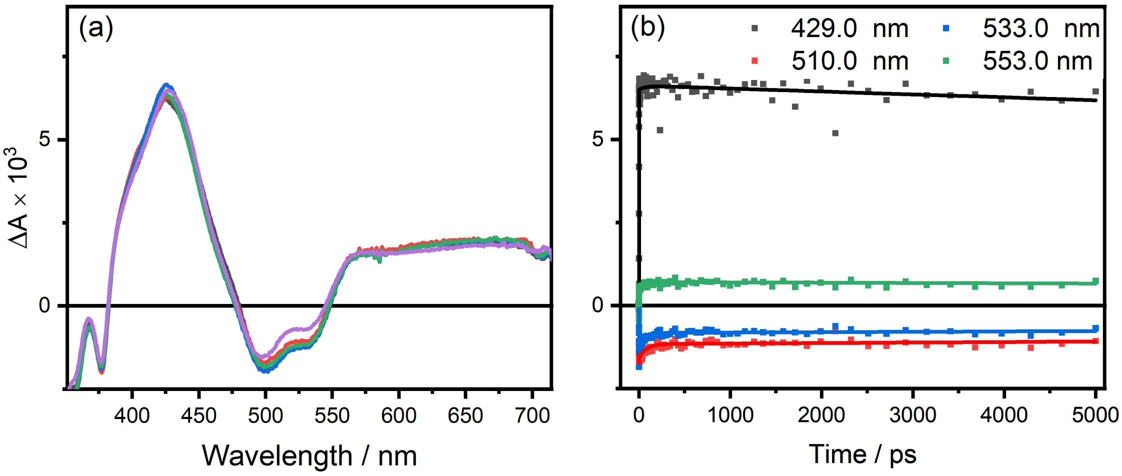

Figure 3.9: Transient absorption spectra of Complex 4 following excitation at 500 nm, in Hexane. Single point kinetics traces are shown at select wavelengths, which are given as insets. The solid line kinetic traces are obtained from global analysis fitting of the data.

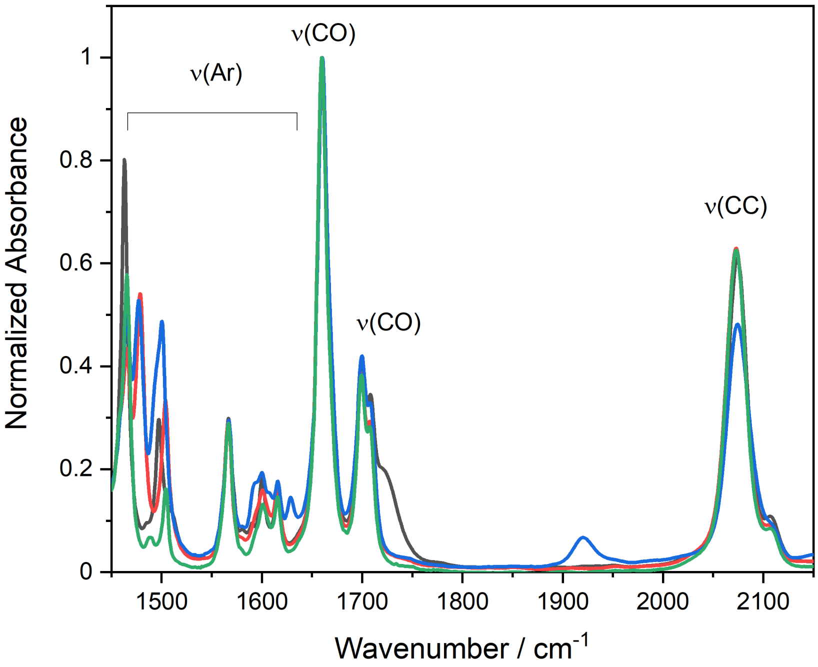

Figure 3.10: FTIR spectra for Complexes 1 (Black), 2 (Red), 3 (Blue) and 4 (Green) recorded in DCM.

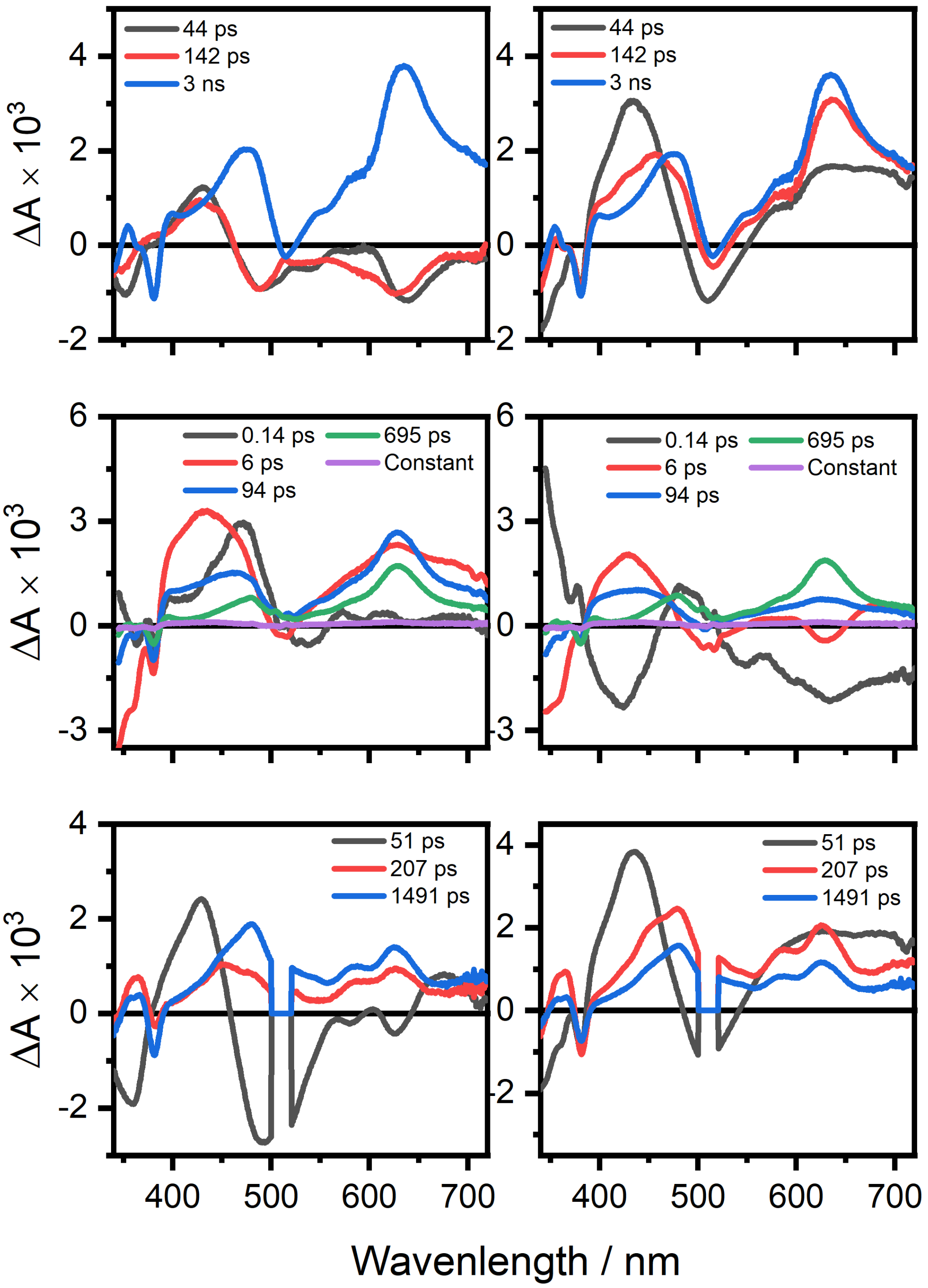

Figure 3.12: Decay associated spectra (left) and evolution-associated spectra (right) for Complexes 2, 3 and 4 in DCM. The lifetimes are given as in insets in the graphs.

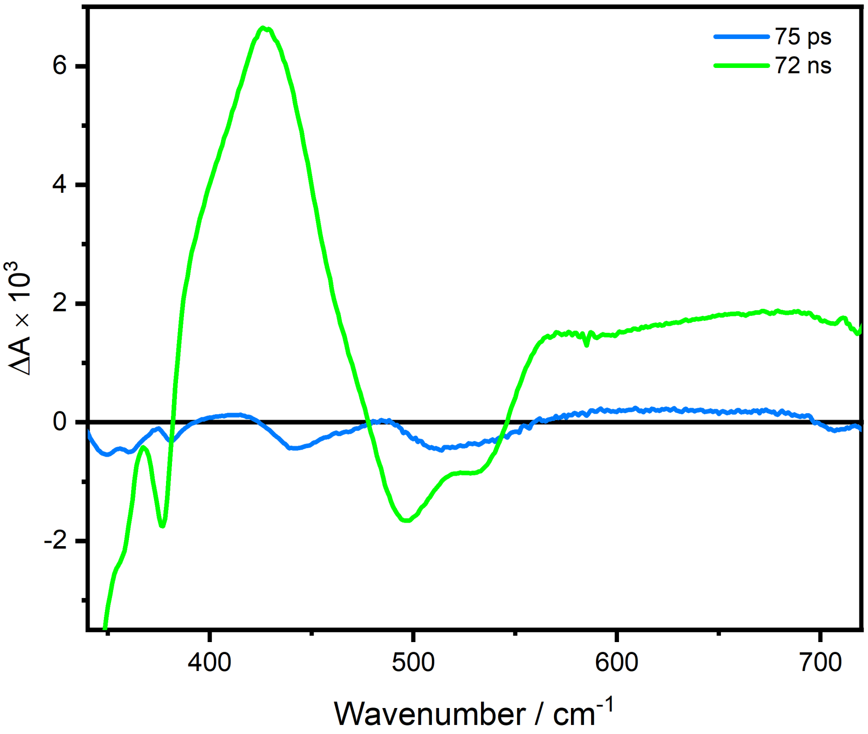

Figure 3.13: Decay associated spectra for Complex 4 in hexane.

Chapter 4

Photophysics and ground state dynamics of two modified Pt(II) donor-bridge-acceptor trans-acetylide complexes bearing a 1,8-Naphthalimide acceptor, whereby the attachment of the donor is modified

4.1 Introduction

In this chapter the ultrafast dynamics of two novel complexes are discussed. This work is inspired by and directly builds upon previous work undertaken in the Weinstein group. Previously, the excited state dynamics of a Pt(II) donor-bridge-acceptor trans-acetylide complex, bearing a 1,8-Naphthalimide (NAP) acceptor and a phenothiazine (PTZ) donor (NAP-Pt-Ph-CH_2-PTZ, Complex 2.3), was extensively studied. A range of techniques were utilised including transient absorption and time-resolved infrared spectroscopy. Following UV-Vis excitation, a Franck-Condon state in Complex 2.3 is populated. This state then decays on a sub 500 fs timescale, to form a CT State. This branches via three pathways: electron transfer to form a ^{3}CSS, and charge recombination to form either a ^{3}NAP state or the ground state. The energy level diagram for the excited state processes following excitation at 400 nm can be seen in Figure 3.1. The ultimate aim of this research is to design a donor-bridge-acceptor system whereby a long lived ^{3}CSS is formed with high yield in addition to a yield that can be modulated via IR excitation of vibrational modes. Modulation of the excited states was achieved in Complex 2.3 by IR excitation of a bridge localised vibrational mode in the branching CT state. Such modulation was shown to be 100% effective in that the yield of the ^{3}CSS was 100% suppressed, with a corresponding increase in yield of the ^{3}NAP state. This was not the desired effect as the aim of the investigation was to increase the yield of the ^{3}CSS, not the ^{3}NAP state. Complex 2.3 was found not to be an ideal case as the ^{3}NAP state is lower in energy than the ^{3}CSS. Therefore the formation of the ^{3}CSS is competing with the formation of the ^{3}NAP state as it is energetically favourable for a molecule to decay into a lower lying state. The spectroscopic investigations of this complex have inspired the synthesis of two novel complexes, NAP-Pt-3-PTZ and NAP-Pt-3-PTZ-PTZ-$(OMe)_2$ (Complexes 2.1-2.3, Figure 4.2), with the aim of gaining a greater understanding of how molecular structure can influence the excited state dynamics of a complex. The molecules have been synthetically designed with the intention of stabilising the ^{3}CSS, and therefore increasing the likelihood that the ^{3}CSS is the lowest energy excited state. To achieve this excited state ordering, the following molecular structure was proposed; both the donor and acceptor are strongly conjugated to the Pt(II) bridge centre. In Complex 2.3, only the acceptor is strongly conjugated to the bridge, whereas the donor is weakly conjugated through a phenyl ring and CH_2 spacer moiety. Both novel complexes have a 1,8-Naphthalimide (NAP) acceptor, which is strongly conjugated to the Pt(II) bridge moiety and at least one strongly conjugated PTZ donor. In NAP-Pt-3-PTZ, (Complex 2.1 (Figure 4.2)) the PTZ donor is attached directly to the bridge, this is to increase conjugation between the donor and the bridge. In NAP-Pt-3-PTZ-PTZ-OMe_2 (Complex 2.2), was designed in addition to Complex 2.1 as a way to potentially extend the lifetime of the^{3}CSS state. Complex

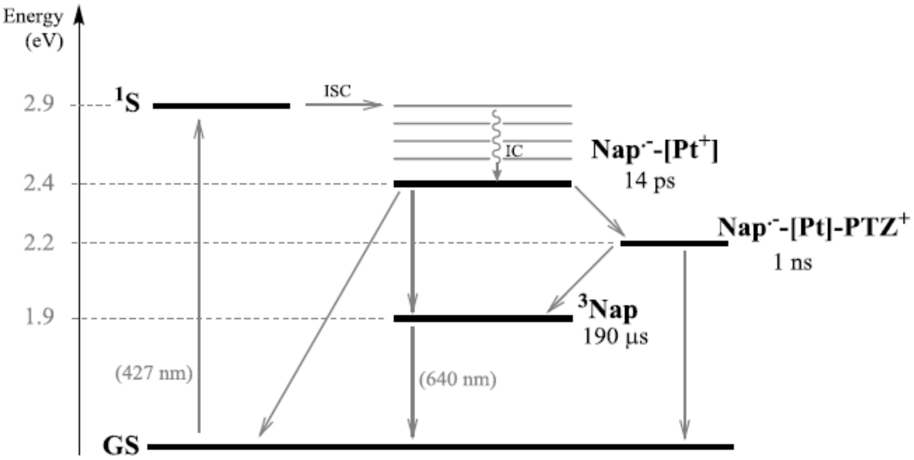

Figure 4.1: Energy diagram for the excited state processes of Complex 2.3, following excitation at 400 nm. Figure courtesy of Paul Scattergood.

2.2 (Figure 4.2) consists of two PTZ donors to form a molecular cascade system, the first donor is attached to the bridge directly, the second is attached to the first donor through its own nitrogen atom. Methoxy groups are appended to the second donor to ensure the oxidation potential is lower, than that of the first donor. Two ^{3}CSS states, CSS$_1$ and CSS$_2$, can be formed due to a difference in oxidation potential between the donors. CSS$_1$ is formed first after sacrificial donation to replenish the Pt centre, followed by the sacrificial donation of an electron from the second donor to the first donor to form CSS$_2$. To investigate the affect of increasing the conjugation between the donor and the Pt bridge the findings from Complexes 2.1 and 2.2 will be compared to the previously reported Complex 2.3 (Figure 4.2). In an ideal scenario, Complexes 2.1-2.2 would be compared to an additional molecule, whereby the acceptor is not strongly conjugated to the Pt bridge but the donor is. However, this brings about certain challenges. In previously studied molecules when the acceptor is not strongly coupled to the bridge, there is no MLCT transition to excite and therefore no electron hole on the platinum is created, and therefore no ^{3}CSS state would be formed. This complex was only studied using DFT calculations and so will be discussed in this section.

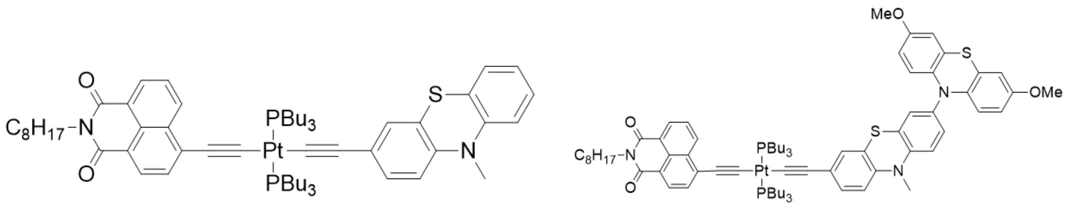

(a) Complex 2.1

(b) Complex 2.2

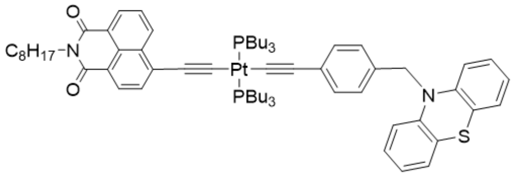

(c) Complex 2.3

Figure 4.2: Complexes 2.1-2.3

4.2 Results

4.3 UV-Vis

The UV-Vis absorption spectra of Complexes are shown in Figure 4.3. The spectra were recorded in CH_2Cl_2 (DCM), covering a spectral range between 230 and 510 nm. The intraligand (IL) π-$\pi*$ transitions centered on the NAP, Ph and PTZ units occur in the region between 230 and 370 nm for all complexes. The intraligand π-$\pi*$ transition centred on the PTZ occurs at 320 nm for Complexes 2.1 and 2.2. The transitions that occur at 248 nm and 300 nm are assigned to the Ph and acetylide (π-$\pi*$) ligand localized transitions. The π-$\pi*$ transitions centred on the NAP ligand occur in the region between 302 and 368 nm. A low energy metal to ligand charge transfer (MLCT) transition is responsible for the broad absorption band with a maxima at 432 nm for Complexes 2.1 and 2.2. This MLCT transition involves charge transfer from the Pt-acetylide bridge to the NAP acceptor ligand. Figure 4.4 shows that the absorption band centred at 432 nm exhibits solvatochromic behaviour, suggesting that the electronic transition responsible for this absorption band has CT character. DFT calculations confirm this assignment, as well as suggesting that this transition also has ligand-to-ligand character. Therefore, the absorption band centred at 432 nm is a assigned to a mixed metal-ligand to ligand charge transfer (ML-LCT) transition. The d-orbitals on the Pt mix with those of the acetylide, leading to the transition being of mixed character. The ML-LCT band is insensitive to the type of donor mutually trans to the acceptor, indicating that the ligand-to-ligand character of this transition arises from the NAP-CC moiety only. The ML-LCT band reported in Complex 2.3 is 430 nm. This is very similar to the ML-LCT transition in Complexes 2.1-2.2, indicating that the donor plays a very small role if any in this transition.

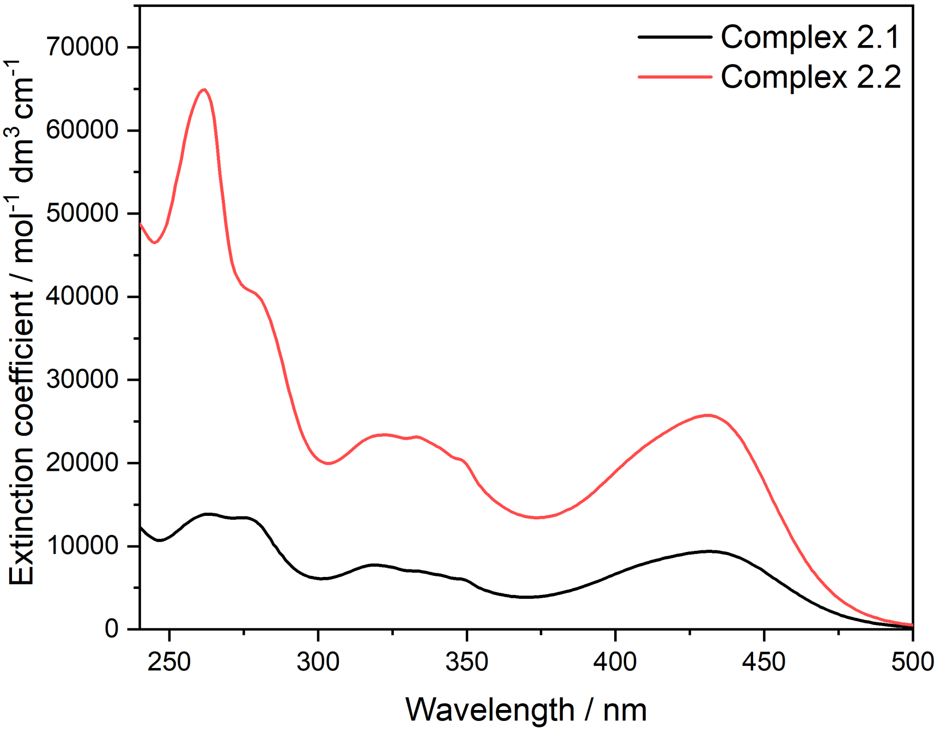

Figure 4.3: UV-Vis spectra of Complex 2.1 (black trace) and Complex 2.2 (red trace) recorded in DCM.

4.4 Emission spectroscopy

The steady state emission spectra in aerated DCM, following excitation at 432 nm, of Complexes 2.1 and 2.2, are shown in Figure 4.5. The emission bands for Complex 2.1 and 2.2 are centred at 502 and 493 nm, respectively. In hexane, the emission from Complexes 2.1 and 2.2 shifts to shorter wavelengths. Such solvatochromic behaviour suggests that the emitting excited state has charge transfer character and is therefore likely to be from

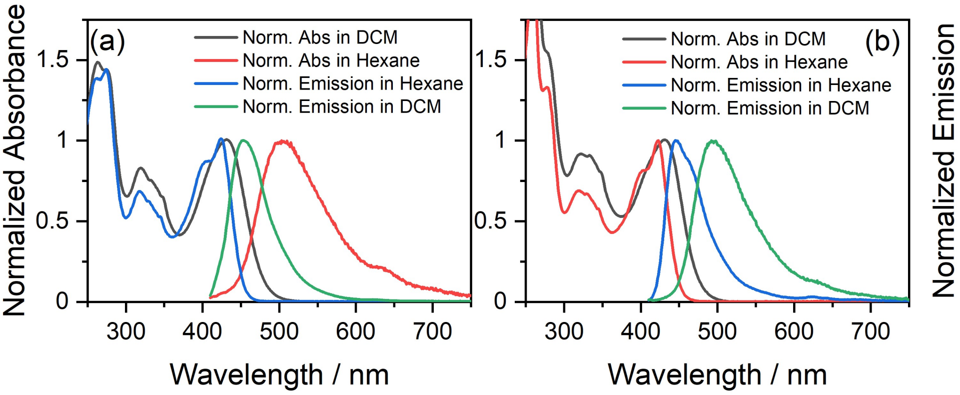

Figure 4.4: UV-Vis and emission spectra of Complex 2.1 (a) and Complex 2.2 (b) recorded in DCM and Hexane.

a MLCT state involving Pt and the NAP ligand. In addition to the emission from a CT state, lower energy emission at approximately 645 nm with a shoulder at 700 nm is also observed in both complexes. The shoulder is due to vibronic progression. It was found that these emission bands were sensitive to the presence of molecular oxygen, and when removed, the intensity of these bands increased. The position of these bands and their sensitivity to the presence of molecular oxygen suggest that they emanate from a triplet excited state located on the NAP fragment of the molecule. The higher energy band at around 500 nm is insensitive to molecular oxygen, indicating the CT state is a singlet excited state. These spectra can be seen in Figure 4.6. The emission spectra in Complexes 2.1-2.2 is similar to that of Complex 2.3. The absorption and emission maxima along with the quantum yields and molar absorption coefficients can be found in Table 4.1.

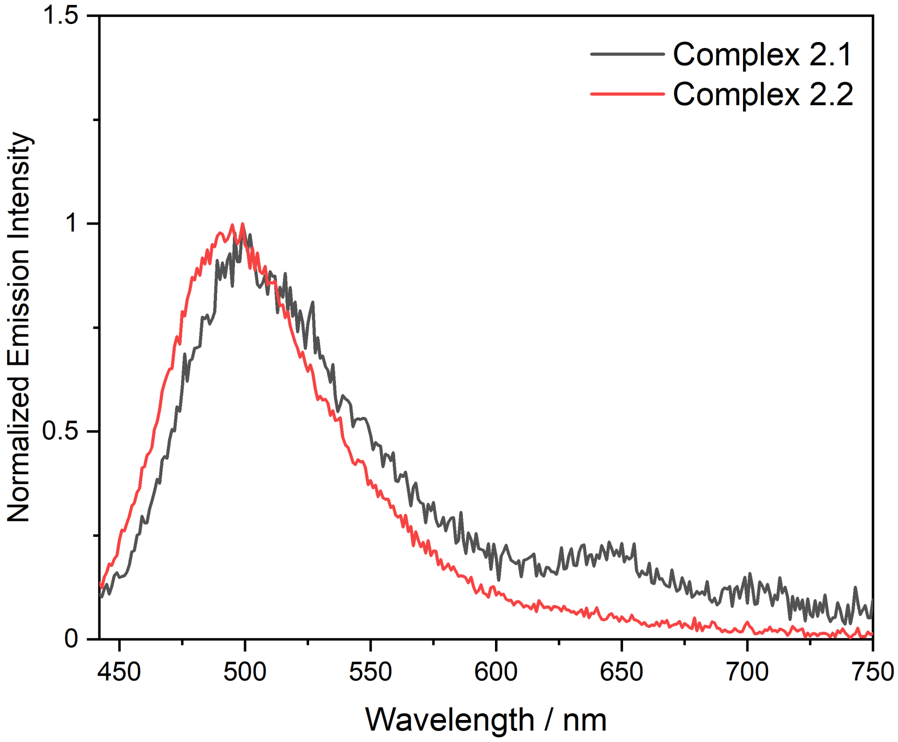

Figure 4.5: Emission spectra of aerated solutions of Complexes 2.1 and 2.2 in DCM.

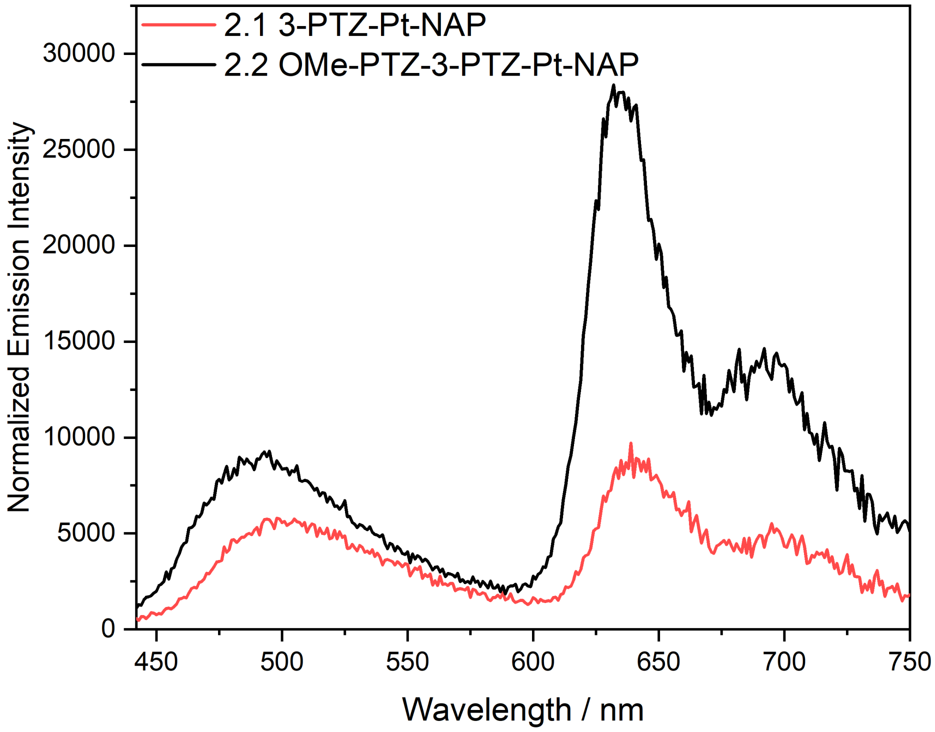

Figure 4.6: Emission spectra of degassed solutions of Complexes 2.1 and 2.2 in DCM

	λ_{abs}	λ_{em}	ϕ_{em}	ε / $mol^{-1}\ dm^{-3}\ cm^{-1}$
2.1	432	502	0.00057	9320
2.2	432	493	0.00031	38500

Table 4.1: Absorption (λ_{abs}) and emission maxima (λ_{em}), quantum yield (ϕ_{em}) and molar absorption coefficient (ε) for Complexes 2.1 and 2.2.

4.5 Transient Absorption

The TA spectra of Complex 2.1 and 2.2 have been recorded in DCM, Acetonitrile (MeCN) and Hexane upon excitation at 400 nm. The excited state dynamics were probed for the two complexes between 340 and 740 nm. All spectra are dominated by coherent artefact signal before approximately 300 fs and have therefore been trimmed accordingly. This does not apply to the the early time data which shows the growth of bands already present at 300 fs. The lifetimes were obtained from global analysis of the time resolved datasets. The pump-probe time delay increases for the different coloured traces are as follows: black, red, blue, green, purple, and yellow.

4.5.1 NAP-Pt-3-PTZ (Complex 2.1)

DCM

For Complex 2.1, in DCM, the early time data (-0.03 to 0.18 ps) shows the growth of two bands centred at 475 and 658 nm. At wavelengths less than 475 nm, bleaching of the ML-LCT absorption band is visible with a peak at 421 nm. A 5 nm blue shift of the ESA band centred at 475 nm occurs from 0.18 ps to 0.3 ps, in addition to the rise of a small absorption band at 566 nm from 0.3 ps to 9 ps. Following the spectral changes between 0.3 and 9 ps, the ESA features at 480 and 566 nm decay by 50 ps, revealing less structured ESA spanning a range from 458 to 690 nm. Due to the decay of overlapping ESA, the

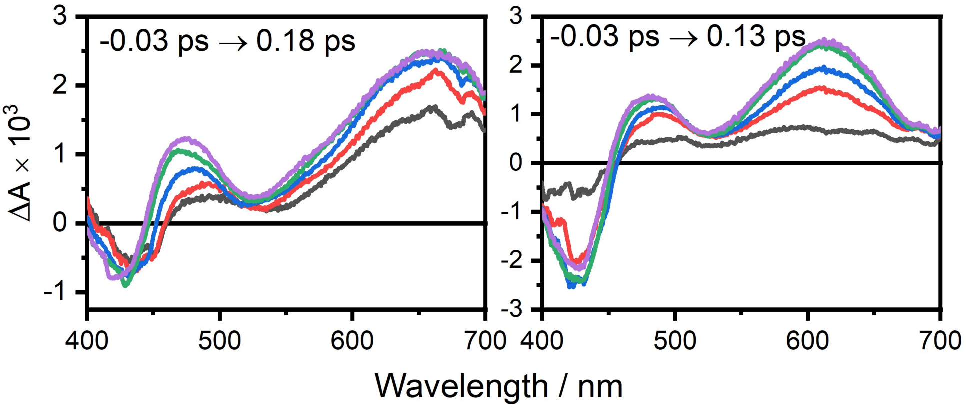

Figure 4.7: Early time transient absorption at 400 nm excitation in DCM of Complex 2.1 (left) and Complex 2.2 (right). Pump probe delay times for Complex 2.1 are -0.03 ps, 0.05 ps, 0.1 ps, 0.14 ps and 0.18 ps. Pump probe delay times for Complex 2.2 are -0.03 ps, 0.02 ps, 0.04 ps, 0.1 ps and 0.13 ps.

bleach signal deepens and shifts from 421 to 431 nm. The final excited state spectrum remains stationary over the remaining pump-probe time delays (100 ps - 6000 ps).

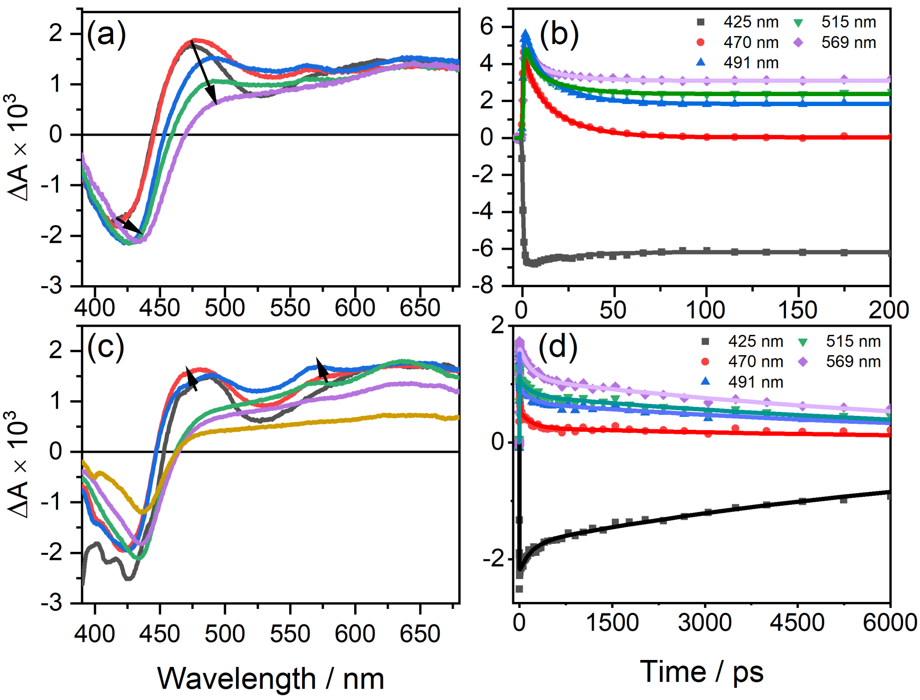

Figure 4.8: Transient absorption at 400 nm excitation in DCM of Complex 2.1 and 2.2. Pump probe delay times are 0.3 ps, 9 ps, 16 ps, 49 ps and 6000 ps for Complex 2.1, panel (a) and 0.15, 0.33, 0.75, 135, 790 and 6000 ps for Complex 2.2, panel (c). Single point kinetics at chosen wavelengths are shown in Graphs, (b) and (d) for the corresponding TA spectra. The wavelengths are given as insets. The fittings are overlaid which have been extracted from global lifetime analysis.)

Transient Absorption in Acetonitrile and Hexane

The transient absorption of Complex 2.1 is shown in Figure 4.9. Immediately following excitation of complex 2.1 (0.04 ps), in MeCN, ESA bands at 468 nm and 560 - 670 nm are observed. In addition to the ESA, bleaching of the ML-LCT absorption band is visible with a peak at 415 nm. Stimulated emission is also observed at 523 nm, producing a dip in the overlapped ESA spectrum. Between 0.04 ps and 0.8 ps there is growth of a shoulder at 448 nm, redshift of the peak centred at 468 nm redshifts to 480 nm, and a rise of an ESA peak at 560 nm. Between 1.6 ps and 10 ps there is a significant change in spectral shape of the ESA. The ESA bands at 480 nm and 560 nm decay over the following 200 ps, revealing less structured ESA spanning a range from 455 nm to 700 nm. Concomitant with this spectral change is partial recovery of the bleaching signal at 415 nm, in addition to a shift of the bleach minimum to 430 nm. Complete decay of the unstructured ESA is observed over the full experimental time window (6000 ps), alongside full recovery of the bleaching signal at 430 nm.

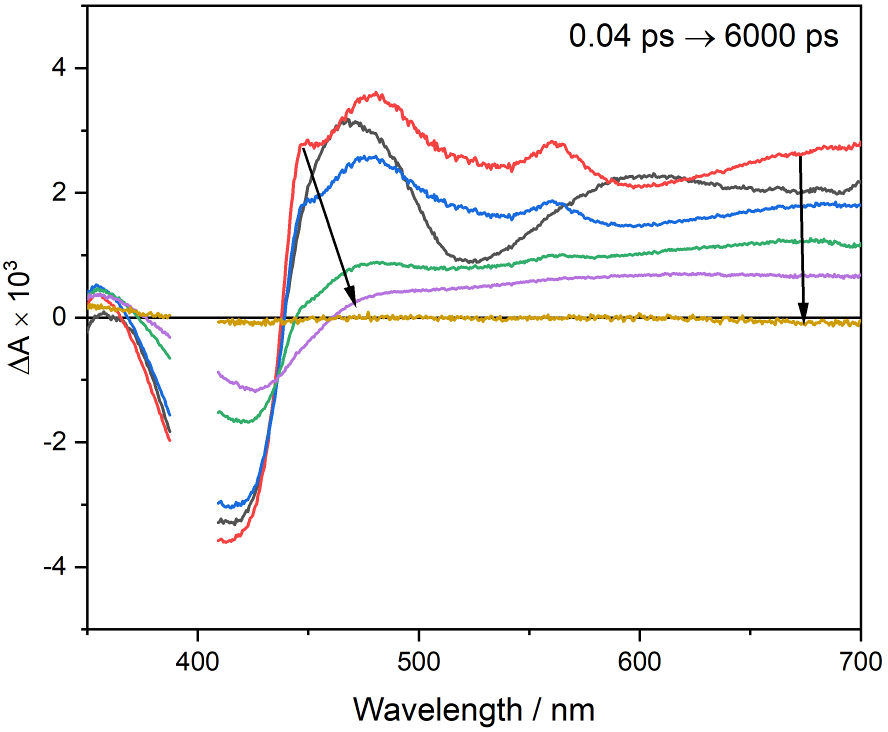

Figure 4.9: Transient absorption at 400 nm excitation in MeCN of Complex 2.1. Pump probe delay times are 0.05 ps, 0.82 ps, 1.70 ps, 7.10 ps, 210 ps and 6000 ps.

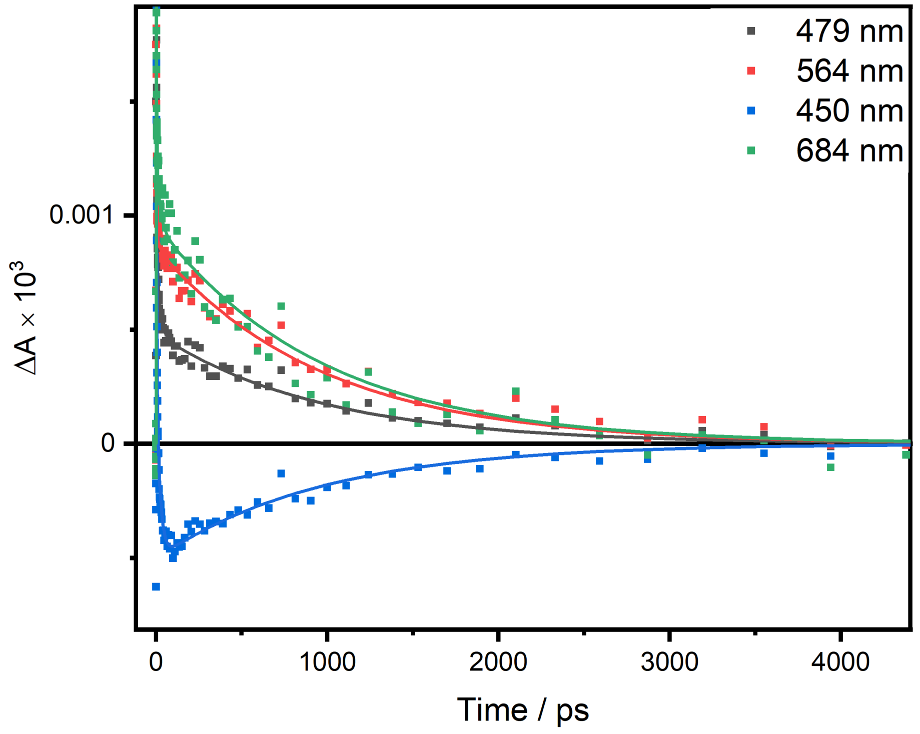

Figure 4.10: Single point kinetics at chosen wavelengths are shown for Complex 2.1 in MeCN, for the corresponding TA spectra (Figure 4.12). The wavelengths are given as insets. The fittings are overlaid which have been extracted from global lifetime analysis.

The transient absorption of Complex 2.1 is given in Figure 4.11. For Complex 2.1, in Hexane, there is an ESA band centred at 490 nm 0.2 ps after excitation. Accompanying the ESA band at 490 nm, there is broad absorption between 567 nm and 688 nm. Bleaching of the ML-LCT absorption band is visible with a peak at 427 nm. Between 0.3 ps and 10 ps there is a rise of broad featureless ESA between 600 nm and 690 nm. Due to the decay of overlapping ESA, the bleach signal partially grows and shifts from 427 to 424 nm. Between 0.2 and 6000 ps (maximum delay) there is a significant change in spectral shape of the ESA features. The ESA feature at 490 nm decays revealing less structured ESA spanning a range from 458 to 690 nm. The final excited state spectrum remains stationary over the remaining pump-probe time delays (50 ps - 6000 ps).

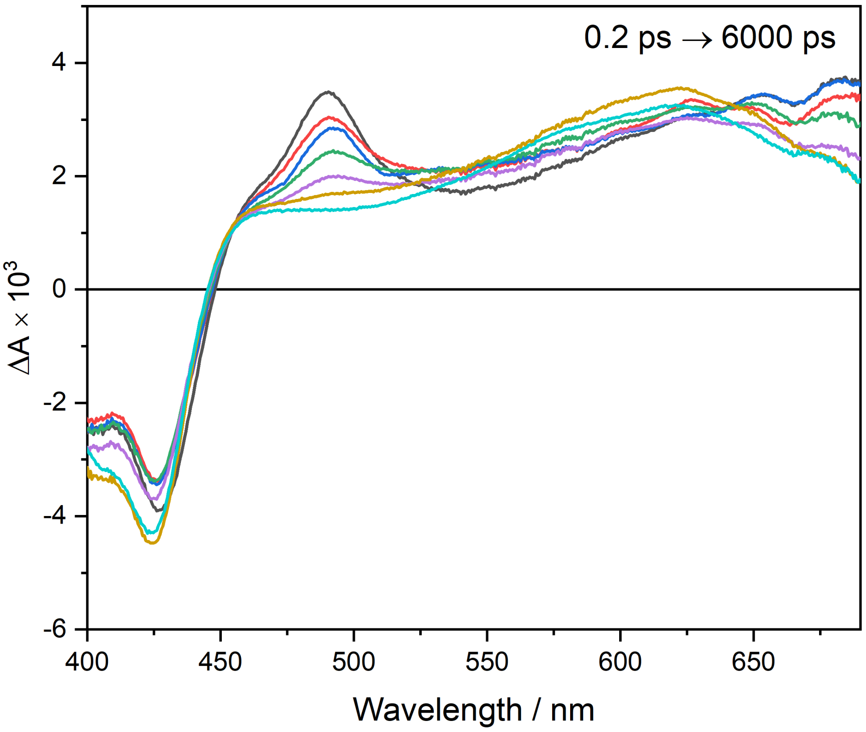

Figure 4.11: Transient absorption at 400 nm excitation in Hexane of Complex 2.1. Pump probe delay times are 0.2 ps, 0.9 ps, 1 ps, 2 ps, 4 ps, 10 ps, 6000 ps.

4.5.2 NAP-Pt-3-PTZ-PTZ-(OMe)$_2$ (Complex 2.2)

DCM

For complex 2.2, in DCM, 0.3 ps after excitation there is an ESA band centered at 480 and 568 nm (Figure 4.8. To the left of the ESA bands, bleaching of the ML-LCT absorption band is visible with a peak at 422 nm. Stimulated emission is also observed at 532 nm, which will obscure any overlapping ESA signal. Between 0.3 and 2 ps there is a redshift in signal at 480 to 488 nm, which is concomitant with the growth of ESA signal at 566 nm and the rise of broad/featureless ESA between 600 and 670 nm. Due to the decay of overlapping ESA, the bleach signal partially grows and shifts from 422 to 434 nm. Between 2 and 6000 ps (maximum delay) there is a significant change in spectral shape of the ESA features. The ESA features at 488 and 566 nm decay revealing less structured ESA spanning a range from 462 to 670 nm.The signal does not decay on the timescale of the experiment. There is partial recovery of the bleaching signal.

Transient Absorption in MeCN

For complex 2.2, in MeCN, 0.08 ps after excitation there is ESA centered at 470 nm and broad featureless ESA which spans a range from 560 to 680 nm. To the left of the ESA bands, bleaching of the ML-LCT absorption band is visible with a peak at 415 nm. Stimulated emission is also observed at 526 nm, which will obscure any overlapping ESA signal. Between 0.08 and 0.3 ps there is a growth of a shoulder at 449 nm and the peak centered at 470 redshifts to 480 nm, there is also a rise of an ESA peak at 562 nm. Between 0.3 and 6 ps there is a significant change in spectral shape of the ESA features. The ESA features at 480 and 562 nm decay revealing less structured ESA spanning a range from 462 to 680 nm. The signal does not decay within the timescale of the experiment. Between 0.08 and 6000 ps (maximum delay) the ESA at 415 to 431 nm redshifts from due to decaying overlapping ESA signal. There is also partial recovery of the bleaching signal.

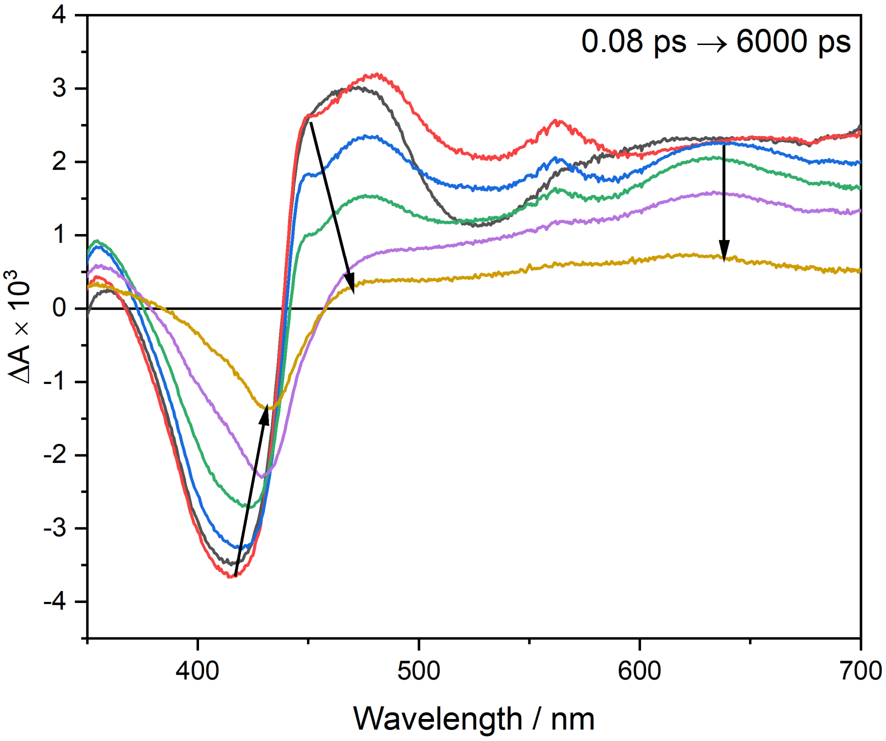

Figure 4.12: Transient absorption at 400 nm excitation in ACN of Complex 2.2. Pump probe delay times are 0.08, 0.30, 1.8, 3.7, 64 and 6000 ps

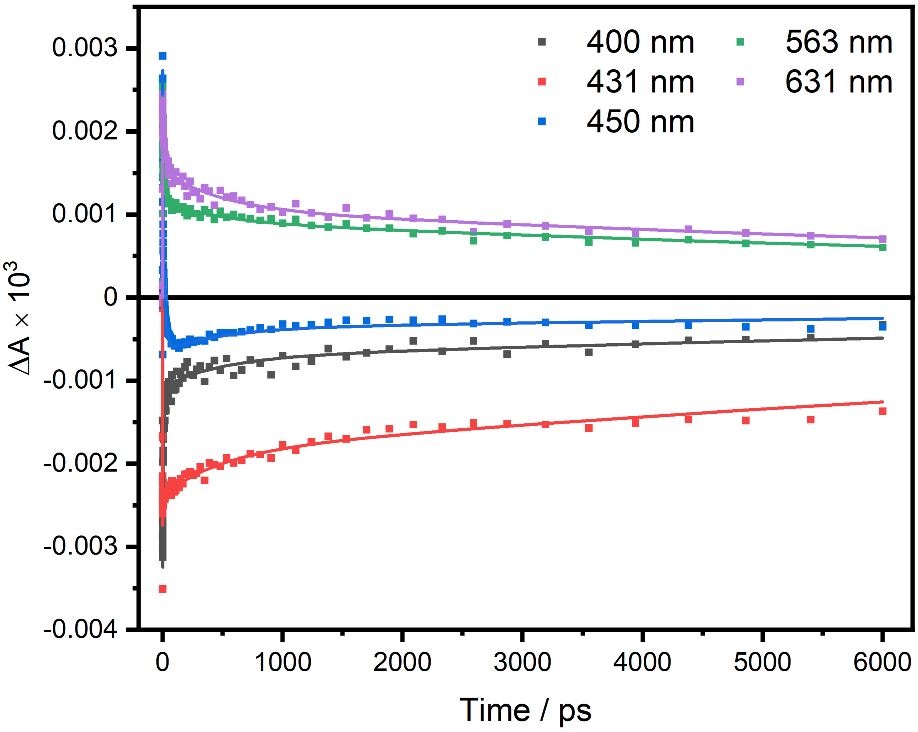

Figure 4.13: Single point kinetics at chosen wavelengths are shown in Figure 4.13 for the corresponding TA spectra of Complex 2.2 in MeCN (Figure 4.12). The wavelengths are given as insets. The fittings are overlaid which have been extracted from global lifetime analysis.

Transient Absorption in Hexane

For Complex 2.2, in Hexane, 0.3 ps after excitation there is an ESA band centered at 492 nm. There is also broad absorption between 542 and 680 nm. To the left of the ESA bands, bleaching of the ML-LCT absorption band is visible with a peak at 425 nm. Stimulated emission is also observed at 546 nm, which will obscure any overlapping ESA signal. Between 0.2 and 6000 ps (maximum delay) there is a significant change in spectral shape of the ESA features. The ESA feature at 492 nm decays revealing less structured ESA spanning a range from 463 to 680 nm. Due to the decay of overlapping ESA, the bleach signal partially grows and shifts from 427 to 424 nm. The signal does not decay on the timescale of the experiment.

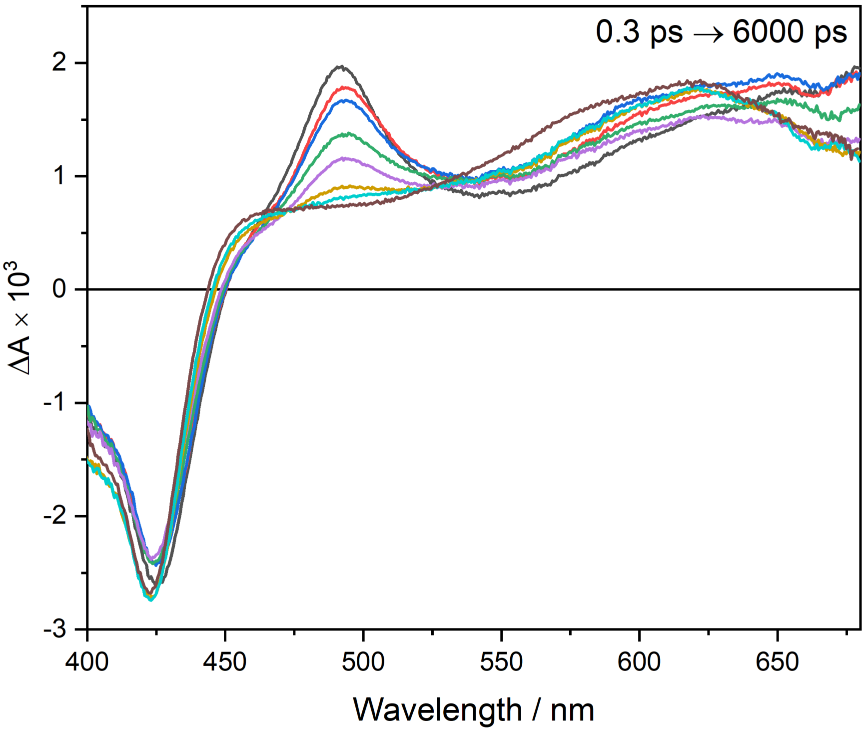

Figure 4.14: Transient absorption at 400 nm excitation in Hexane of Complex 2.2. Pump probe delay times are 0.25, 0.92, 1.1, 2.0, 3.7, 9.73 and 6000 ps

4.6 Fluorescence up-conversion spectroscopy (FLUPS)

4.6.1 Fluorescence up-conversion spectroscopy of NAP-Pt-3-PTZ (Complex 2.1)

The pump-probe time delay increases for the different coloured traces as follows: black, red, blue, green, and purple to yellow to cyan. In Complex 2.1, upon excitation at 400 nm, broad emission with a maxima at 472 nm grows in with instrument response. Between 0.3 and 12 ps the band redshifts to 479 nm along with simultaneous decay and narrowing of the band. The band loses almost all signal intensity within the first 12 ps. Between 12 and 195 ps (maximum time delay) the signal continues to decay. However at 195 ps, there is a small residual signal which does not decay on the timescale of the experiment. The emission at 472 nm is assigned to the vibrationally hot MLCT state which is of mixed triplet and singlet nature due to Pt (II) exhibiting strong spin orbit coupling. A 1 ps lifetime is assigned to vibrational cooling and solvent reorganisation of the MLCT state and population the ^{3}NAP state. Two lifetimes, 10 ps and a constant were required to fit the decay of the spectra. This first lifetime is assigned to the decay of the state of charge transfer character and the constant is required to fit the decay of the long lived ^{3}NAP localised ligand state.

4.6.2 Fluorescence up-conversion spectroscopy of NAP-Pt-3-PTZ-PTZ-(OMe)$_2$ (Complex 2.2)

For Complex 2.2, upon excitation at 400 nm broad emission with a maxima at 475 nm grows in with instrument response. Between 0.3 and 1.2 ps the band redshifts to 484 nm along with simultaneous decay and narrowing of the band. The band loses almost all signal intensity within the first 11 ps. Between 11 and 195 ps (maximum time delay) the signal continues to decay. However at 195 ps, there is a small residual signal which does not decay on the timescale of the experiment. The emission at 475 nm is assigned to the vibrationally hot MLCT state which is of mixed triplet and singlet nature.

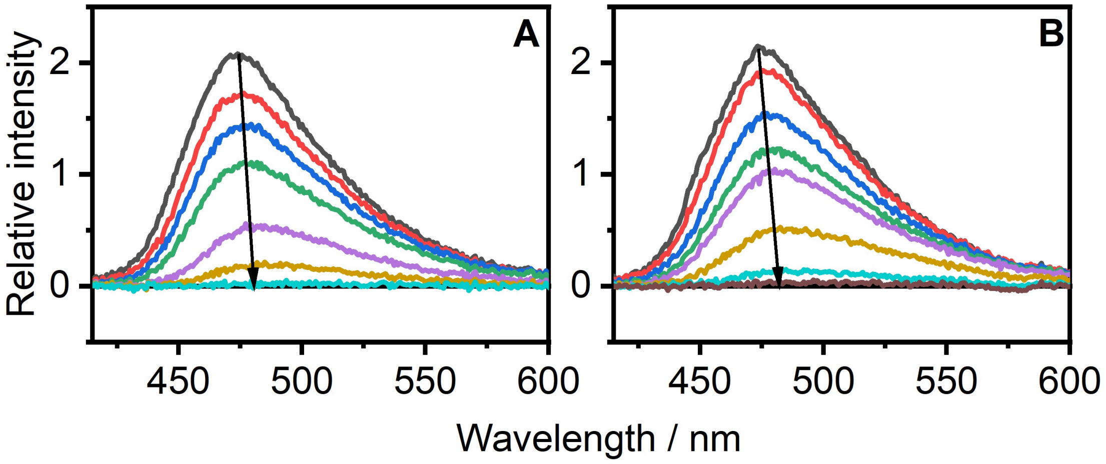

Figure 4.15: FLUPS - Time-resolved emission spectra for Complexes 2.1 (Panel A) and 2.2 (Panel B) upon excitation at 400 nm. Time delays for panel A are 0.32, 0.42, 0.51, 0.70, 2.38, 12.2 and 195 ps. Time delays for panel B are 0.237, 0.325, 0.415, 0.507, 0.602, 1.23, 11.4, 195 ps.

4.7 FTIR

The ground state absorption spectra of complexes 2.1 and 2.2 were recorded in DCM between 1550 and 2220 cm^{-1}. Complexes 2.1 has absorption bands at 1654 and 1693 cm^{-1} with a shoulder at 1722. Complex 2.2 has absorption bands at 1654 and 1693 cm^{-1}. These absorption bands are assigned to the asymmetric/symmetric NAP-localised carbonyl ν(C=O) vibrations. The absorption bands present in Complexes 2.1 and 2.2 at 2086 cm^{-1} with a shoulder at 2140 cm^{-1} are assigned to the bridge-localised acetlyide ν(C≡C) vibration. Complexes 2.2 both have an absorption band at 1584 cm^{-1} which is assigned to the ν(Ar) ring stretching modes.

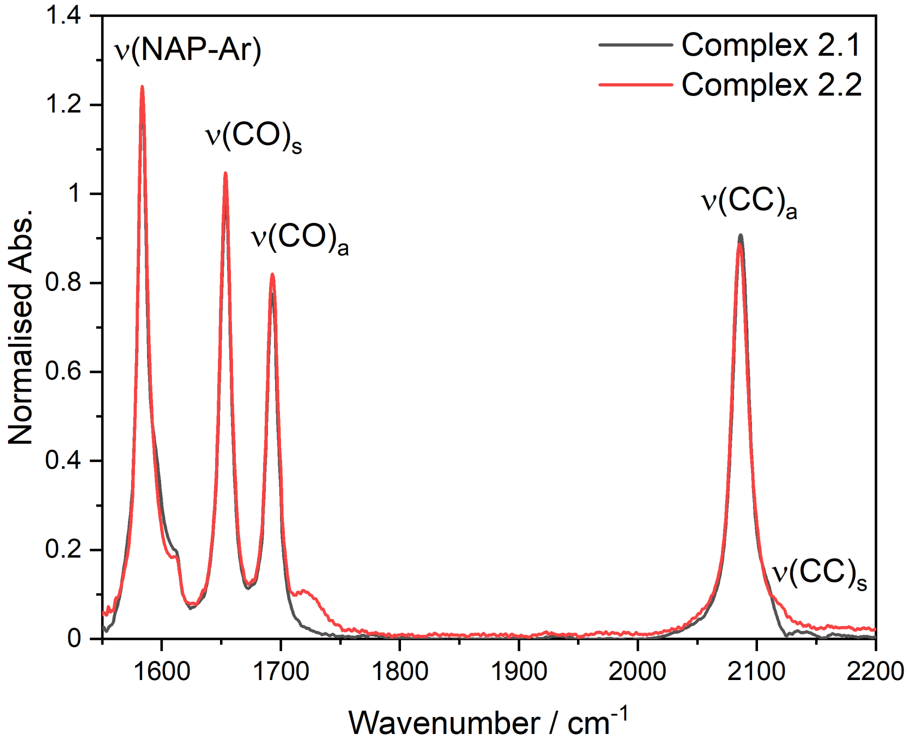

Figure 4.16: FTIR spectra of Complexes 2.1 (black) and 2.2 (red).

4.8 TRIR

4.8.1 NAP-Pt-3-PTZ (Complex 2.1)

The pump-probe time delay increases for the different coloured traces as follows: black, red, blue, green, and purple to yellow to cyan to brown. The TRIR spectra of Complex 2.1 are shown in Figure 4.17. The high frequency region has been trimmed spectrally from 1870 to 2160 cm^{-1} and the data has been trimmed temporally to 1.6 ps. After excitation at 400 nm, there is a band at 2030 cm^{-1} which is assigned to the transient ν(CC) vibration in the initially populated excited state. There is also a band at 1942 cm^{-1}, which is assigned as ^{3}NAP state. There is also a bleaching signal at 2088 cm^{-1} which is assigned to the ν(CC) ground state vibration at 2086 cm^{-1}. Between 1.1 and 6.8 ps there is a shift in peak position of the transient ν(CC) band from 2030 to 2036 cm^{-1}. This is assigned to vibrational cooling. The band at 1942 cm^{-1} also becomes sharper due to the decay of the neighbouring/overlapping broad absorption. Over the following 50 ps the ν(CC) transient band at 2036 cm^{-1} decays fully. The ^{3}NAP transient at 1942 cm^{-1} only partially decays within the experimental time window along with partial recovery of the bleaching signal. The low frequency region has been trimmed spectrally from 1560 to 1732 cm^{-1} and has been trimmed temporally to 1.6 ps. After excitation at 400 nm, there are bands at 1596, 1610 and 1638 cm^{-1} which are assigned to carbonyl vibrations in the initially populated excited states. Accompanying the transient carbonyl bands is the transient at 1564 cm^{-1}, which are assigned to ν(Ar) signals in the initially populated excited state. Bleaching signals at 1655 and 1692 cm^{-1}1 are also observed which are assigned to the ν(CO) ground state vibrations at 1654 and 1693 cm^{-1}. Between 1.6 and 6.8 ps there is a shift in peak position of the transient ν(CO) band from 1638 to 1641 cm^{-1}. This is assigned to vibrational cooling. Over the following 1860 ps there is uniform decay of the ν(CO) transient signal at 1610 cm^{-1} and the transient ν(Ar) signal at 1564 cm^{-1}, revealing two transients at 1575 and 1629 cm^{-1}, which were previously hidden by overlapping ESA. There is a small amount of recovery of the bleaching signals at 1655 and 1692 cm^{-1}.

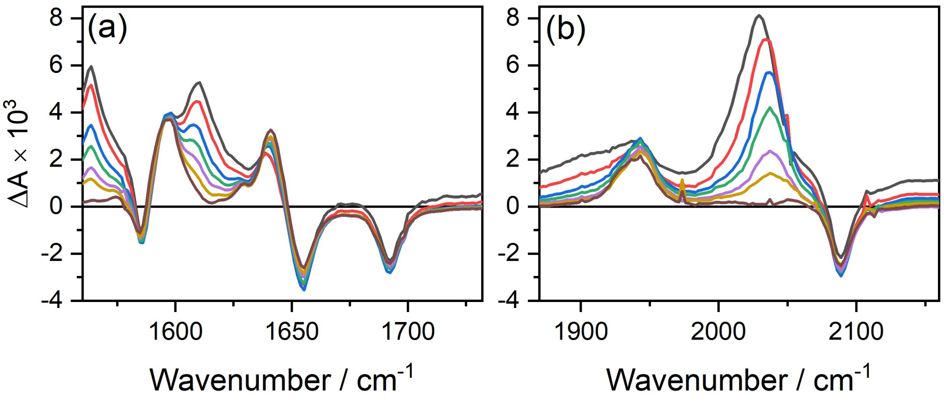

Figure 4.17: Time-resolved infrared spectra of Complex 2.1 following excitation at 400 nm, in DCM, for low (panel (a) and high (panel (b) frequency probe regions. Time delays are 1.6, 2.8, 6.8, 11, 18, 29 and 1900 ps.

4.8.2 NAP-Pt-3-PTZ-PTZ-(OMe)$_2$ (Complex 2.2)

DCM

The high frequency region has been trimmed spectrally from 1880 to 2155 cm^{-1} and the data has been trimmed temporally to 1.6 ps. After excitation at 400 nm, there is a band at 2024 cm^{-1} which is assigned to the transient ν(CC) vibration in the initially populated excited state. There is also a band at 1940 cm^{-1}, which is assigned as ^{3}NAP state. There is also a bleaching signal at 2088 cm^{-1} which is assigned to the ν(CC) ground state vibration at 2086 cm^{-1}. Between 1.6 and 4.2 ps there is a shift in peak position of the transient ν(CC) band from 2024 to 2034 cm^{-1}. This is likely to be vibrational cooling. Over the following 300 ps the ν(CC) transient band centred at 2034 cm^{-1} decays fully. The ^{3}NAP transient at 1948 cm^{-1} only partially decays within the experimental time window along with partial recovery of the bleaching signal at 2088 cm^{-1}. The low frequency region has been trimmed spectrally from 1560 to 1733 cm^{-1} and has been trimmed temporally to 1.6 ps. After excitation at 400 nm, there are transient bands at 1598, 1612 and 1639 cm^{-1} which are assigned to carbonyl vibrations in the initially populated excited states. Accompanying the transient carbonyl bands is the transient band at 1569 cm^{-1}, which is assigned to ν(Ar) signal in the initially populated excited states. Bleaching signals at 1655 and 1692 cm^{-1} are also observed which are assigned to the ν(CO) ground state vibrations at 1654 and 1693 cm^{-1}. Between 1.6 and 6.8 ps there is a shift in peak position of the transient ν(CO) band from 1639 to 1642 cm^{-1}. This is assigned to vibrational cooling. Over the following 300 ps there is uniform decay of the ν(CO) transient signal at 1612 cm^{-1} and the transient ν(Ar) signal at 1564 cm^{-1}, revealing two sharper transient bands at 1596 and 1642 cm^{-1}, which were previously overlapped with ESA. The bleaching signals at 1655 and 1692 cm^{-1} do not fully recover by 1864 ps (maximum delay).

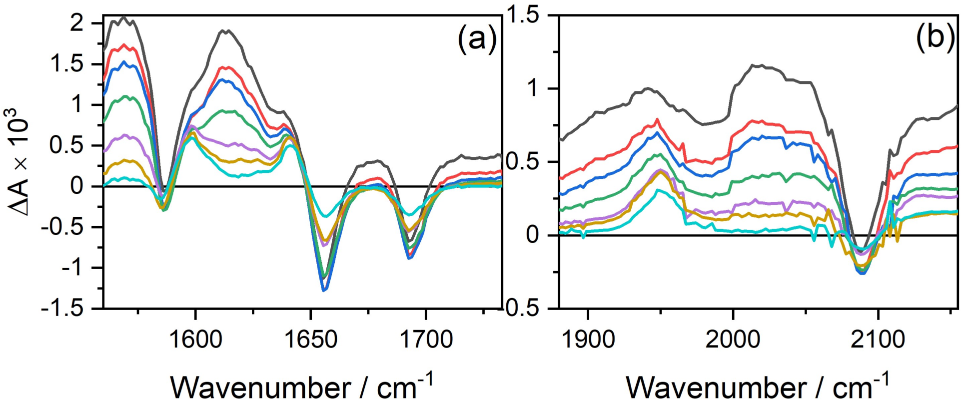

Figure 4.18: Time-resolved infrared spectra of Complex 2.2 following excitation at 400 nm, in DCM, for both high and low frequency probe regions. Time delays are 1.6, 2.8, 4.2, 6.8, 29, 72 and 1900 ps.

Hexane

The high frequency region has been trimmed spectrally from 1860 to 2120 cm^{-1} and the data have been trimmed temporally to 0.39 ps. In Complex 2.2, in hexane, after excitation at 400 nm, there is a band at 2024 cm^{-1} which is assigned to the transient ν(CC) vibration in the initially populated excited state. There are also a bands at 1900 and 2120 cm^{-1} assigned to the same excited state. There is also a band at 1930 cm^{-1}, which is assigned as the ^{3}NAP state. This is assigned as a ^{3}CT state. There is also a bleaching signal at 2090 cm^{-1} which is assigned to the ν(CC) ground state vibration at 2090 cm^{-1}. Between 1 and 2.2 ps there is a shift in peak position of the transient ν(CC) band from 2024 to 2031 cm^{-1}. This is likely to be vibrational cooling. This blueshift, reveals the band at 1930 cm^{-1} more clearly. Between 0.39 and 3600 ps, the bands at 1900, 2030 and 2120 cm^{-1} decay to leave the band at 1940 cm^{-1} and the bleaching signal at 2090 cm^{-1}. The ^{3}NAP transient at 1948 cm^{-1} only partially decays within the experimental time window along with partial recovery of the bleaching signal.

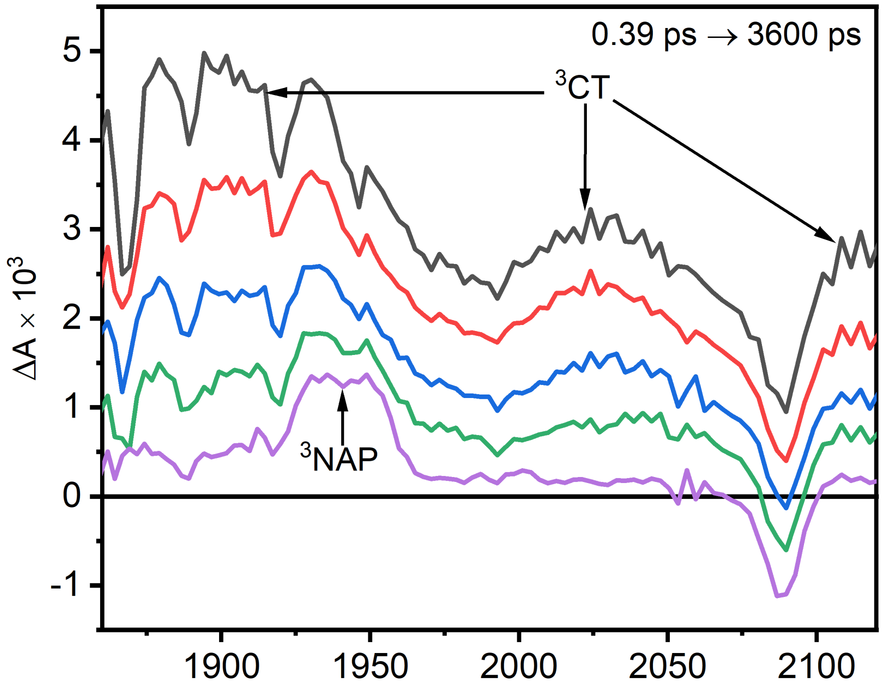

Figure 4.19: Time-resolved infrared spectra of Complex 2.2 following excitation at 400 nm, in Hexane, for high frequency probe regions.

	FTIR / cm^{-1}		TRIR / cm^{-1}	
Complex	carbonyl region	acetylide region	carbonyl region	acetylide region
2.1	1654, 1693, 1722	2086, 2140	1596, 1610, 1638	1942, 2030 / 2036
2.2	1654, 1693	2086, 2140	1590, 1625, 1645	1948, 2024 / 2034
2.3	16	2073, 2120	1608, 1620, 1643 / 1585, 1625	1897, 2023/ 2050

Table 4.2: A table of the carbonyl and acetylide vibrational frequencies present in Complexes 2.1 and 2.2 and 2.3 for both FTIR and TRIR experiments. The forward slashes indicate the peak frequency at different times during the TRIR experiment

4.9 Discussion

4.9.1 NAP-Pt-3-PTZ (Complex 2.1)

Transient Absorption (DCM)

The bands present at 480 and 566 nm are consistent with those previously reported in the spectroelectrochemistry of the NAP radical ion. Therefore, it is likely that this excited state has an electron density distribution on the NAP ligand consistent with that of the previously studied NAP radical anion. This suggests that the new excited state formed has CT character, whereby the NAP is formally reduced. The bands at 480 and 566 nm, associated with the CT state, decay with a lifetime of 3.8 ps into the ^{3}NAP state and 19 ps into the ground state. From DFT calculations the excited state is assigned as having mixed CT and ILCT character. This state will be referred to as the CT state from here after. Between 0.3 and 49 ps there is a significant change in spectral shape of the ESA features, which indicates a change of electronic state. The bands at 480 and 566 nm associated with the mixed CT and ILCT state decay revealing broad featureless ESA between 600 and 690 nm, which is characteristic of the ^{3}NAP excited state localised on the [NAP-CC] moiety. The decay of this state is assigned a constant as a lifetime (470 ns). There is no band present at 516 nm, which in previously studied NAP and PTZ bearing molecules was indicative of the PTZ radical cation having formed. The band present at 566 nm, which is thought be the NAP radical ion is present in spectroelectrochemistry for NAP-Pt-Cl, therefore is not indicative of the ^{3}CSS forming.[74] The rate of charge separation for 2.1 is significantly increased due to the increased coupling between the acceptor and Pt bridge moeity. There is no formation of a ^{3}CSS state despite increased coupling between donor and Pt bridge. This is a significantly different formation of excited states compared to what is seen in Complex 2.3, where the donor is not strongly coupled to the Pt (II) bridge. This could be due to the PTZ donor moeity being highly conjugated to the Pt bridge moeity, meaning that the ^{3}CSS can't be defined as a ^{3}CSS anymore. The electron on the PTZ donor and the Pt are no longer separated in space. Although the ET rate is determined by coupling, the donor has been incorporated into the structure of the bridge, so they are not separate entities. In Complex 2.3, the CV of the PTZ doesn't shift, which proves that there is not much communication between PTZ and the Pt. However, in Complex 2.1 the electron which comes from the HOMO (highest occupied molecular orbital) is now shared between Pt bridge and the PTZ donor.

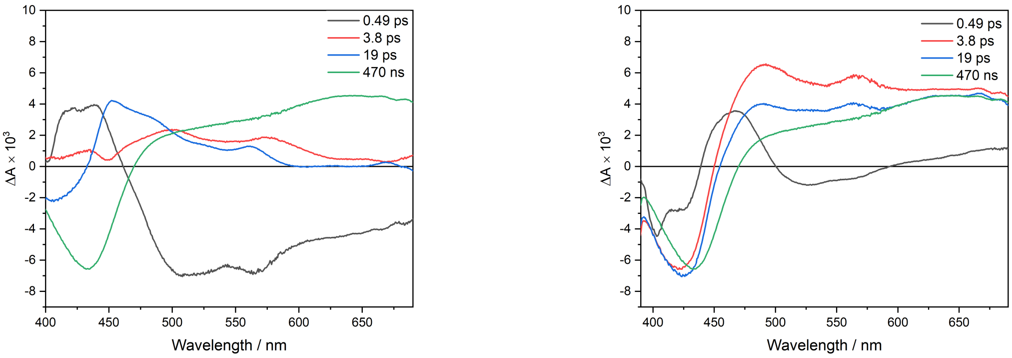

Figure 4.20: Decay associated (left) and evolution associated (right) spectra for Complex 2.1, in DCM

Transient Absorption (Hexane)

In Complex 2.1, the ESA centered at 490 nm and between 567 and 688 nm is assigned to a state with mixed CT and ILCT character. A lifetime of 4 ps, is assigned to the decay of this state. This is the same lifetime as that extracted from the TA undertaken in DCM. The excited state populated in hexane appears to have less CT character and more ILCT character than in DCM as there is no ESA band at 566 nm, which is assigned to the NAP radical anion. This state decays into a ^{3}NAP state, which like in DCM does not decay on the timescale of the experiment and has a constant assigned to its decay. The dip in the excited state absorption spectrum could potentially be attributed to stimulated emission from the initially excited state, noting that the steady state emission spectrum has a peak at 505 nm.

Transient Absorption (MeCN)

A 2 ps lifetime is assigned to vibrational cooling and solvent reorganisation of the MLCT state. The peaks at roughly 480 and 560 nm (NAP radical anion) are assigned to the initally populated CT state. The broad absorption spanning between 480 and 700 nm is assigned to the ^{3}NAP. Two lifetimes, 21 ps and a 964 ps were required to fit the decay of the spectra. This first 21 ps lifetime is assigned to the decay of the state of charge transfer character and the 964 ps is required to fit the decay of the long lived ^{3}NAP localised ligand state. In Complex 2.1 in MeCN the signal recovers fully, unlike in DCM and Hexane. The dynamics are accelerated in ACN in Complex 2.1, by a factor of roughly 470 for the decay of the ^{3}NAP state.

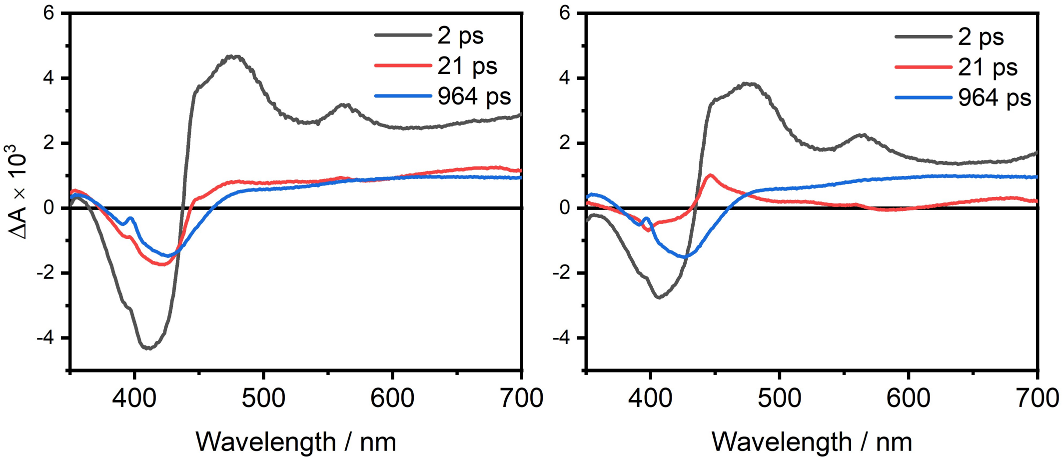

Figure 4.21: Decay associated (left) and evolution associated (right) spectra for Complex 2.1, in MeCN

4.9.2 FLUPS

A 1 ps lifetime is assigned to vibrational cooling and solvent reorganisation of the MLCT state and also the decay into the ^{3}NAP state. Two lifetimes, 10 ps and a constant were required to fit the decay of the spectra. This first lifetime is assigned to the decay of the state of mixed charge transfer and intraligand character and the constant is required to fit the decay of the long lived ^{3}NAP localised ligand state. It is important to note that the 10 ps and constant lifetimes have very small contributions in the DAS.

4.9.3 TRIR (DCM)

In Complex 2.1, at the initial time delay the bands positioned at 1563 and 1609 cm^{-1} are present, along with the presence of the band at 1597 and 1641 cm^{-1}. the initially excited states are populated on a sub ps timescale. There is a significant change in ESA

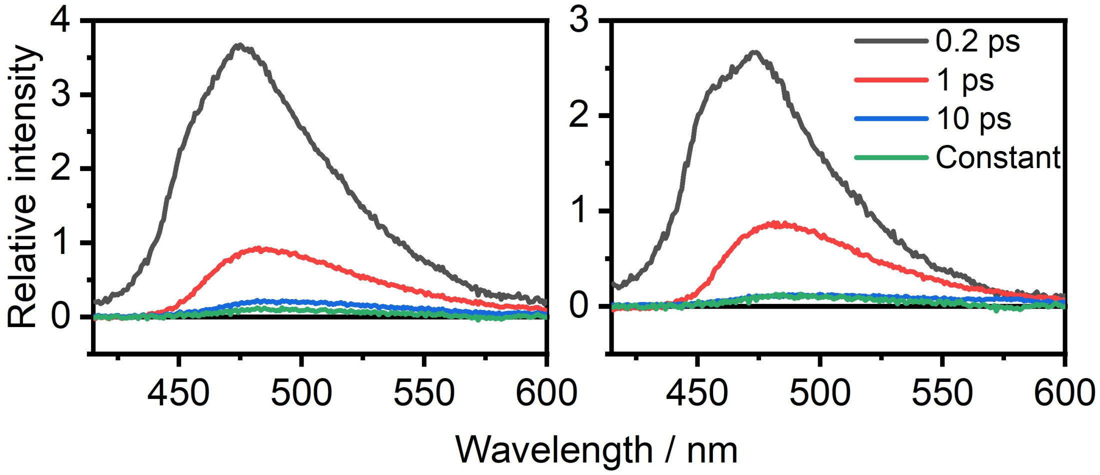

Figure 4.22: Evolution and decay associated spectra and for Complexes 2.1 in DCM. The lifetimes are given as in insets in the graphs.

i.e decay in the bands positioned at 1609 and 1563 cm^{-1}. The decay of these bands is also concomitant with the decay of the band at 2029 cm^{-1}, indicating that these three bands belong to the same excited state. These ν(CO) bands are consistent with those previously reported in the FTIR spectrum of the one-electron reduced NAP-Pt-Cl complex.[74] These three bands are attributed to the NAP^{-} anion and therefore are assigned to the CT state. A lifetime of 17 ps is assigned to decay of the CT state into the ground state. This corroborates with the 19 ps lifetime extracted from TA for the decay of the CT state. This excited CT state is likely to be a triplet state a result of the Pt orbitals facilitating fast intersystem crossing due to increased spin-orbit coupling. The bands at 1597 cm^{-1} and 1641 cm^{-1} are also present at the initial time delay. They are assigned to the ^{3}NAP state. While the bands at 1563 and 1609 cm^{-1} associated with the CT state decay fully, there is little change in bands assigned to the ^{3}NAP state and a small growth in the bleaching signals. This indicates that the the ^{3}CT state decays directly into the ^{3}NAP state. A lifetime of 1.1 ps is assigned to the decay of the ^{3}CT state into the ^{3}NAP state. A constant is assigned to decay of the final ^{3}NAP lowest lying state. Both the TRIR and TA data indicate that there is no formation of a ^{3}CSS state. The dynamics seen in the low frequency region are similar to what is seen in a previously studied compound NAP-Pt-Ph,[74] increasing the conjugation of the donor causes the donor to no longer act like a donor. There is no significant shift in ν(CO) bands which would usually indicate a change in electron density and therefore a PTZ$^+$ cation forming, which is what is seen in previously studied molecules such as PTZ-Ph-Pt-NAP.[74]

The EAS and DAS associated with all the lifetimes above are shown in Figure 4.24. The blue shift of the band at 2030 to 2036 cm^{-1}, which is vibrational cooling is assigned a lifetime of 1 ps. The ν(CC) band present at 2030 cm^{-1} is assigned to the CT state. A 16 ps lifetime is assigned to decay of this CT state. There is also a band at 1942 cm^{-1} which is assigned to the ^{3}NAP state. This band is present alongside the CT band at 2030 cm^{-1}. The ^{3}NAP state decays with a lifetime on the scale of several nanoseconds and it is represented with a constant. The high frequency TRIR data shows that two different electronic states are formed simultaneously, due to several transient bands belonging to different excited states being present at once. This is in agreement with the low frequency TRIR and TA data, where it is evident that a combination of states have been populated. The formation of these states is accelerated compared to that in Complex 2.3. Averaging the TA and TRIR lifetimes gives an average of 2 ps for the decay of the CT state. The lifetime of the CT state in Complex 2.3 is 14 ps.[75] Therefore the decay of the CT state has been accelerated by a factor of 7. The CT also decays via an additional pathway into the ^{3}NAP state, as well as the ground state. The EAS and DAS associated with all the lifetimes above are shown in Figure 4.24. The lifetimes extracted from both low and high frequency TRIR are consistent with those extracted from TA and FLUPS, all lifetimes can be found in Table 4.3.

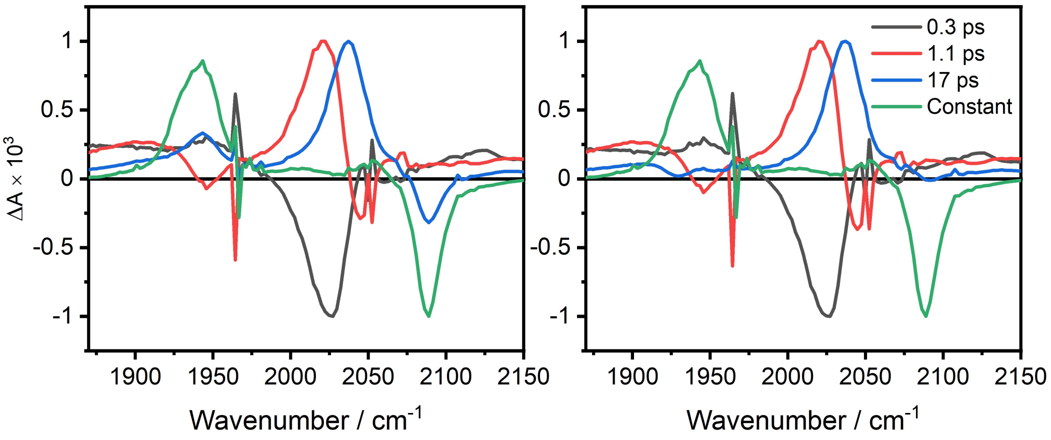

Figure 4.23: Time-resolved infrared spectra GLA of Complex 2.1 following excitation at 400 nm, in DCM, for low frequency probe regions.

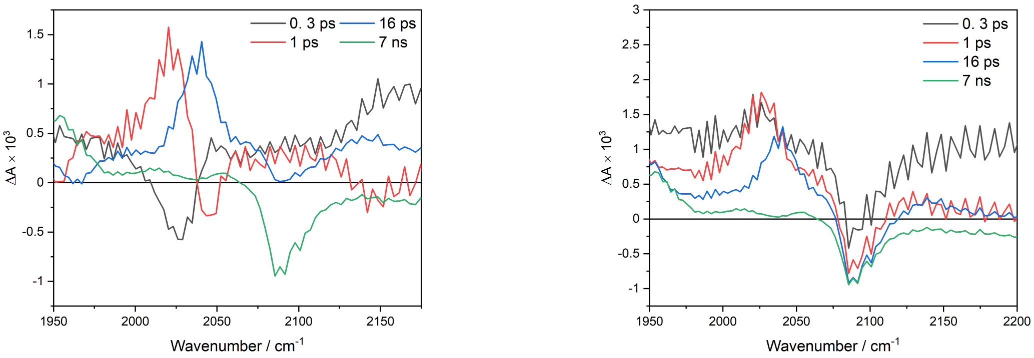

Figure 4.24: Decay associated spectra for Complex 2.1, in DCM, for high frequency probe regions.

4.9.4 DFT calculations

Density difference calculations (electron density difference between S_0 and corresponding triplet state) have been performed by Heather Carson in the Meijer group. The calculations are consistent with the spectroscopic data which shows that the ^{3}NAP state is T_1, the lowest lying triplet state, with an energy of 2.074 eV. This corroborates with the energy estimated from the emission ^{3}NAP state conducted in Hexane. T_2, is predicted to be a ^{3}CSS state. However, from the experimental work, it was hypothesised that no ^{3}CSS had been formed and that T_2 was a state with charge transfer character but without significant electron density loss from the donor. When comparing Complex 2.1 to the complex where the donor is also strongly coupled but the acceptor is weakly couple the ordering of the states is reversed. The ^{3}CSS is the lowest state and second lowest state is ^{3}NAP. Also the energy of the T_1 state is 0.3 eV lower in Complex 2.1, compared to when the acceptor is weakly coupled. This implies that the coupling of the acceptor does have a significant impact on the ordering and energies of the states.

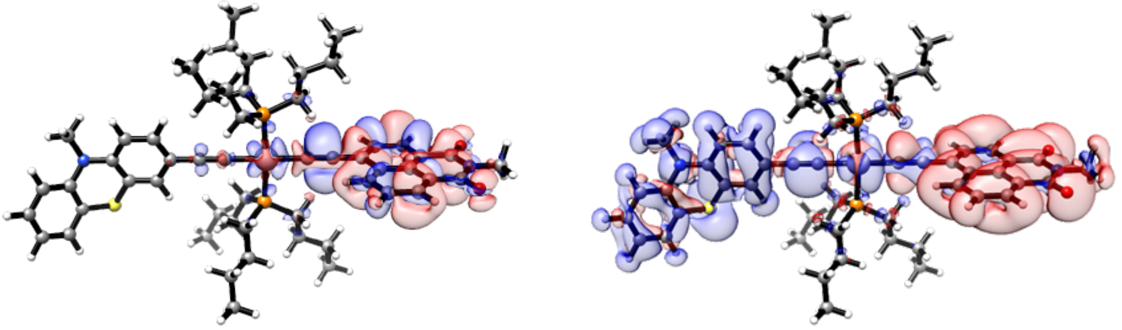

Figure 4.25: T_1 (left) and T_2 (right) electron density difference diagrams for Complex 2.1. Blue indicates loss of electron density, whereas red indicates gain in electron density.

4.10 NAP-Pt-3-PTZ-PTZ-(OMe)$_2$ (Complex 2.2)

4.10.1 FLUPS (DCM)

A 1.1 ps lifetime is assigned to vibrational cooling and solvent reorganisation of the MLCT state. Two lifetimes, 17 ps and a constant were required to fit the decay of the spectra. This first lifetime is assigned to the decay of the state of charge transfer character and the constant is required to fit the decay of the long lived ^{3}NAP localised ligand state. There is a discrepancy between the TRIR and TA lifetimes with the FLUPS lifetime. This is due to the maximum time delay being 195 ps in FLUPS, therefore the lifetime assigned to decay of CT state from the FLUPS measurement will not be as reliable as that from TRIR and TA.

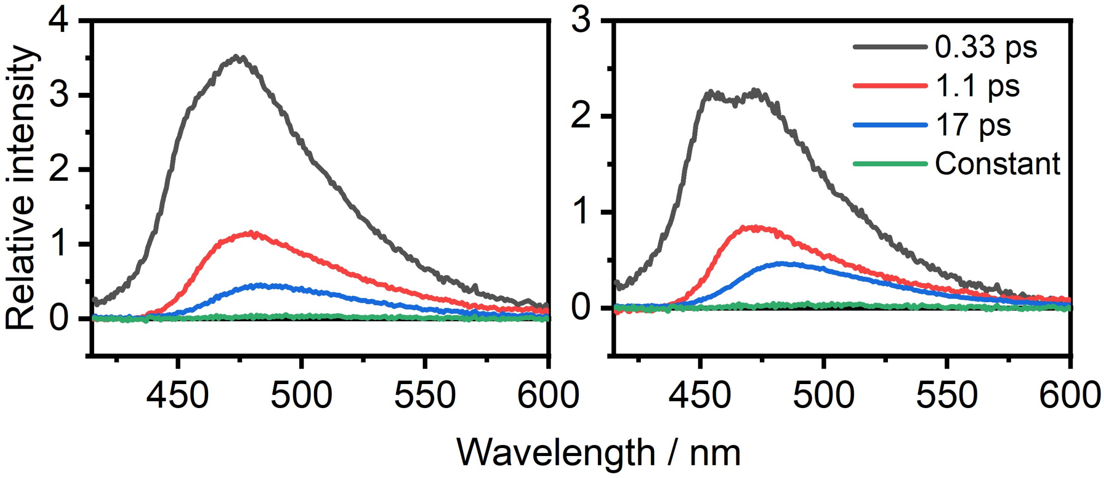

Figure 4.26: Evolution and decay associated spectra and for Complexes 2.2 in DCM. The lifetimes are given as in insets in the graphs.

4.10.2 Transient Absorption (DCM)

The bands present at 484 and 570 nm are consistent with those previously reported in the spectroelectrochemistry of the NAP radical ion. Therefore, it is likely that this excited state has an electron density distribution on the NAP ligand consistent with that of the previously studied NAP radical anion. This suggests that the new excited state formed has CT character, whereby the NAP is formally reduced. The bands at 484 and 570 nm, associated with the CT state, decay with a lifetime of 6.4 (vibrational relaxation) and 208 ps. From DFT calculations the excited state is assigned as having mixed CT and ILCT character. This state will be referred to as the CT state from hereafter. Between 0.3 and 135 ps there is a significant change in spectral shape of the ESA features, which indicates a change of electronic state. The bands at 480 and 566 nm associated with the mixed CT and ILCT state decay revealing broad The featureless ESA between 600 and 690 nm, which is characteristic of the ^{3}NAP excited state localised on the [NAP-CC] moiety. There is no band present at 516 nm as in Complex 2.1 which in previously studied NAP and PTZ bearing molecules, such as in Complex 2.3, would be indicative of the PTZ radical cation having formed. The band present at 566 nm, which is thought be the NAP radical ion is present in spectroelectrochemistry for NAP-Pt-Cl, therefore is not indicative of the ^{3}CSS forming.[74]

4.10.3 Transient Absorption (Hexane)

In Complex 2.2, the ESA centred at around 490 nm and between 550 and 675 nm is assigned to a state with mixed CT and ILCT character. The decay of this initial excited state is assigned a lifetime of 6 ps, 1.5 times longer than that of Complex 2.1, showing that the extra donor extends the lifetime of the excited states in both DCM and hexane. Like in Complex 2.1, the excited state populated in hexane appears to have less CT character and more ILCT character than in DCM as there is no strong ESA band at 566 nm, which is assigned to the NAP radical anion. Similar to Complex 2.1, this state decays into a ^{3}NAP state, which like in DCM does not decay on the timescale of the experiment and has a constant assigned to its decay.

4.10.4 TRIR (Hexane)

In Complex 2.2, the ESA bands at 1900, 2030 and 2120 cm^{-1} correspond to a state with CT character whereas the band at 1940 cm^{-1} corresponds to a ILCT state, therefore this corroborates with the TA that a state of mixture of CT and ILCT states are formed. This state then decays into a pure ILCT state i.e a ^{3}NAP state, which like in the TA, does not decay on the timescale of the experiment.

4.10.5 TRIR (DCM)

In Complex 2.2, at zero time, ESA bands positioned at 1569 and 1612 cm^{-1} are present, along with the presence of the band at 1598 and 1639 cm^{-1}. A sub ps lifetime is assigned to the population of initial excited states. There is a significant change in ESA i.e decay in the bands positioned at 1612 and 1569 cm^{-1}. The decay of these bands is also concomitant with the decay of the band at 2024 cm^{-1}, indicating they belong to the same excited state. These ν(CO) bands are consistent with those previously reported in the FTIR spectrum of the one-electron reduced NAP-Pt-Cl complex.[74] These three bands are attributed to the NAP$^-$ anion and therefore are assigned to the CT state. A lifetime of 4 ps is assigned to decay of this CT state. The bands at 1598 and 1639 $^{-1}$ are also present at the initial time delay. They are assigned to the ^{3}NAP state. While the bands at 1569 and 1612 cm^{-1} associated with the CT state decay fully, there is little change in bands assigned to the ^{3}NAP state and a small growth in the bleaching signals. This indicates that the the CT state decays directly into the ^{3}NAP state. The dynamics seen in the low frequency region is similar to what is seen in a previously studied compound NAP-Pt-Ph.[74] A constant is assigned to decay of final ^{3}NAP state. Both the TRIR and TA data corroborate that there is no formation of a ^{3}CSS. There is no significant shift in ν(CO) bands which would usually indicate a change in electron density and therefore indication of the PTZ$^+$ cation forming, which is what is seen in previously studied molecules such as PTZ-Ph-Pt-NAP.[74] The ν(CC) band present at 2034 cm^{-1} is assigned to the CT state. A 4.1 ps lifetime is assigned to decay of this CT state. There is also a band at 1942 cm^{-1} which is assigned to the ^{3}NAP state. This band is present alongside the CT band at 2034 cm^{-1}. The ^{3}NAP state decays with a lifetime on the scale of several nanoseconds and it is represented with a constant. An additional lifetime of 120 ps is needed to fit the decay of the ^{3}NAP and the CT state. The high frequency TRIR data, similar to that of Complex 2.1, shows that two different electron states are formed simultaneously, as there are several transient bands belonging to different excited states being present at once. This is in agreement with the low frequency TRIR and TA data, where it is evident that a combination of states have been populated. The formation of these states is accelerated compared to that in Complex 2.3. The lifetime of the CT state in Complex 2.3 is 14 ps.[75] Averaging the TA and TRIR lifetimes gives an average lifetime of 4.8 ps for the decay of the CT state in Complex 2.2 into the ^{3}NAP state. The rate of decay of the CT state has been increased by a factor of 3, by connecting the PTZ donor through the phenyl ring, thus increasing the driving force for charge recombination. In Complex 2.1 the CT state decays quicker than in Complex 2.2. The addition of the second PTZ donor increases the lifetime of the CT state decaying into the ground state by a factor of 9. The EAS and DAS associated with all the lifetimes above are shown in Figure 4.28. The lifetimes extracted from both low and high frequency TRIR are consistent with those extracted from TA, all lifetimes can be found in Table 4.3. The FLUPS lifetimes vary from the lifetimes extracted from TA and

TRIR. The FLUPS experiment is measuring the emission emulating from emissive states and also only has a maximum delay of 200 ps. Therefore the lifetimes extracted may not be consistent with that of TA and TRIR. When comparing these DBA complexes to similar complexes (NDI-Pt-Ph-CH_2-PTZ, NDI-Pt-Cl, NDI-Pt-Ph and NAP-Pt-Ph-CH_2-PTZ) found in the literature,[73,74] the striking difference is that the ^{3}CSS is no longer formed due to the modifications on the donor.

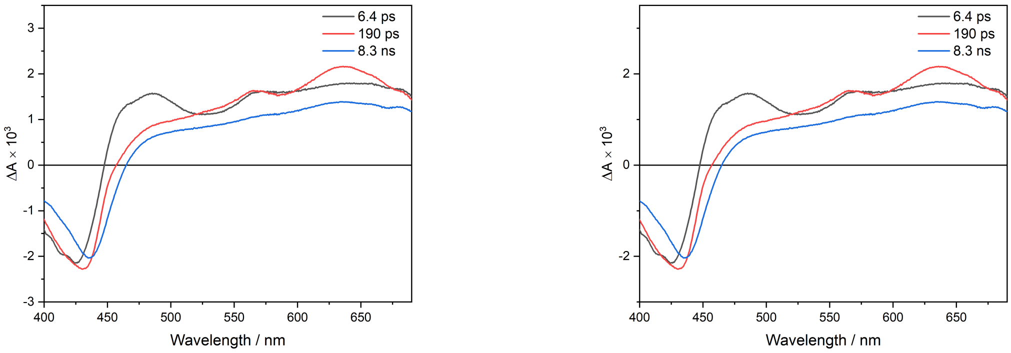

Figure 4.27: Decay associated spectra for Complex 2.2, in DCM, duplicate figure

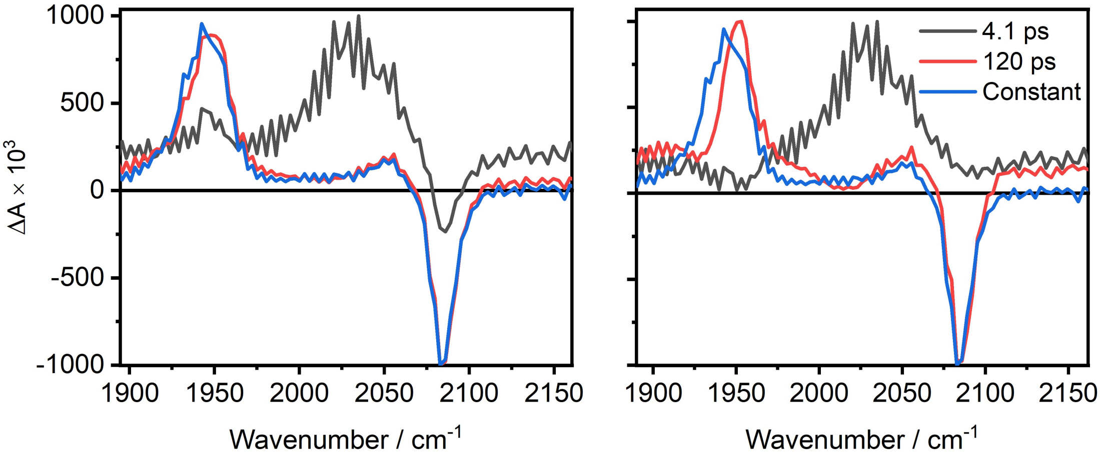

Figure 4.28: Decay associated spectra for Complex 2.2, in DCM, for high frequency probe regions.

4.11 Conclusions

The excited state spectra in Complex 2.1 and Complex 2.2 are fairly consistent with one another. In both complexes NAP$^-$ anion and ^{3}NAP bands are both present at zero time,

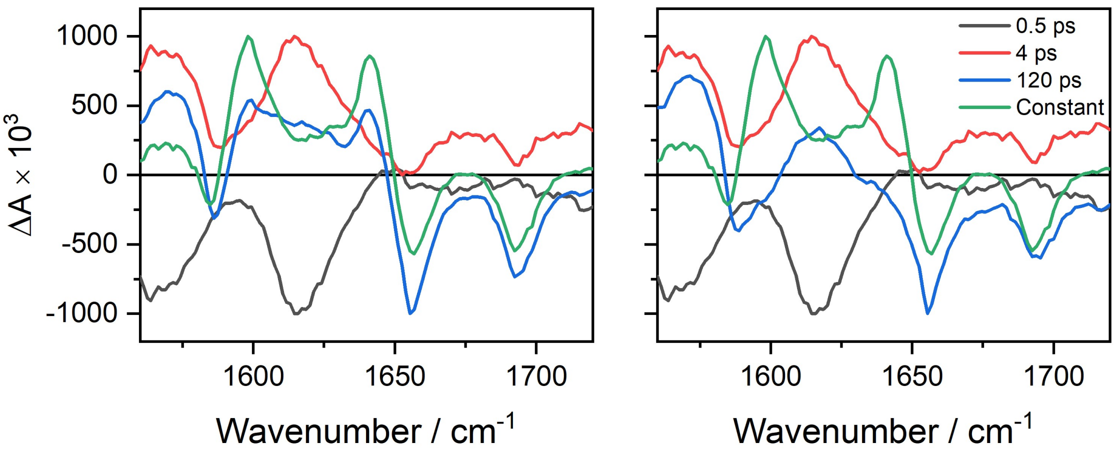

Figure 4.29: Decay associated spectra for Complex 2.2, in DCM, for low frequency probe regions.

	τ / ps (TA)	τ / ps (HF TRIR)	τ / ps (LF TRIR)	τ / ps (FLUPS)
2.1	0.49 ps	0.02 ps	0.3 ps	0.2 ps
	3.8 ps	1.1 ps	1 ps	1 ps
	19 ps	16 ps	16 ps	10 ps
	Constant	Constant	Constant	Constant
2.2	0.2 ps	0.5 ps	0.5 ps	0.4 ps
	6.4 ps	4 ps	4 ps	1.1 ps
	208 ps	120 ps	120 ps	17 ps
	Constant	Constant	Constant	Constant

Table 4.3: GLA lifetimes associated with Complex 2.1 and 2.2.

followed by the decay of the NAP$^-$ anion bands at 1563 and 1609 cm^{-1} into the the ^{3}NAP state, which like in Complex 2.1 do not decay by the maximum time delay (1864 ps). However, the kinetics of the two compounds do differ significantly. The lifetime of the CT state in Complex 2.2 is 4.8 ps (averaged from TA and TRIR), which is roughly 1.4 times slower than that of Complex 2.1. The additional PTZ donor with methoxy groups appended allows for the lifetime of the CT state to be extended by a factor of 9. The attachment of the PTZ donor which increases the coupling between the bridge and the donor creates an additional pathway for the decay of the CT state into the ^{3}NAP state. This was seen in previous work,[75] whereby removal of the CH$_2$ spacer also created an additional pathway into the ^{3}NAP state. The energy level diagrams for Complexes 2.1 and 2.2 can be seen in Figure 4.30.

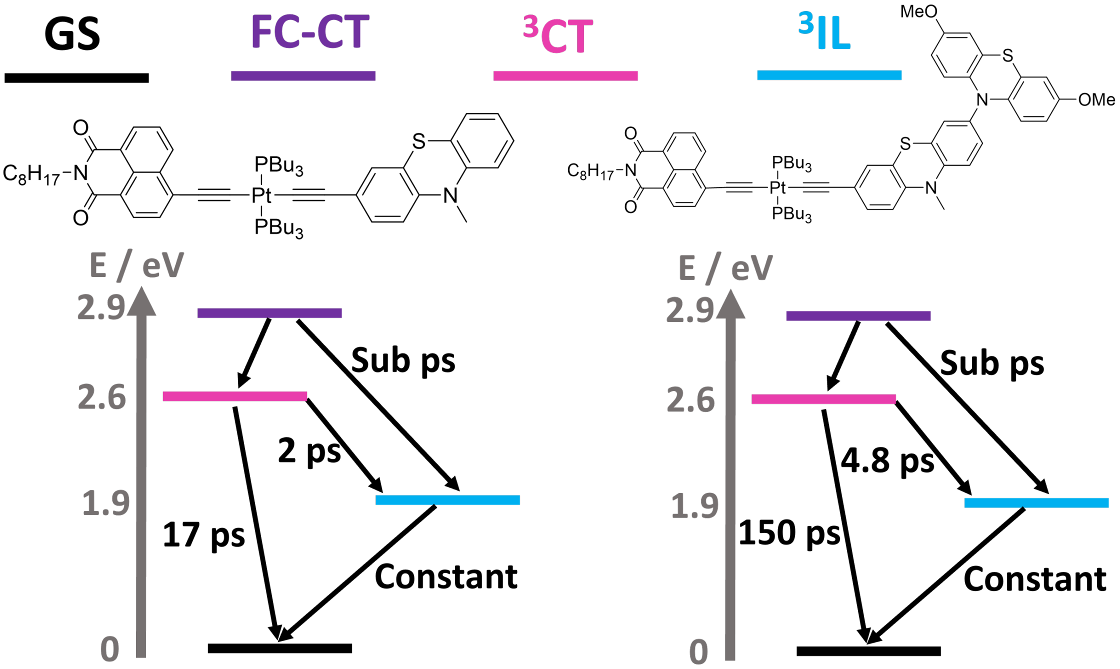

Figure 4.30: An energy level diagram showing the excited state processes following excitation at around 400 nm, in DCM, for Complexes 2.1 and 2.2 (left to right). The energies of the states have been estimated using emission in DCM and hexane.

Chapter 5

Photophysics and ground state dynamics of two of modified Pt(II) donor-bridge-acceptor trans-acetylide complexes bearing a 1,4,5,8-naphthalene diimide acceptor

The ultrafast dynamics of two novel Pt(II) donor-bridge-acceptor trans-acetylide complexes have been studied and compared to the original 'unmodified' complex (Complex 1), employing a variety of techniques including steady-state measurements, ultrafast TA spectroscopy and TRIR spectroscopy and 2DIR spectroscopy. Both molecules have an NDI acceptor and at least one PTZ donor. Complex 1 is the original unmodified complex, Complex 3.1 has the PTZ donor is attached directly to the bridge instead of through the nitrogen atom, this is to increase conjugation between the donor and the bridge. Complex 3.2 has two PTZ donors to form a molecular cascade system, the first donor is attached to the bridge directly, the second is attached to the first donor through its own nitrogen atom. The second donor has methoxy groups appended to it to ensure the oxidation potential is lower, than that of the first donor. This is so that theoretically two ^{3}CSS states can be formed,^{3}CSS$_1$ and ^{3}CSS$_2$. ^{3}CSS$_1$ is formed first, followed by the sacrificial donation of an electron from the second donor to the first donor to form CSS$_2$. This is designed to mimic a small scale artificial photosynthetic cascade. To provide clarity on the findings from Complexes 3.1 and 3.2 I will discuss results previously reported on Complex 1 to make comparison. Complex 1 contains an electronically identical acceptor, but contains a spacer between the PTZ donor which is attached through the nitrogen.

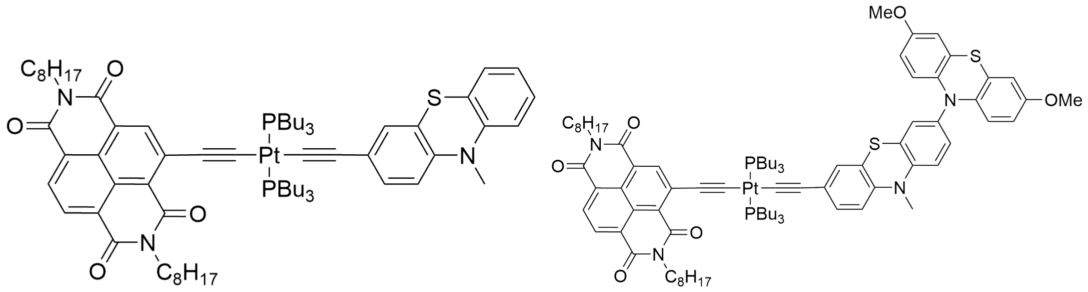

(a) Complex 3.1 (b) Complex 3.2

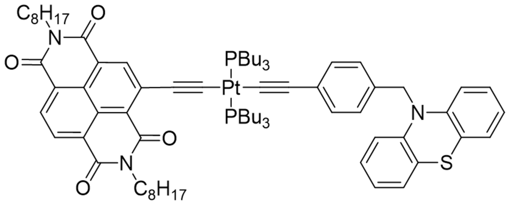

(c) Complex 1

Figure 5.1: Complexes 3.1, 3.2 and 1

5.1 Results

5.1.1 UV-Vis absorption spectroscopy

The UV-Vis absorption spectra of Complexes 3.1 and 3.2 are shown in Figure 5.2. The spectra were recorded in CH_2Cl_2 (DCM), covering a spectral range between 230 and 600 nm. The intraligand (IL) π-$\pi*$ transitions centered on the NDI, Ph and PTZ units occur in the region between 230 and 390 nm for all complexes. The intraligand π-$\pi*$ transition centred on the PTZ occurs at 258 nm for Complex 3.1 and at 261 nm for Complex 3.2. The transitions that occur at 287 and 327 nm in Complex 3.1 and at 283 and 343 are assigned to the acetylide and phenyl (π-$\pi*$) ligand localized transitions. The π-$\pi*$ transitions centred on the NDI ligand occur at 360 and 380 nm in Complex 3.1 and 3.2. A low energy metal to ligand charge transfer (MLCT) transition is responsible for the broad absorption band with a maxima at 500 nm for Complexes 3.1 and 3.2. This MLCT transition involves charge transfer from the Pt-acetylide bridge to the NDI acceptor ligand. Figure 5.2 shows that the absorption band centred at 500 nm exhibits solvatochromic behaviour, suggesting that electronic transition responsible for this absorption band has CT character. DFT calculations confirm this assignment, as well as suggesting that this transition also has ligand-to-ligand character. Therefore, the absorption band centred at 500 nm is a assigned to a mixed metal-ligand to ligand charge transfer (ML-LCT) transition. The d-orbitals on the Pt mix with those of the acetylide, leading to the transition being of of mixed character. The spectra are consistent with the UV-Vis spectra of Complex 1 indicating that the ML-LCT band is insensitive to the type of donor mutually trans to the acceptor, indicating that the ligand-to-ligand character of this transition arises from the NDI-CC moiety only.

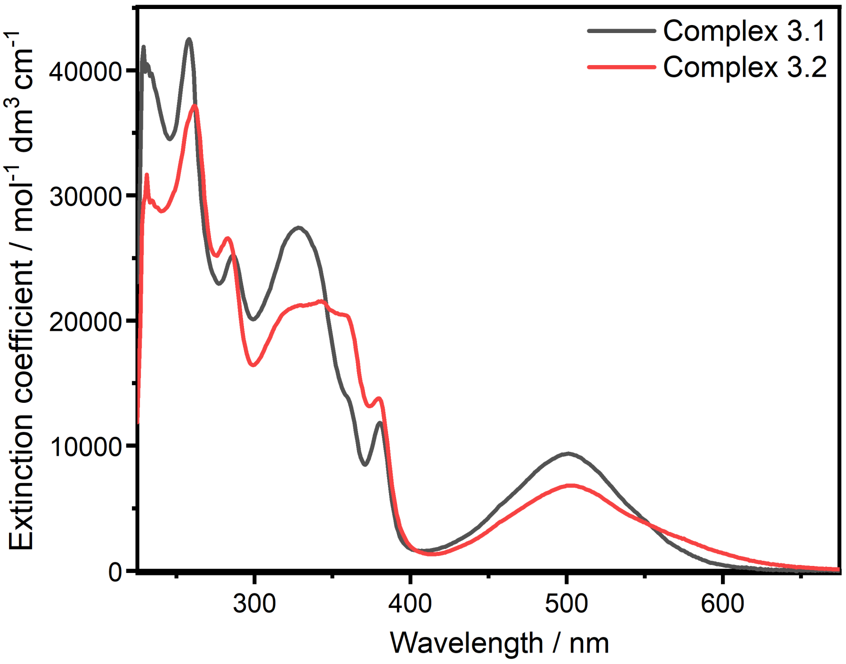

Figure 5.2: UV-Vis absorption spectra for Complexes 3.1 (Black) and 3.2 (Dashed red) recorded in DCM, at room temperature.

5.1.2 FTIR spectroscopy

The ground state vibrational absorption spectra of complexes 3.1 and 3.2 were recorded in DCM between 1550 and 2130 cm^{-1}. Complexes 3.1 has absorption bands at 1659 and 1700 cm^{-1} with a shoulder at 1708 cm^{-1}. Complex 3.2 has absorption bands at 1660 and 1700 cm^{-1} with a shoulder at 1708. This is similar to what was reported in Complex 1. These absorption bands are assigned to the asymmetric/symmetric NDI-localised carbonyl ν(C=O) vibrations. There are two absorption bands present in Complexes 3.1 and 3.2 due to the presence of the two acetylide bands. They are positioned at 2073 with a shoulder cm^{-1} at 2120 and are assigned to the bridge-localised asymmetric and symmetric acetlyide ν(C≡C) vibration. The asymmetric shoulder band in Complex 3.1 and 3.2 is broader than that in Complex 1. Complexes 3.1 and 3.2 both have an absorption band at 1600 with a shoulder at 1616 cm^{-1} which are assigned to the ν(Ar) ring stretching modes.

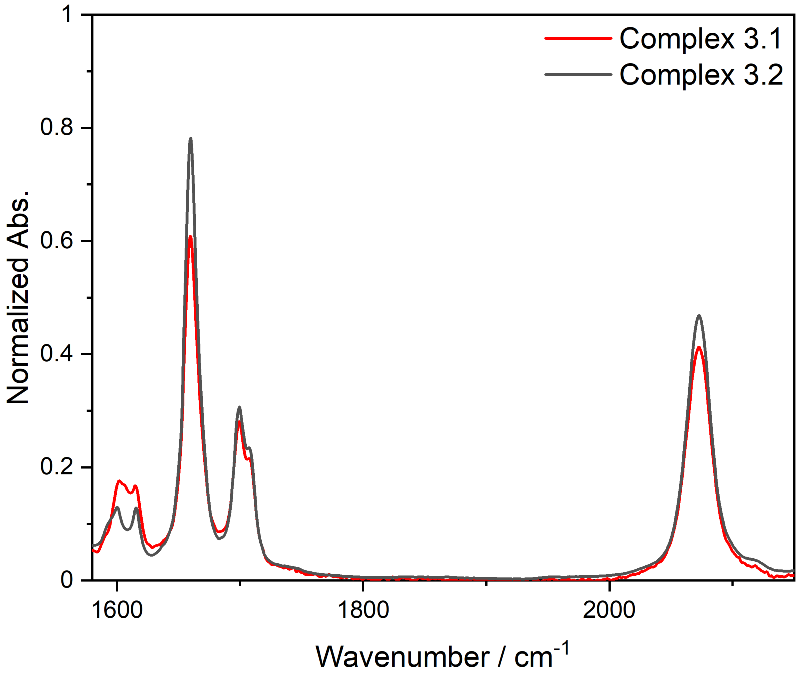

Figure 5.3: FTIR absorption spectra for Complexes 3.1 (Black) and 3.2 (Red) recorded in DCM, at room temperature.

5.1.3 Emission spectroscopy

Figure 5.4 shows the steady state emission spectra of complexes 3.1 and 3.2, in aerated DCM, following excitation at 500 nm (ML-LCT absorption band). The emission maxima for complexes 3.1 and 3.2 appear at 630 nm. There is no band present in the near-IR region as seen in Complexes 2.1 and 2.2, suggesting that the ordering of the states is different due to the change in acceptor. It is likely that similar to Complex 1, a lower lying state is quenching any emission emanating from the ^{3}NDI state.

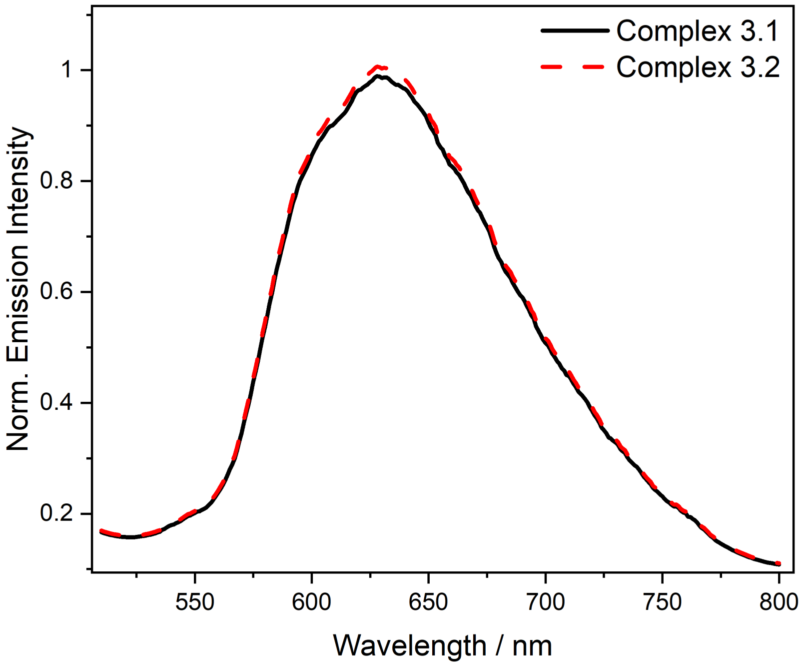

Figure 5.4: Aerated emission spectra for Complexes 3.1 (Black) and 3.2 (Red dashed) recorded in DCM, at room temperature.

5.1.4 Transient Absorption (DCM)

The TA spectra of Complexes 3.1 and 3.2 have been recorded in DCM, upon excitation at 500 nm. The excited state dynamics, following excitation, were probed for the two complexes between 395 and 700 nm. All spectra are dominated by sub ps coherent artefact signal and have therefore been trimmed accordingly. The lifetimes were obtained from global analysis of the time resolved data sets. All decay trace colours increase in chronological order from black to red to blue to green to purple to yellow to cyan to brown.

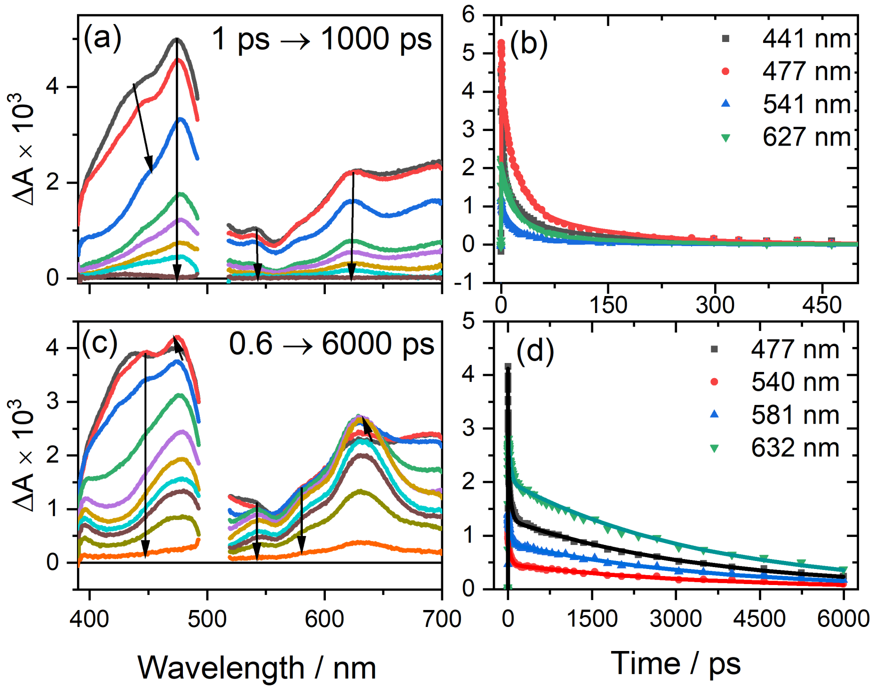

Figure 5.5: TA spectra for Complexes 3.1 and 3.2 following excitation of the ML-LCT transition in DCM are shown in Graphs (a) and (c). The given time delays for a and c are 1.0, 1.4, 5.5, 26, 41, 63, 99 and 1000 ps, and 0.60, 0.86, 1.50, 4.1, 9.2, 26, 68, 150, 1600 and 6000 ps respectively. Single point kinetics at chosen wavelengths are shown in Graphs, (b) and (d) for the corresponding TA spectra. The wavelengths are given as insets. The fittings are overlaid which have been extracted from global lifetime analysis.)

NDI-Pt-3-PTZ (Complex 3.1)

In complex 3.1, 1 ps after excitation, there are two adjacent ESA bands centred at 436 nm and 474 nm. There is also an ESA band at 624 nm with a shoulder at 578 nm, which overlaps with broad ESA between 615 and 700 nm. There is also an ESA band at 541 nm. The spectra has been cut between 492 and 518 nm due to pump scatter, thus obscuring the bleaching of the ML-LCT transition expected at 500 nm. Between 1 and 1.4 ps the ESA band at 436 redshifts to 443 nm. Between 1.4 and 5.4 ps there is a change in spectral shape in the ESA features. The ESA band at 443 nm along with the broad ESA between 615 and 700 nm decay, revealing the sharper ESA band at 624 nm with a shoulder at 578 nm. Between 5 and 1000 ps (maximum delay) the shape of the spectra remains constant while there is uniform decay of the signal. By 1000 ps virtually all signal has decayed.

NDI-Pt-3-PTZ-PTZ-(OMe)$_2$ (Complex 3.2)

In complex 3.2, 0.6 ps after excitation, there are two adjacent ESA bands centred at 437 nm and 474 nm. There is also an ESA band at 631 nm with a shoulder at 580 nm, which overlaps with broad ESA between 615 and 700 nm. The spectra has been cut between 493 and 520 nm due to pump scatter, thus obscuring the bleaching of the ML-LCT transition expected at 500 nm. Over the following 1 ps there is a significant change in spectral shape in the ESA features. There is a redshift of the signal from 437 nm to 447 nm, and the growth of a ESA signal at 474 and 631 nm. There is also growth of a peak at 541 nm, which is concomitant with the growth of the signals at 474 and 631 nm. By 4 ps the ESA band at 447 nm along with the broad ESA between 615 and 700 nm have decayed, revealing a sharper ESA band at 630 nm with a shoulder at 580 nm. Between 4 and 6000 ps (maximum delay) the shape of the spectra remains constant while there is uniform decay of the signal.

5.1.5 Transient Absorption (Hexane)

The TA spectra of Complexes 3.1 and 3.2 have been recorded in Hexane, upon excitation at 500 nm. The excited state dynamics, following excitation, were probed for the two complexes between 395 and 700 nm. All spectra are dominated by sub ps coherent artefact signal and have therefore been trimmed accordingly.

NDI-Pt-3-PTZ (Complex 3.1)

In Complex 3.1, there is an ESA band centred at 421 nm 0.4 ps after excitation. There is also an ESA band at 613 nm, which overlaps with broad ESA between 591 and 687 nm. There is also an ESA band at 539 nm. The same peak is seen in DCM. The bleaching of the ML-LCT transition is at 500 nm. Between 0.4 and 300 ps the ESA band at 421 nm red shifts to 429 nm and the band at 613 nm decays to reveal broad absorption between

573 and 687 nm. Between 300 and 6000 ps (maximum delay) the shape of the spectra remains constant while there is decay of the ESA band at 429 nm.

NDI-Pt-3-PTZ-PTZ-(OMe)$_2$ (Complex 3.2)

In Complex 3.2, similar to what was observed in Complex 3.1, 0.77 ps after excitation, there is an ESA band centred at 421 nm. There is also an ESA band at 613 nm, which overlaps with broad ESA between 600 and 700 nm. There is also an ESA band at 540 nm. The bleaching of the ML-LCT transition is at 500 nm, but this is slightly obscured by pump scatter. By 180 ps the ESA band at 421 nm red shifts to 424 nm and the band at 613 nm decays to reveal broad absorption between 575 and 700 nm. Between 180 and 2700 ps there is uniform decay of the signal, while the shape of the spectra remains constant. Between 2700 and 6000 ps (maximum delay) the shape of the spectra remains constant while there is decay of the ESA band at 429 nm.

5.1.6 Time Resolved Infrared Spectroscopy

NDI-Pt-3-PTZ (Complex 3.1)

The TRIR spectra of Complex 3.1 are shown in Figure 5.7. The low frequency region has been trimmed spectrally from 1550 to 1800 cm^{-1} and has been trimmed temporally to 1.6 ps. Before 1.6 ps the spectra are dominated by coherent artefact signals. After excitation at 520 nm, there are bands at 1625 (with a shoulder at 1645) and 1590 cm^{-1} which are assigned to carbonyl vibrations in the initially populated excited state. Bleaching signals at 1660 and 1700 cm^{-1} are also observed which are assigned to the ν(CO) ground state vibrations at 1660 and 1700 cm^{-1}. Accompanying the transient carbonyl bands is the band at 1560 cm^{-1}, which is assigned to ν(Ar) signal in the initially populated excited state. Between 1.6 and 1864 ps there is uniform decay of the ν(CO) transient signals at 1660 and 1670 cm^{-1} and the transient ν(Ar) signal at 1560 cm^{-1}. Concomitant with this decay is the recovery of the bleaching signals at 1660 and 1700 cm^{-1}1. The high frequency region has been trimmed spectrally from 1800 to 2115 cm^{-1} and the data have been trimmed temporally to 0.4 ps. Before 0.4 ps the spectra are dominated by coherent

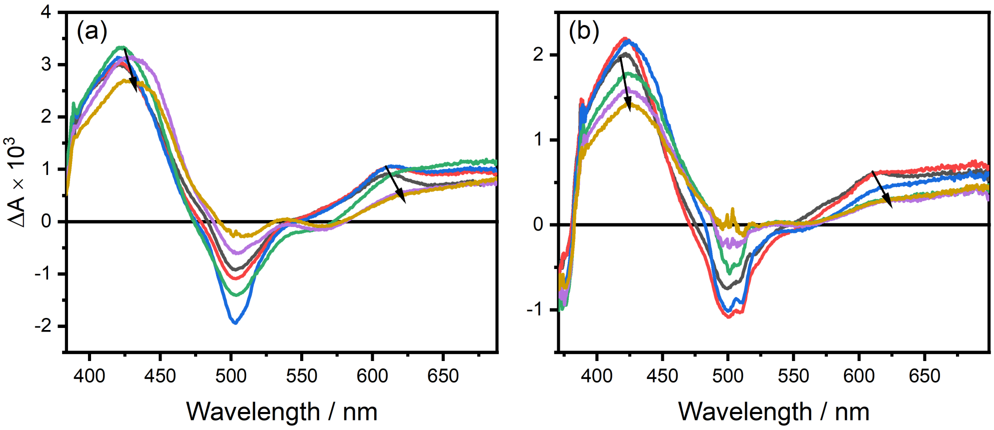

Figure 5.6: TA spectra for Complexes 3.1 and 3.2 following excitation of the ML-LCT transition in Hexane are shown in Graphs (a) and (b). The given time delays for a and b are 0.40, 0.72, 15, 306 and 6000 ps and 0.77, 3.8, 180, 2700, 4600 and 6000 ps respectively.)

artefact signals. After excitation at 520 nm, there is a band at 1897 and 2020cm^{-1} which is assigned to the transient ν(CC) vibration in the initially populated excited state. There is also a bleaching signal at 2073 cm^{-1} which is assigned to the ν(CC) ground state vibration at 2073 cm^{-1}. Between 1.6 and 1900 ps there is uniform decay of the transient ν(CC) peaks at 1897 and the peak at 2020 shifts to 2023 cm^{-1}, along with partial recovery of the bleach, which is still present at 1900 ps (maximum delay).

NDI-Pt-3-PTZ-PTZ-(OMe)$_2$ (Complex 3.2)

The TRIR spectra of Complex 3.2 are shown in Figure 5.8. The low frequency region has been trimmed spectrally from 1556 to 1740 cm^{-1} and has been trimmed temporally to 0.8 ps. Before 0.8 ps the spectra are dominated by coherent artefact signals. After excitation at 520 nm, there are bands at 1608, 1620 and 1643 cm^{-1} which are assigned

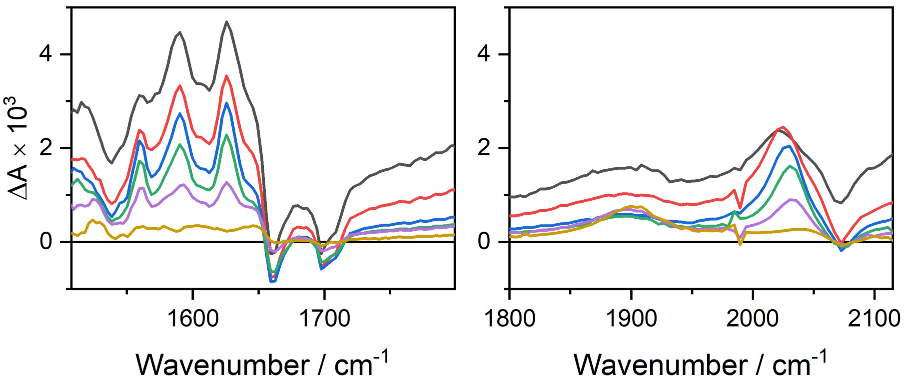

Figure 5.7: TRIR spectra for Complex 3.1, following excitation of the ML-LCT band in DCM. The time delays for both graphs are 0.4, 1.6, 4.2, 11, 44 and 1800 ps.

to carbonyl vibrations in the initially populated excited state. Bleaching signals at 1662, 1700 and 1709 cm^{-1}1 are also observed which are assigned to the ν(CO) ground state vibrations at 1660 and 1700, 1708 cm^{-1}. Between 0.8 and 1100 ps there is decay of the ν(CO) transient signals at 1608, 1620 and 1643 cm^{-1}. Concomitant with this decay is the growth of new transient bands at 1585 and 1625 cm^{-1}, the two bands are assigned to transient ν(CO) vibrations. The bleaching signals at 1662, 1700 and 1709 cm^{-1} also grow in on the same timescale. Between 1100 and 2800 ps (maximum delay) there is uniform decay of the signal, however, the signal is still present at the maximum delay. The high frequency region has been trimmed spectrally from 1750 to 2140 cm^{-1} and the data have been trimmed temporally to 1.6 ps. Before 1.6 ps the spectra are dominated by coherent artefact signals. After excitation at 520 nm, there is a band at 1897 and 2023 cm^{-1} which is assigned to the transient ν(CC) vibration in the initially populated excited state. There is also a bleaching signal at 2073 cm^{-1} which is assigned to the ν(CC) ground state vibration at 2073 cm^{-1}. Between 1.6 and 1900 ps there is uniform decay of the transient ν(CC) peaks at 1897 and 2023 cm^{-1} which reveals a shoulder at 2050 cm^{-1}, along with partial recovery of the bleach, which is still present at 1900 ps (maximum delay).

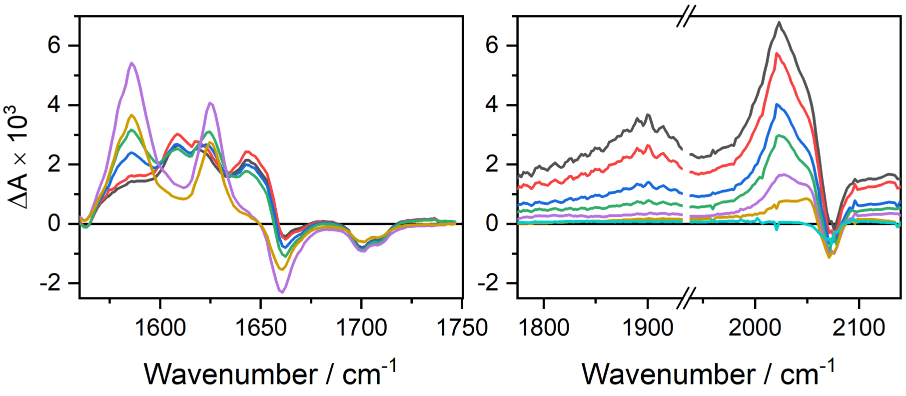

Figure 5.8: (OMe-PTZ-3-PTZ-Pt-NDI) TRIR spectra for Complex 3.2, following excitation of the ML-LCT band in DCM. The time delays for both graphs are 0.8, 2, 14, 34, 1100 and 2800 ps.

	FTIR / cm^{-1}		**TRIR / cm^{-1}**	
Complex	carbonyl region	acetylide region	carbonyl region	acetylide region
1	1659, 1699, 1708	2072, 2107	1612, 1647 / 1592, 1626	1885 / 1963 / 1928 / 2097
3.1	1660,1700, 1708	2073, 2120	1590, 1625, 1645	1897, 2020
3.2	1660, 1700, 1708	2073, 2120	1608, 1620, 1643 / 1585, 1625	1897, 2023/ 2050

Table 5.1: A table of the carbonyl and acetylide vibrational frequencies present in Complexes 1, 3.1 and 3.2, for both FTIR and TRIR experiments. The forward slashes indicate the peak frequency at different times during the TRIR experiment

5.2 Discussion

5.3 Transient Absorption

5.3.1 NDI-Pt-3-PTZ (Complex 3.1)

In Complex 3.1 in DCM, the ESA band present at zero time at 437 nm along with the featureless ESA between 600 and 700 nm, is characteristic of the spectra of the ^{3}IL excited state localised on the [NDI-CC] moiety denoted the ^{3}NDI state. The ESA signals present at 474, 541 and 624 nm are assigned to the NDI$^-$ anion. The bands at 474, 541 and 624 nm are consistent with those previously reported in the spectroelectrochemistry of the NDI radical ion. Therefore, it is likely that the new excited state has an electron density distribution on the NDI ligand consistent with that of the previously studied NDI$^-$ radical anion.[46,72] There are no ESA bands which are assigned to the PTZ+ cation.[76–78] This suggests that the new excited state formed is a ^{3}CT state, whereby the NDI is formally reduced, but there is no significant electron loss from the donor. The ^{3}CT has been formed rapidly with a lifetime of 2.4 ps. One DAS lifetime of 32 ps is required to fit the decay of this ^{3}CT state. It is hard to directly compare the rate of charge separation to previously studied complexes such as Complex 1, which share the same strongly conjugated acceptor but weakly conjugated donor, as the nature of the state is different. In Complex 1 a full ^{3}CSS state is formed, unlike in Complex 3.1 where it is a ^{3}CT state. Therefore the comparison will be made to the ^{3}IL(CT) state in Complex 1. Comparing the formation of these two similar states it is clear that in Complex 3.1 the ^{3}CT state is formed at a rate of two times (1.88) faster. The rate of decay of the ^{3}CT state is 25 times quicker than in Complex 1. The corresponding EAS and DAS spectra are shown in Figure 5.9. There is some small residual signal present at 1000 ps at 437 nm, which is assigned to the ^{3}IL excited state, for which a constant was required in order to fit the decay.

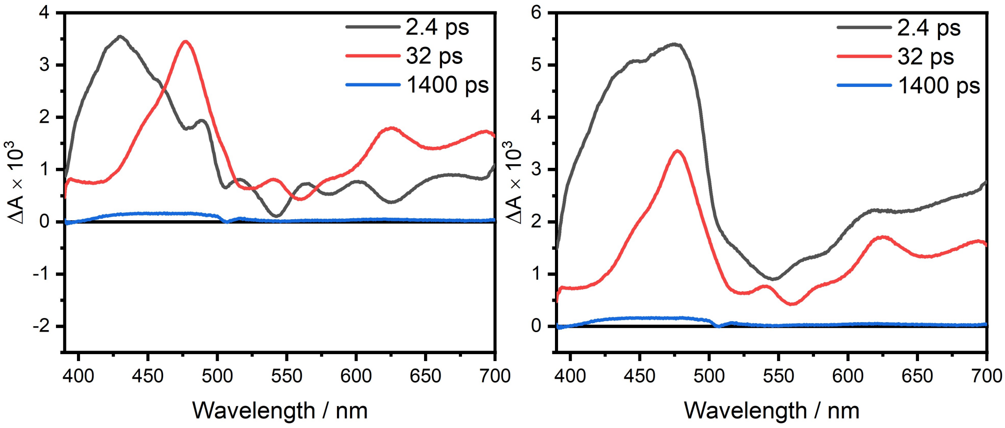

Figure 5.9: Decay associated spectra (left) and evolution-associated spectra (right) for the transient absorption of Complex 3.1 (3-PTZ-Pt-NDI).

5.3.2 NDI-Pt-3-PTZ-PTZ-(OMe)$_2$ (Complex 3.2)

In Complex 2.2, the ESA signals present at 474 and 631 nm along with growth of signal at 541 nm are assigned to NDI- anion. This is indicative that a ^{3}CT state has been formed rapidly with a lifetime of 3 ps. This is similar to the rate of formation of the ^{3}CT state in Complex 2.1. This is consistent as the modifications are on the donor, shows that coupling between donor and Pt bridge doesn't affect rate of electron transfer between Pt bridge and acceptor. One DAS lifetime of 42 ps is required to fit first decay of this ^{3}CT state, which will be called ^{3}CT state$_1$. Then a second DAS lifetime of 3470 ps is required to fit the decay of the second ^{3}CT state, which will be denoted ^{3}CT state$_2$. It is clear that the additional PTZ donor increases the lifetime of the ^{3}CT state and therefore decreases the rate of charge recombination. The additional PTZ donor increases the lifetime of the ^{3}CT by a factor of 5 compared to Complex 2.1. There are no clear ESA bands which are assigned to the PTZ$^+$ cation[76–78] in the TA therefore TRIR is needed to clarify further the identity of the ^{3}CT state$_2$. The corresponding EAS and DAS spectra are shown in Figure 5.10.

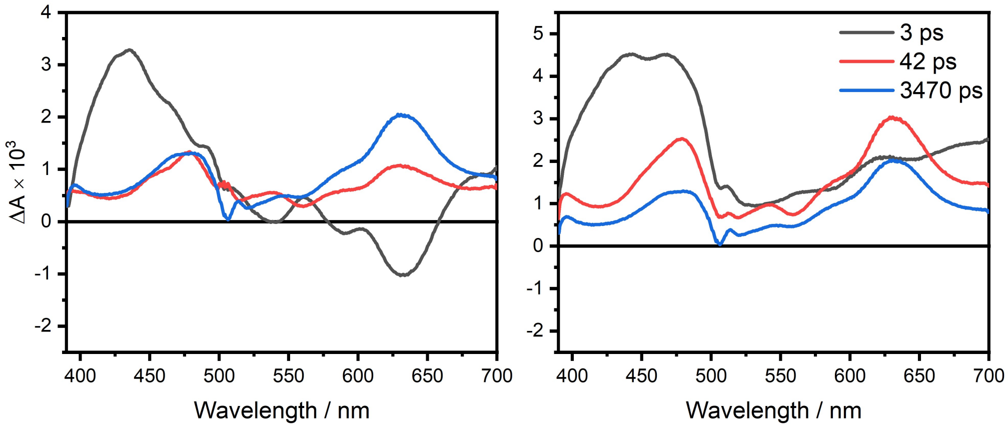

Figure 5.10: Decay associated spectra (left) and evolution-associated spectra (right) for the transient absorption of Complex 3.2 (OMe-PTZ-3-PTZ-Pt-NDI)

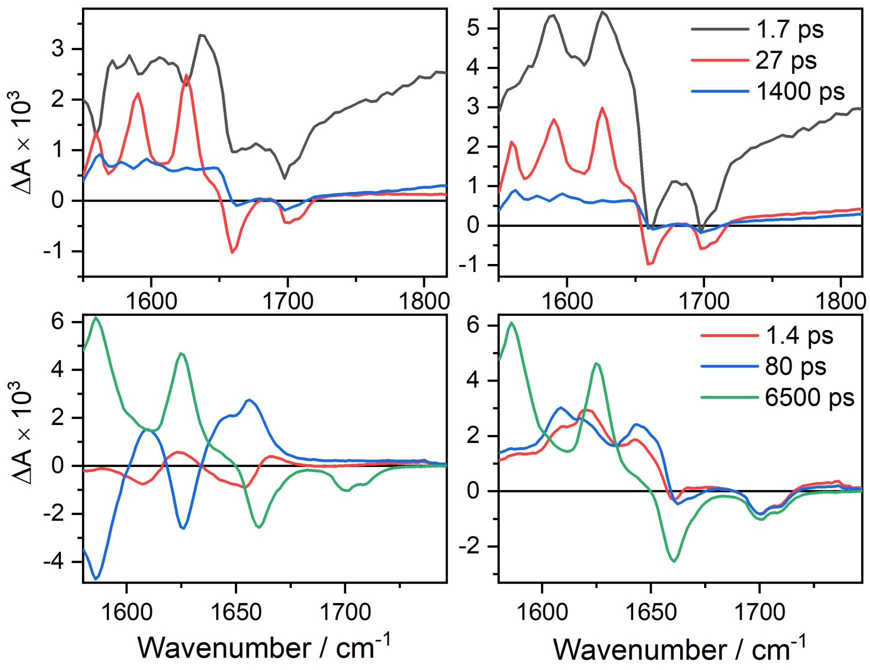

Figure 5.11: Top panels show the GLA for the TRIR of Complex 3.1, bottom panels show the GLA for the TRIR for CompleX 3.2

5.4 TRIR

5.4.1 NDI-Pt-3-PTZ (Complex 3.1)

In Complex 3.1 in DCM, there is no distinctive transient acetylide band at around 2100 cm^{-1} which is seen in other NDI complexes i.e in Complexes 1-4, which indicates formation of a ^{3}CSS. The ESA bands at 1589 and 1626 cm^{-1} are already present at zero time.

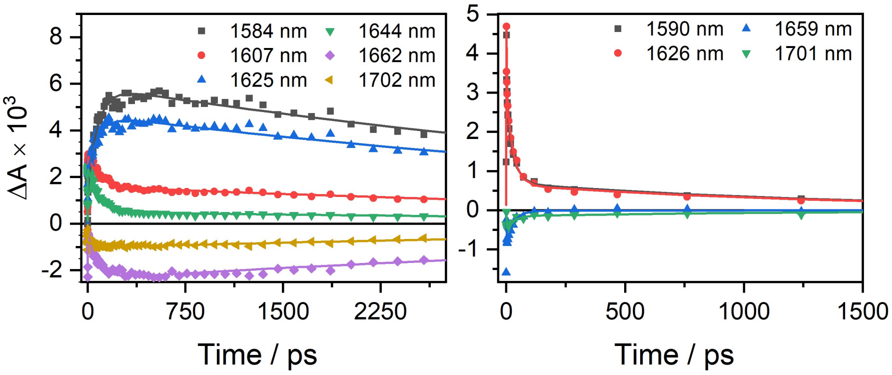

Figure 5.12: Kinetics of left panel (OMe-PTZ-3-PTZ-Pt-NDI) and right panel (3-PTZ-Pt-NDI).

These ESA bands are consistent with previously reported NDI-localised excited state carbonyl vibrations. In previous complexes a change in electron density is seen, whereby the ν(CO) bands shift to lower energies. This doesn't necessarily discount the possibility that a ^{3}CSS has formed, as a ^{3}CSS could have formed almost instantaneously. However, combining the findings from both the TA and TRIR data, it is more likely that this is a CT state, as there is no shift in the carbonyl bands. The bands that are assigned to the ^{3}NDI state are also present and at late time there is either shift back to the ^{3}NDI state or decay of the other ESA band just reveals this state more clearly. DFT theory calculations suggest that the first two triplet states, T_1 and T_2 are both ^{3}CSS so it is possible that a ^{3}CSS has been formed. There has been no ^{3}CSS formed which was also seen in Complex 2.1, which is an analogous compound with a 1,8-Naphthalimide acceptor instead of NDI. It is clear that when the donor is a strongly conjugated donor it has a significant impact on whether or not a ^{3}CSS is formed. This could be due to the fact that the PTZ donor being highly conjugated to the Pt bridge moeity, so that the electron on the PTZ and the Pt are no longer separated in space. Although the ET rate is determined by coupling, as the donor has been incorporated into the structure of the bridge, they are no longer separate entities. In previously studied complexes such as Complex 1, the CV of the PTZ doesn't shift, which proves that there is not much communication between PTZ and the Pt. However, in Complex 3.1, the electron which comes from the HOMO (highest occupied molecular orbital) is now shared between Pt bridge and the PTZ.

5.4.2 NDI-Pt-3-PTZ-PTZ-$(OMe)_2$ (Complex 3.2)

For Complex 3.2 the bands present initially at 1608, 1620 and 1643 cm^{-1} are consistent with previously reported NDI-localised excited state carbonyl vibrations. There is a blueshift of the transient ν(CO) signals from 1608, 1620 and 1643 cm^{-1} to 1585 and 1625 cm^{-1}. The shift in the transient ν(CO) signals indicates a change in the electronic environment around the NDI-localised vibrations, suggesting a change in electronic state. These new ν(CO) bands are consistent with those previously reported in the FTIR spectrum of the one-electron reduced NDI-Pt-Cl complex.[72] Therefore, it is likely that the new excited state has an electron density distribution on the NDI ligand consistent with that of the NDI radical anion. This suggests that the new excited state formed is a ^{3}CT state, whereby the NDI is formerly reduced. One DAS lifetime of 6500 ps (Figure 5.12 and 5.11) was required to fit the decay of the ^{3}CT state. The FTIR frequencies are all similar for Complexes 1, 3.1 and 3.2 but Complex 3.2 is much more similar to Complex 1 in the excited state. The carbonyl vibrations shift to lower energies in Complex 1 and 3.2, whereas in Complex 3.1 they are already present and lower energy at zero time. This can be seen clearly in Table 5.1, which shows the carbonyl and acetylide vibrational frequencies present in Complexes 1, 3.1 and 3.2, for both FTIR and TRIR experiments. The lifetimes for both TA and TRIR of Complex 3.1 and 3.2 can be found in Table 5.2. However, unlike in Complex 1 there is no peak present at around 2120 cm^{-1} where the ^{3}CSS normally is. Complex 3.2 is more similar to Complex 1 than Complex 3.1 despite the first donor being conjugated strongly in Complex 3.1 and 3.2 as the second donor in Complex 3.2 is weakly conjugated to the first donor. When comparing these DBA complexes to complexes to those found in literature with the same attachment of the NDI acceptor[79] a key difference is that unlike in complexes found in the literature the ^{3}CSS is no longer formed due to the modifications on the donor. It is hypothesised that when the donor is strongly conjugated i.e bonded through the aromatic ring it no longer acts as an efficient donor. This could be because the aromatic ring is too stable and does not wish to donate electrons. In Complex 3.2 there is a stronger donor attached to a weaker donor which increases electron donating ability. The nitrogen needs to be directly bonded into the donor for it to be an efficient donor. It would be useful to add methoxy groups onto Complex 2.1 and 3.1 in order to increase electron donation ability and to see if this would have any effect on the excite states formed.

Complex	τ / ps (TA)	τ / ps (TRIR)
3.1	2.4 ps	1.7 ps
	32 ps	27 ps
	Constant	Constant
3.2	-	0.02 ps
	3.0 ps	1.4 ps
	42 ps	80 ps
	3500 ps	6500 ps

Table 5.2: Table to show TA and TRIR lifetimes for Complexes 3.1 and 3.2.

5.5 DFT calculations

Density difference calculations (electron density difference between S_0 and corresponding triplet state) have been performed by by Heather Carson in the Meijer group. The calculations predict that T_1, the lowest lying triplet state, is a ^{3}CSS with an energy of 1.487 eV. This is the lowest energy out of all complexes studided in this thesis. However, from the experimental work, it was hypothesised that no ^{3}CSS had been formed and that T_1 was a state with charge transfer character but without significant electron density loss from the donor. T_2, is predicted to be a ^{3}NDI state. When comparing Complex 3.1 to the complex where the donor is also strongly coupled but the acceptor is weakly coupled the ^{3}CSS is also the lowest state. Also the energy of the T_1 state is 0.09 eV higher in Complex 2.1, compared to when the acceptor is weakly coupled. This implies that the coupling of the acceptor does not have as much of significant impact on the ordering and energies of the states when compared to NAP bearing molecules.

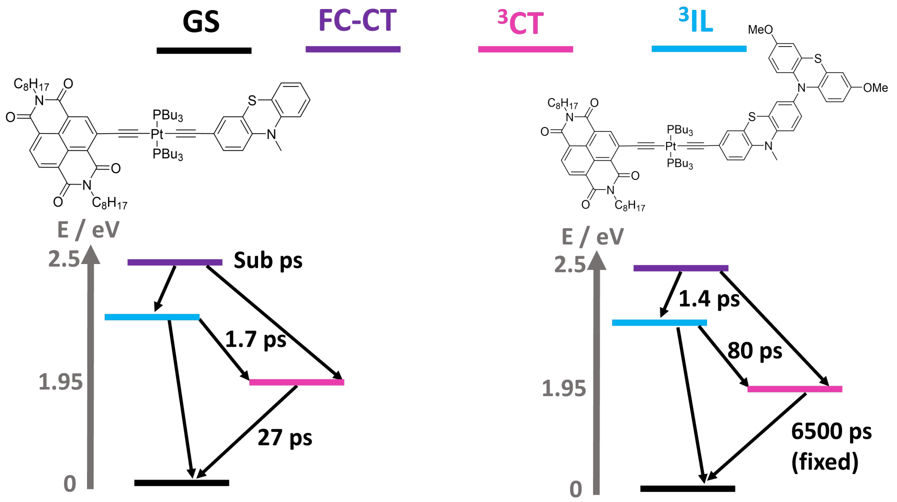

Figure 5.13: An energy level diagram showing the excited state processes following excitation at 500 nm, in DCM, for Complexes 2.1 and 2.2 (left to right). The energies of the states have been estimated using emission in DCM and hexane.

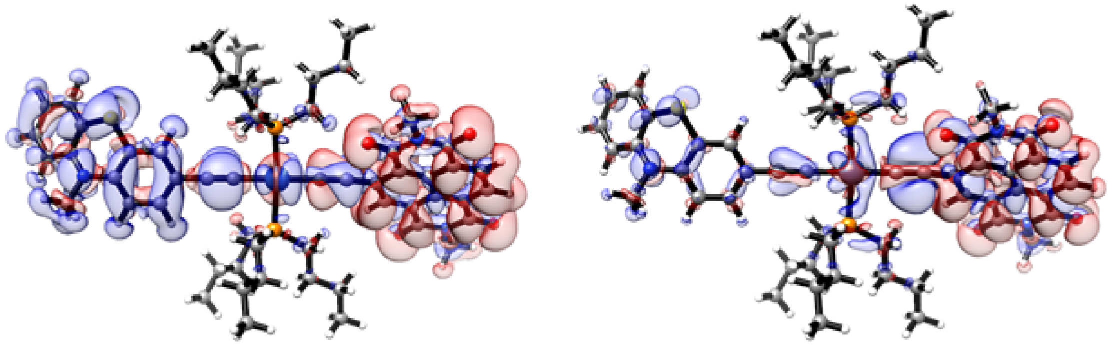

(a) T_1 (b) T_2

Figure 5.14: T_1 and T_2 electron density difference diagrams for Complex 3.1. Blue indicates loss of electron density, whereas red indicates gain in electron density.

5.6 Conclusions

Both Complex 3.1 and 3.2 undergo branching after the initial FC-CT state is formed, to form at least two states. The two most likely states being a ^{3}NDI state and a ^{3}CT state. In Complex 3.1, the ^{3}CT state state has fully decayed by 1000 ps, leaving only a small residual signal assigned to the ^{3}NDI state. The most striking difference seen between the complexes is in the low frequency TRIR data and the dynamics of the states. In Complex 3.2, in the low frequency data there is a shift in the carbonyl frequencies to lower energy, indicating a change in excited state. However, in Complex 3.1 the carbonyls are already at the lower frequency position at early time and so no shift in energy is seen at all throughout the experiment. This is very different to other previously studied NDI bearing donor-bridge-acceptor complexes. The other clear difference between the two complexes is the longevity of the states. The final ^{3}CT state is still present at 6000 ps in Complex 3.2, which is owed to the additional donor increasing the lifetime of the state by a factor of 5. There is no ^{3}CSS formation in either complex. Therefore, it is clear that the combination of a strongly coupled donor and acceptor did not achieve the desired effect i.e a long lived charge separated state. This could be due to the fact that the donor is so strongly conjugated it no longer acts as an efficient donor. This could be because the aromatic ring is too stable and therefore it is no longer favourable to donate electrons.

Chapter 6

Vibrational modulation of the excited dynamics of a series of Donor-Brideg-Acceptor complexes

In this chapter, a UV_{pump}-IR_{pump}-IR_{probe} pulse sequence is utilised to interrogate the effect of bridge localised vibrations on the charge-separation (”Vibrational Control”) in the Pt(II) trans-acetylide complexes investigated in chapters 3-5. The influence of molecular structure and driving force of charge separation on the efficiency of vibrational control is examined by comparing a series of Donor-Bridge-Acceptor molecules.

6.1 Previous Work

The vibrational control of electron transfer has been previously studied in the analogous complexes NAP-Pt-Ph-CH_2-PTZ and NDI-Pt-Ph-CH_2-PTZ.[75] The complexes studied here differ only by the strength of the acceptor. NAP is a weaker acceptor than NDI, which alters the dynamics substantially between the complexes. In NAP-Pt-Ph-CH_2-PTZ, the Franck-Condon state is populated via excitation with a laser pulse centred at 400 nm. This state then decays on a sub 500 fs timescale, to form a CT State. The CT state branches over three pathways: 1. to a ^{3}CSS, 2. to a ^{3}NAP state, 3. charge recombination to form the ground state. Three-Pulse experiments were conducted on NAP-Pt-

Ph-CH_2-PTZ in the following manner. 2 ps after excitation at 400nm the asymmetric acetylide absorption band in the CT state (1908 cm^{-1}) was selectively excited. The effect of the perturbation of the acetylide vibration on the subsequent excited state branching was then measured with a broadband IR probe at time delays, T. As a result of the excitation acetylide vibrational mode and after normalisation to the number of IR photons absorbed, it was found that the yield of the ^{3}CSS decreased from 10% ± 1 to 0%. This result demonstrated that the pathway to forming the ^{3}CSS was fully ”switched off”. Effectively, the ET from the PTZ donor moiety to the oxidised bridge was suppressed, while charge recombination to form the ^{3}NAP state was increased by 10 ± 1%. It is hypothesised that the excitation of the acetylide bond leads to an increase in energy gap between the CT state and ^{3}CSS, which makes the CT to ^{3}CSS pathway unfeasible. However, the CT to ^{3}NAP pathway is now either more favourable due to IR excitation or simply the yield of ^{3}NAP increases as a direct result of the CT to ^{3}CSS competing pathway becoming hindered(Figure 6.1). In NDI-Pt-Ph-CH_2-PTZ the ^{3}CSS formation rate is significantly

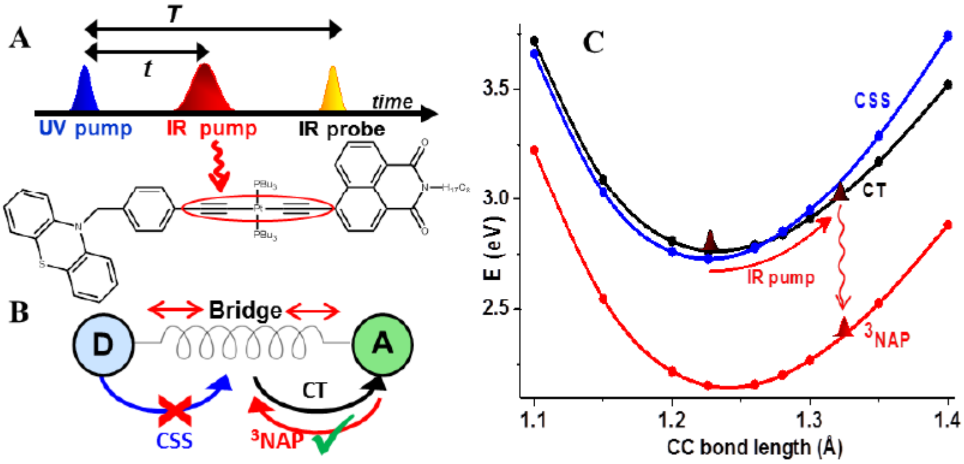

Figure 6.1: A, Shows the order of the UV, IR pump and IR probe and where the IR pump excites the molecule, B, shows the excitation affects the electron transfer pathways, C shows how the elongation of the acetylide bond leads to the CT to ^{3}CSS pathway becoming unfeasible and the CT to ^{3}NAP becoming more favourable. Scheme Courtesy of Milan Delor.

slower than that of NAP-Pt-Ph-CH_2-PTZ, despite NDI being a stronger donor; (1/800 ps) vs (1/14 ps), for the NDI and NAP variants, respectively. The decrease in the charge-separation rate is likely due to the decreased driving force of electron transfer; 0.1 eV vs 0.24 eV for the NDI and NAP variants, respectively. The driving force is decreased as a consequence of the reduced energy gap between the initial IL(CT) state and the ^{3}CSS. Despite the difference in the strength of the acceptors, the vibrational control of the electron transfer observed in the molecules was similar. In NAP-Pt-Ph-CH_2-PTZ the reduction in yield of the ^{3}CSS was 10% and in NDI-Pt-Ph-CH_2-PTZ a 7% decrease in the population of the IL(CT) (corresponding to a subsequent decrease in the ^{3}CSS population as the IL(CT) decays into the ^{3}CSS) was observed (Figure 6.2).

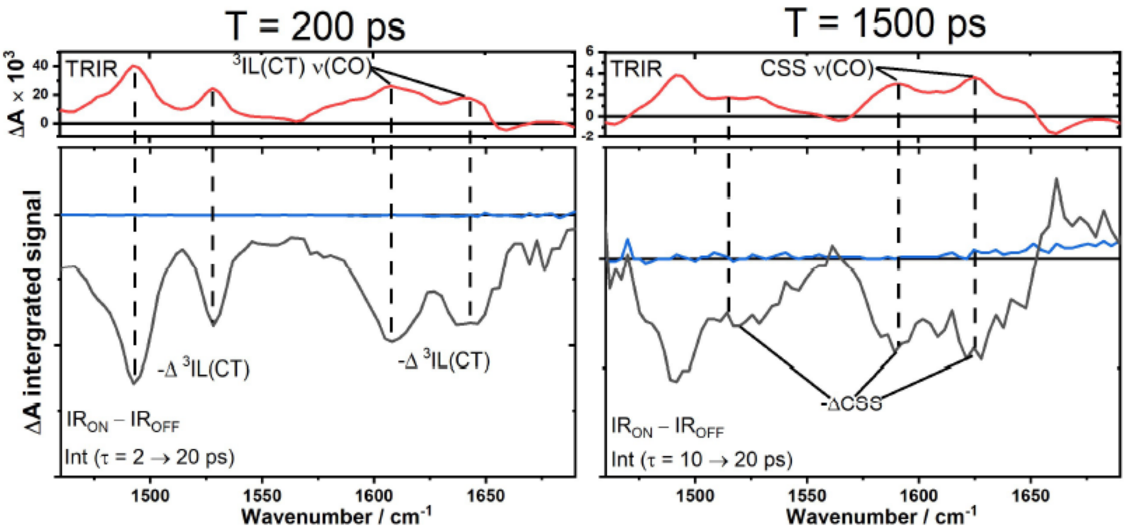

Figure 6.2: (left panel) vibrational control signal of NDI-Pt-Ph-CH_2-PTZ at T = 200 ps, in addition to the corresponding TRIR signal (red trace). (right panel) vibrational control signal of NDI-Pt-Ph-CH_2-PTZ at T = 1500 ps, in addition to the corresponding TRIR signal (red trace) Graph courtesy of Alexander Auty.

6.2 Results and Discussion of T-2DIR for Complexes 2-4

A series of Pt(II) DBA complexes containing the NAP acceptor have been previously studied where the driving force of the formation of the ^{3}CSS is varied by: (1) removal of the CH_2 spacer between the phenyl ring and the donor ligand, and (2) addition of methoxy groups to the PTZ donor. It was previously reported that the larger the driving force of charge separation, the weaker the vibrational control effect i.e., the change in yield of the ^{3}CSS, as a result of excitation of the bridge-localised acetylide mode, becomes smaller..[47]

In this chapter, the influence of vibrational control on the electron transfer in a series of novel Pt(II) Donor-Bridge-Acceptor complexes (both NDI and NAP-containing complexes) is examined. The photophysics of these molecules have already been presented and discussed in Chapter 3, 4 and 5. A schematic of the pump-pump-probe set-up used to collect the data presented in this chapter is shown in Figure 6.3. For all the three-pulse experiments presented in this chapter, the time delay between the UV-Vis pump and IR pump, τ, is set to between 1 and 5 ps. A careful choice of τ is important, in order to ensure that the IR pump can selectively excite the acetylide mode in the appropriate electronic state. In this case the CT state is pumped, as this is the precursor state to the ^{3}CSS. Complexes 1-4 are shown in Figure 6.4.

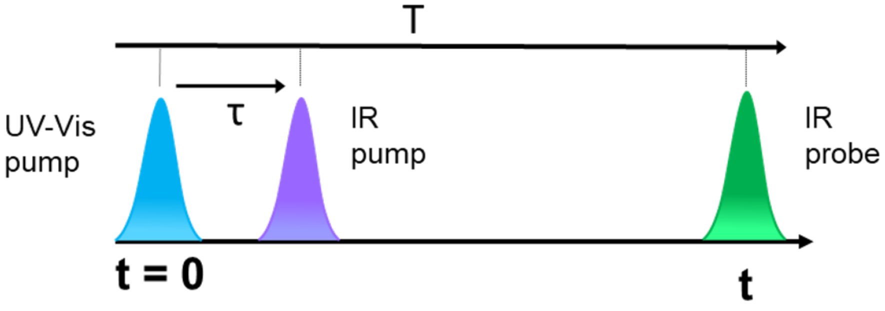

Figure 6.3: Vibrational control experimental set up, where τ, is the time delay between the UV-Vis and the IR pump and T, is the time delay between the UV-Vis pump and the IR probe.

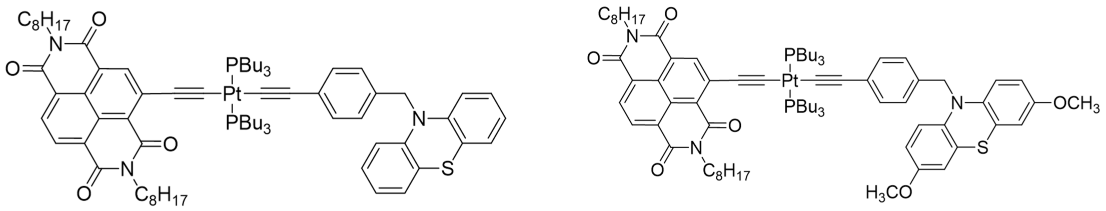

(a) Complex 1

(b) Complex 2

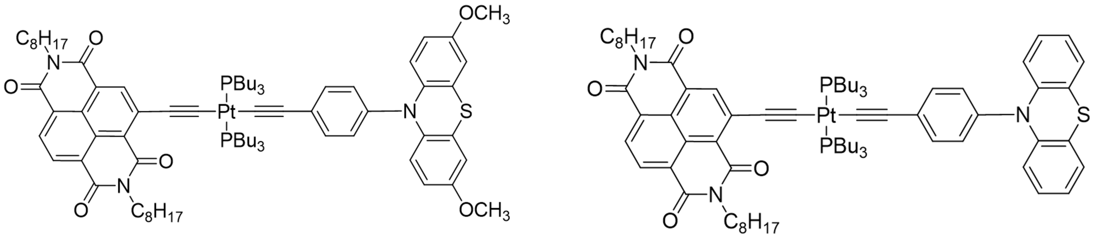

(c) Complex 3

(d) Complex 4

Figure 6.4: Complexes 1-4

6.2.1 NDI-Pt-Ph-Ch$_2$-PTZ-(OMe)$_2$ (Complex 2)

The time delay between the UV$_{pump}$-IR$_{pump}$, is set to 5 ps in the three-pulse experiments of Complex 2. The UV$_{pump}$-IR$_{pump}$-IR$_{probe}$ results are shown in Figure 6.5. The top panel shows the IR Pump OFF data which is equivalent to a UV$_{pump}$-IR$_{probe}$ (TRIR) experiment. The bottom panel shows the IR pump ON - OFF data, which is the differential TRIR signal with the addition of the IR Pump. The visible pump was set to 500 nm, tuned to the ML-LCT transition of Complex 2. The the IR pump energy is set to 1970 cm^{-1}, which corresponds to the acetylide vibration in the ^{3}IL state, indicated by the dashed purple line in Figure 6.5. In the IR Pump ON-OFF data, the black trace at T = 6 ps, after IR at 1970 excitation cm^{-1}, exhibits the self response bleach at the same spectral position as the IR pump. In addition to the self response a corresponding excited state absorption peak is observed at 1895 cm^{-1}. In the red differential spectrum, at T = 200 ps, there is the potential of a very small positive peak at 2067 cm^{-1} corresponding to the ground state v(CC) bleach. This possibly indicates a very marginal increase in the amount of ground state recovery. There is also a negative peak at 2099 cm^{-1} indicating a potential decrease in the population of ^{3}CSS. Clearly these signals are very comparable to the magnitude of the baseline fluctuations, and therefore no concrete conclusions can be drawn. However, a small positive peak is more definitively observed (relative to those outlined above) at 1975 cm^{-1}, suggesting the possibility of a small increase in the population of the ^{3}IL state.

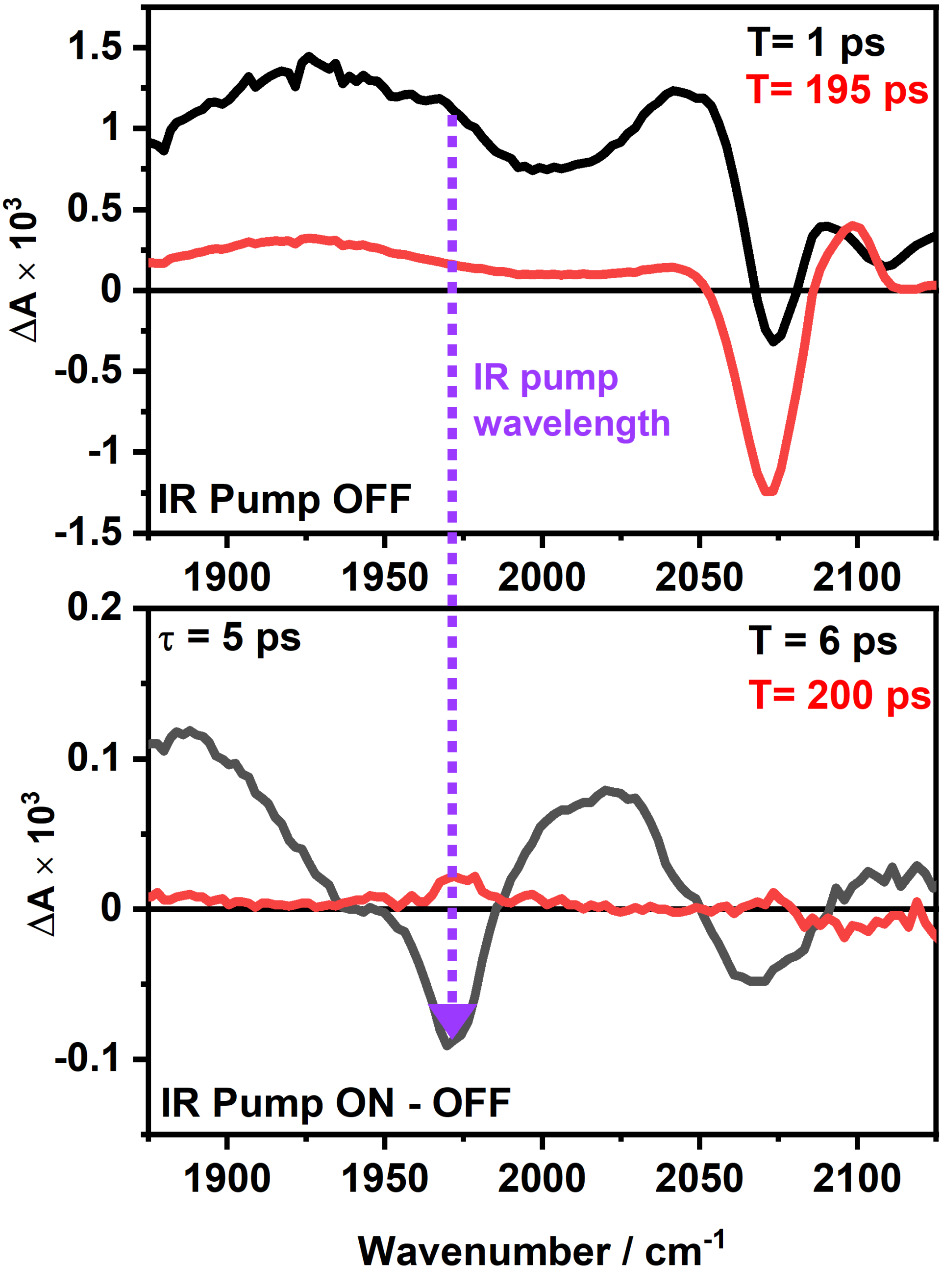

Figure 6.5: TRIR for T = 1, 195 ps (top panel), Vibrational control (bottom panel) for τ = 5 ps, T = 6, 200 ps for NDI-Pt-Ph-Ch$_2$-PTZ-(OMe)$_2$ (Complex 2).

6.2.2 NDI-Pt-Ph-PTZ-(OMe)$_2$ (Complex 3)

The UV$_{pump}$-IR$_{pump}$-IR$_{probe}$ results are shown in Figure 6.6. The top panel shows the IR Pump OFF data which is equivalent to a TRIR experiment. The bottom panel shows the IR pump ON - OFF data, which is TRIR with the addition of the IR Pump. The time delay between the UV$_{pump}$-IR$_{pump}$, τ, is set to 1 ps in Complex 3. The visible pump was set to 500 nm, tuned to the ML-LCT transition of Complex 3, whereas the IR pump is set to 1970 cm^{-1} which is tuned to the vibration of the acetylide band in the excited ^{3}IL state. The purple dashed arrow indicates the band that the IR pump is targeting. In the IR Pump ON-OFF data, the black trace at T = 2 ps, following IR excitation shows the self response bleach at 1970cm^{-1}, in addition to a corresponding ESA peak at 1945 cm^{-1}. The red trace at T = 200 ps doesn't contain any prominent features, following loss of the memory of the initial IR excitation. This indicates that IR excitation of the acetylide mode does not induce any observable changes in yield of excited states 200 ps after the initial UV excitation. The 200 ps time delay is chosen to ensure that the IR probe is only interrogating the relative changes in excited state yield as a result of the IR excitation at 1 ps. At 200 ps the vibrational memory is lost, so any peaks we see are solely due to changes in excited state yield. At 200 ps the final ^{3}CSS is fully formed, therefore the changes in excited state yield of the ^{3}CSS can be examined solely due to IR excitation. Theory calculations predict that the ^{3}CSS in Complex 3 has the lowest energy (1.53 eV) of all complexes studied in this chapter. The large energy gap between the precursor state and the ^{3}CSS is a potential reason for observing no vibrational control effect in this molecule. In NAP analogues that were previously studied, appending the methoxy groups and removal of the CH$_2$ spacer also increased the precursor state - ^{3}CSS state energy gap, resulting in a hindering of the vibrational control effect.

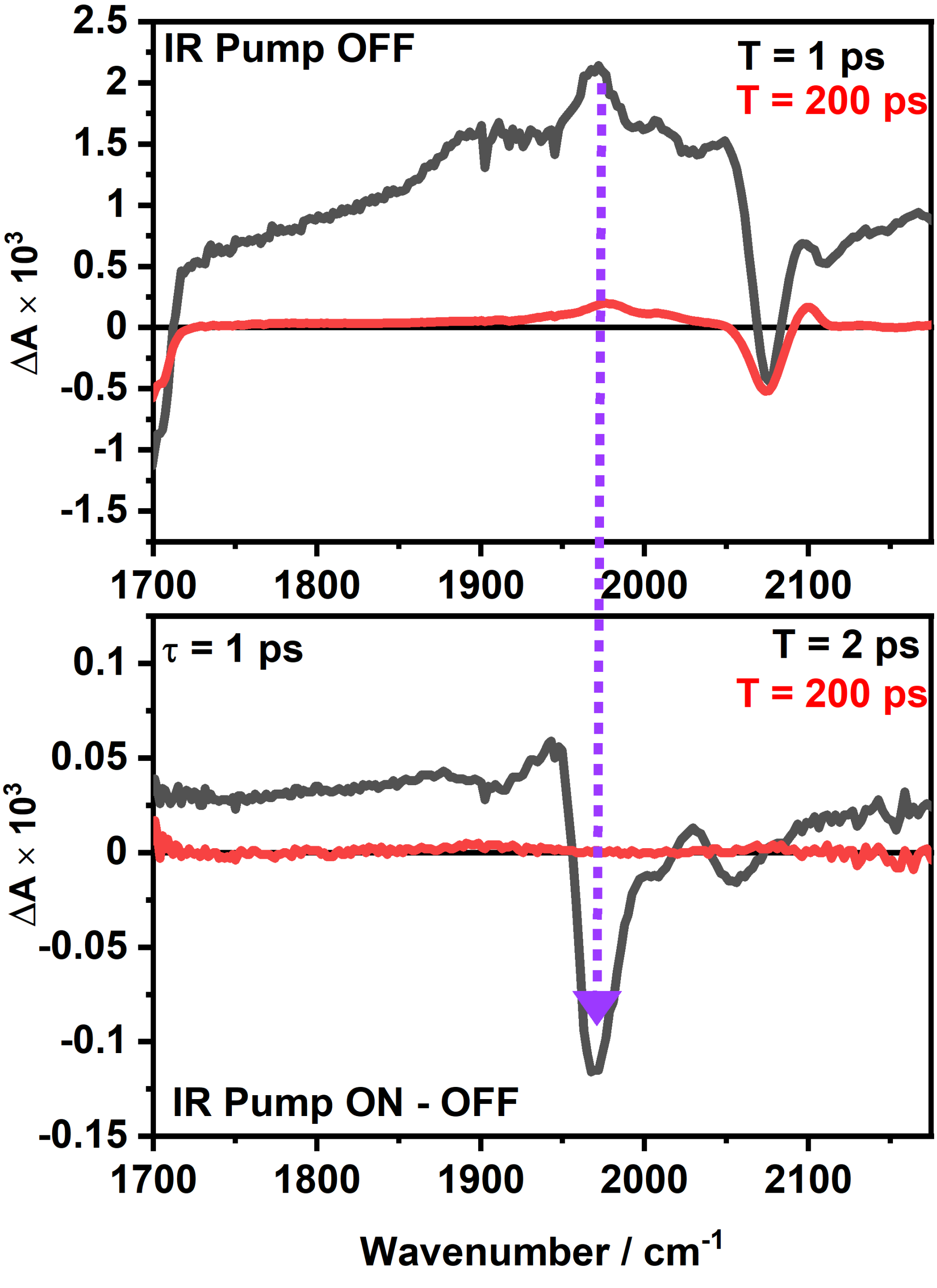

Figure 6.6: TRIR for T = 1, 200 ps (top panel), Vibrational control (bottom panel) for τ = 1 ps, T = 2, 200 ps for NDI-Pt-Ph-PTZ-$(OMe)_2$ (Complex 3)

6.2.3 NDI-Pt-Ph-PTZ (Complex 4)

The TRIR (top panel) and the vibrational control (bottom panel) experimental data for Complex 4 are shown in Figure 6.7. In Complex 4, the time delay between the UV$_{pump}$-IR$_{pump}$, τ, is 2 ps. The visible pump was set to 500 nm, tuned to the ML-LCT transition of Complex 4. The black trace shows the self response peaks due to IR excitation at 1970 cm^{-1}. The IR pump is tuned to the ^{3}IL excited state. The red trace shows the changes in yield of the ^{3}CSS state solely due to IR excitation. The inset shows the positive peak at 2071 cm^{-1} which corresponds to the bleach of the acetylide peak in the ^{3}CSS state in the TRIR. This indicates an increase in bleach recovery. There is a negative peak at 2096 cm^{-1} which corresponds to the transient of the acetylide peak in the ^{3}CSS state in the TRIR. This represents a decrease in ^{3}CSS. An absolute change of 1.25% in the yield of the ^{3}CSS has been estimated by taking ratio of vibrational control signal and TRIR signal at the same UV$_{pump}$-IR$_{probe}$ time delay. When this ratio is normalised to number of IR photons absorbed, which is estimated to be 15%, this is calculated by taking a ratio of the magnitude of the bleach of the IR Pump signal, where you pump, and the transient of the corresponding signal in the TRIR, at the same time delay. The normalised yield is 8%. This yield can be converted into a relative yield change, by considering the yield of the ^{3}CSS, which in the case of complex 4 is estimated to be ca. 66%. The relative yield change in the ^{3}CSS is therefore 12%. This is a similar value to that reported in previously studied NDI complexes, i.e Complex 1 (NDI-Pt-Ph-PTZ), which reported a 7% decrease in ^{3}CSS. Theory calculations also predicted that in this complex no selective excitation would be achievable between the ^{3}NDI and ^{3}CSS state and only acceleration would be possible.

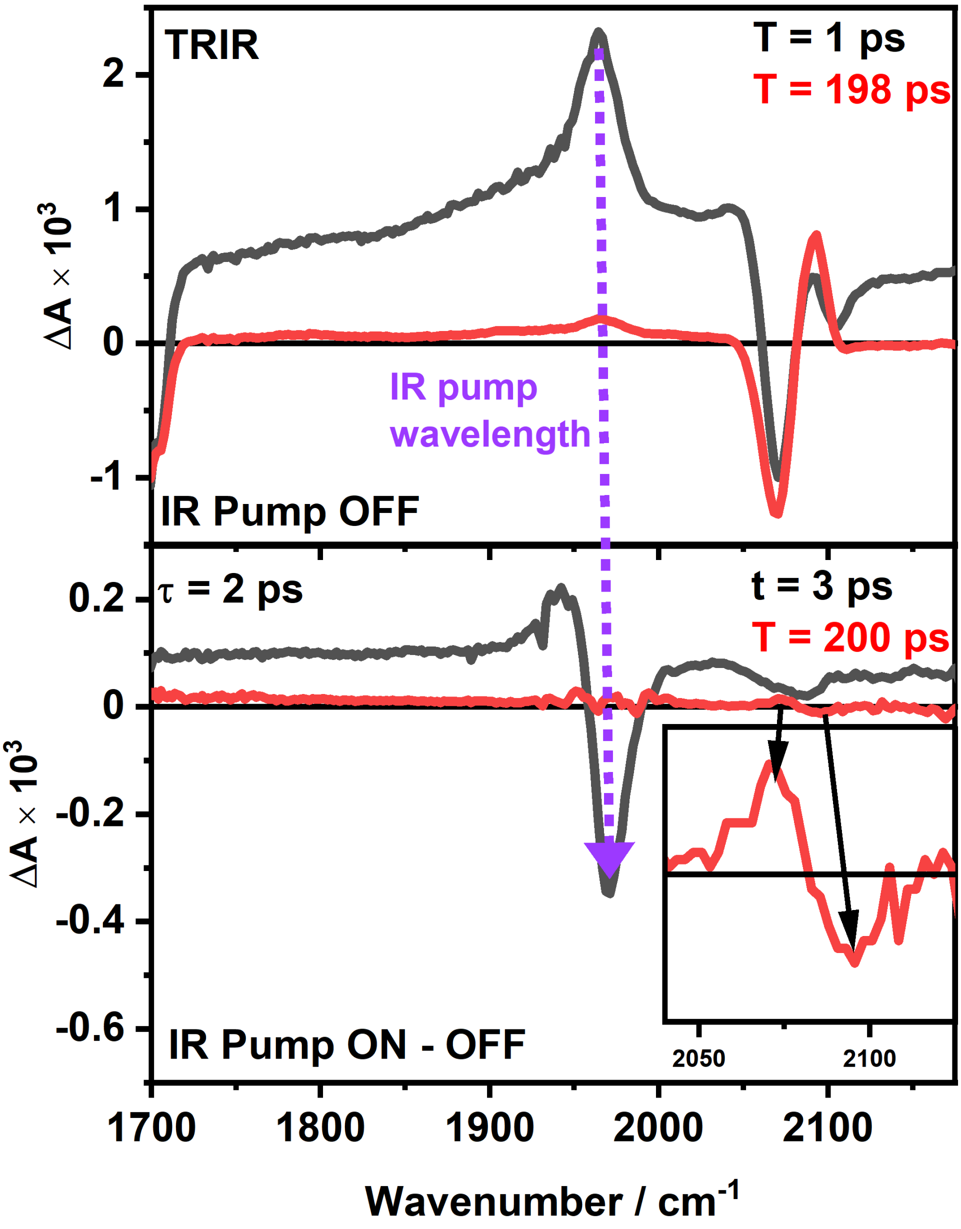

Figure 6.7: TRIR for T = 1, 198 ps (top panel), Vibrational control for τ = 2 ps, T = 3, 200 ps, for NDI-Pt-Ph-PTZ (Complex 4)

6.3 Ground and excited state vibrational spectroscopy of of Complex 2.1 and 3.1

6.3.1 2DIR sprectroscopy of NAP-Pt-3-PTZ (Complex 2.1)

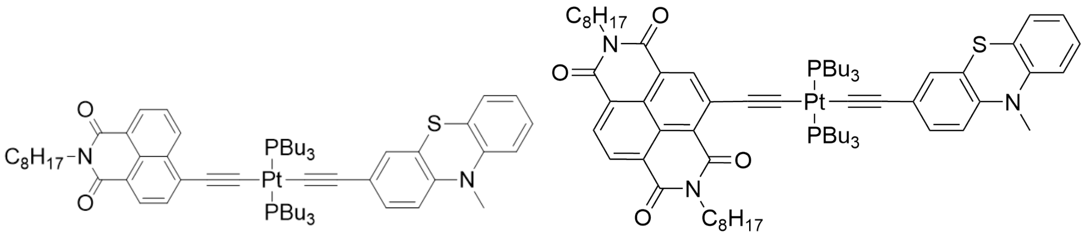

(a) Complex 2.1

(b) Complex 3.1

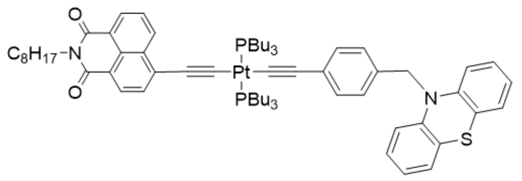

(c) Complex 2.3

Figure 6.8: Complexes 2.1-2.3

Vibrational energy transfer in the electronic ground state, following perturbation of the acetylide modes on the Pt(II) bridge, has been studied in Complex 2.1. Using two broadband IR pumps and a broadband probe, the coupling between the asymmetric acetlyide mode and the ν(CO) and ν(Ar) modes has been investigated and the results are shown in Figure 6.9. Figure 6.9, panels (a) and (b), show the self-response peaks of Complex 2.1 at 465 fs and 45 ps, following excitation of the asymmetric ν(CC) mode at 2090 cm^{-1}. The blue peak positioned at 2090 cm^{-1} represents the bleaching of the $0 \rightarrow 1$ vibrational transition and corresponds to both a reduction in ground state population of the mode and stimulated emission from the $1 \rightarrow 0$ transition. The red peak positioned at 2070 cm^{-1} is the ESA resulting from the $1 \rightarrow 2$ transition of the asymmetric ν(CC) mode, which is blue shifted (20 cm^{-1}) relative to the bleach due to the anharmonicity of the vibrational potential. This anharmonic shift is consistent with previously reported Pt(II) acetylide complexes.[75,80] The majority of the 2D-IR signal decayed by 45 ps. It should be noted that the 2D signal scale bar of the heat maps at a time delay of 45 ps is a factor of 100 times less of that of the early time figure of 465 fs in Figure 6.9. Panels (c) and (d) show three

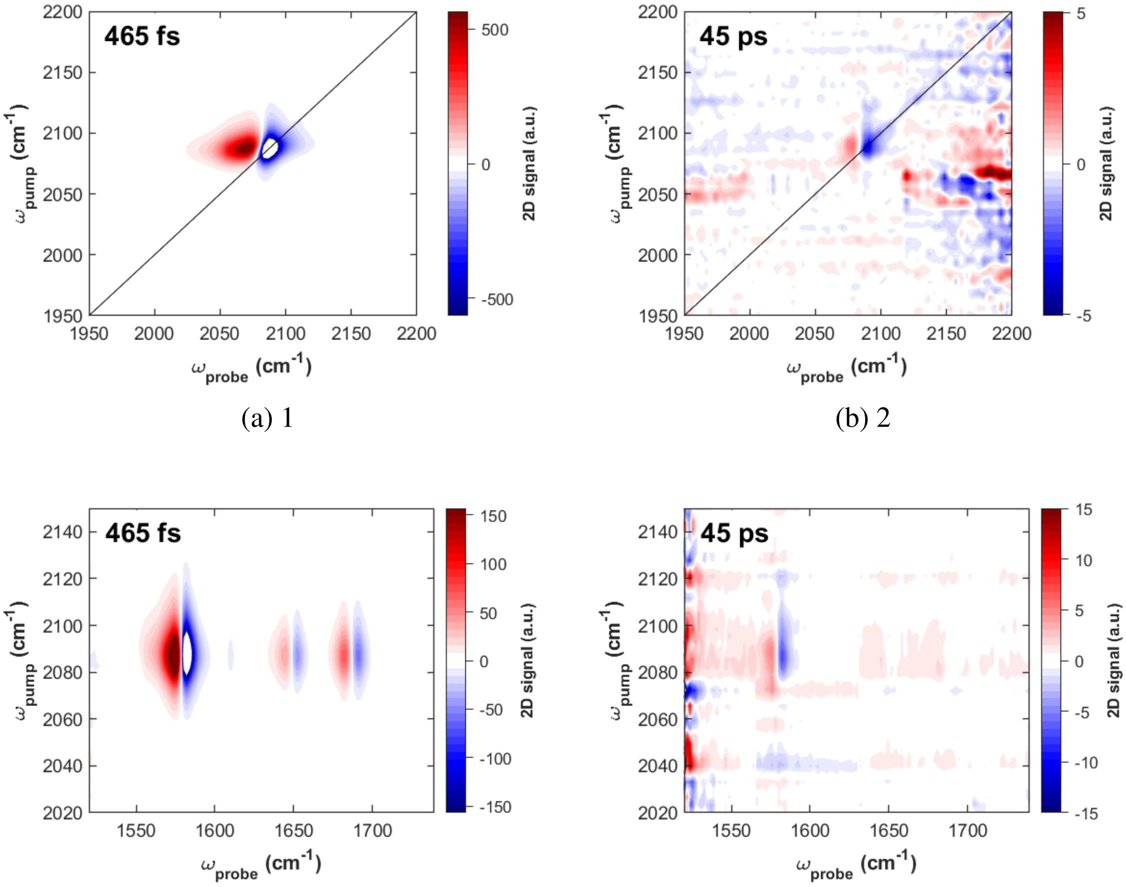

(a) 1

(b) 2

(c) 3

(d)

Figure 6.9: 2DIR of Complex 2.1 in DCM at 465 fs and 45 ps in both high (a and b) and low (c and d) frequency probe regions with pump excitation centred at 2090 cm^{-1}.

cross peak pairs of bleaches and transients at 465 fs and 45 ps, positioned at 1582, 1654 and 1692 cm^{-1} (bleach positions), following excitation of the asymmetric ν(CC) mode at 2090 cm^{-1}. The bleach at 1582 cm^{-1} is assigned to the ν(Ar) vibration on the NAP acceptor. The bleaches at 1654 and 1692 are assigned to ν(CO) vibrations on the NAP acceptor. The accompanying transient signals are positioned at 1574, 1654, 1683 cm^{-1} and demonstrate that the acetylide modes are coupled to the NAP localised modes. These signals are present at zero time, which indicates that excitation of the ν(CC) mode results in an instantaneous response of the aromatic and carbonyl modes. This indicates the carbonyl and acetylide modes are coupled to one another through space. However, from the kinetics it is clear that there is a delayed growth of the carbonyl peaks as they reach maximum signal after that of the acetylide modes, indicating that there could be some population transfer through the molecules' bonds. The ν(CC) modes reach maximum signal at 478 fs. The kinetics shown in Figure 6.10, show that both the recovery of the ν(CC) and the ν(CO) bleaches are biexponential and both recovery fully on the timescale of the experiment (80 ps). The two lifetimes associated with biexponential recovery of ν(CC) bleach are 1.2 and 12 ps. The two lifetimes associated with biexponential decay of the accompanying $1 \rightarrow 2$ ν(CC) transient are 0.95 and 11 ps. The two lifetimes associated with the recovery of the ν(CO) bleaches are 1.1 and 10 ps (symmetric), and 1.3 and 9 ps (asymmetric). The lifetimes associated with biexponential decay of ν(CC) transient, 0.95 and 11 ps, correspond to the ultrafast IVR of the excited ν(CC) mode, followed by slower cooling of the molecule with the surrounding environment (solvent) . The 1.1 ps lifetime is assigned to the initial anharmonic population, the second 10 ps is assigned to their population via IVR from the ν(CC) mode. The transient of the ν(CO) symmetric mode is also decays bi-exponential, the first lifetime is 0.5 ps and the second is 2.9 ps. These lifetimes are consistent with IVR in previously studied Pt(II) based compounds.[75] The transient of the ν(CO) asymmetric mode is also bi-exponential, the first lifetime is 1 ps and the second is 11 ps. The vibrational life times associated with Complex 2.1 are very similar to previously studied complexes.[43] This indicates that the donor conjugation does not have a significant affect on the vibrational coupling between the acetylide bridge and carbonyl acceptor modes in the ground state.

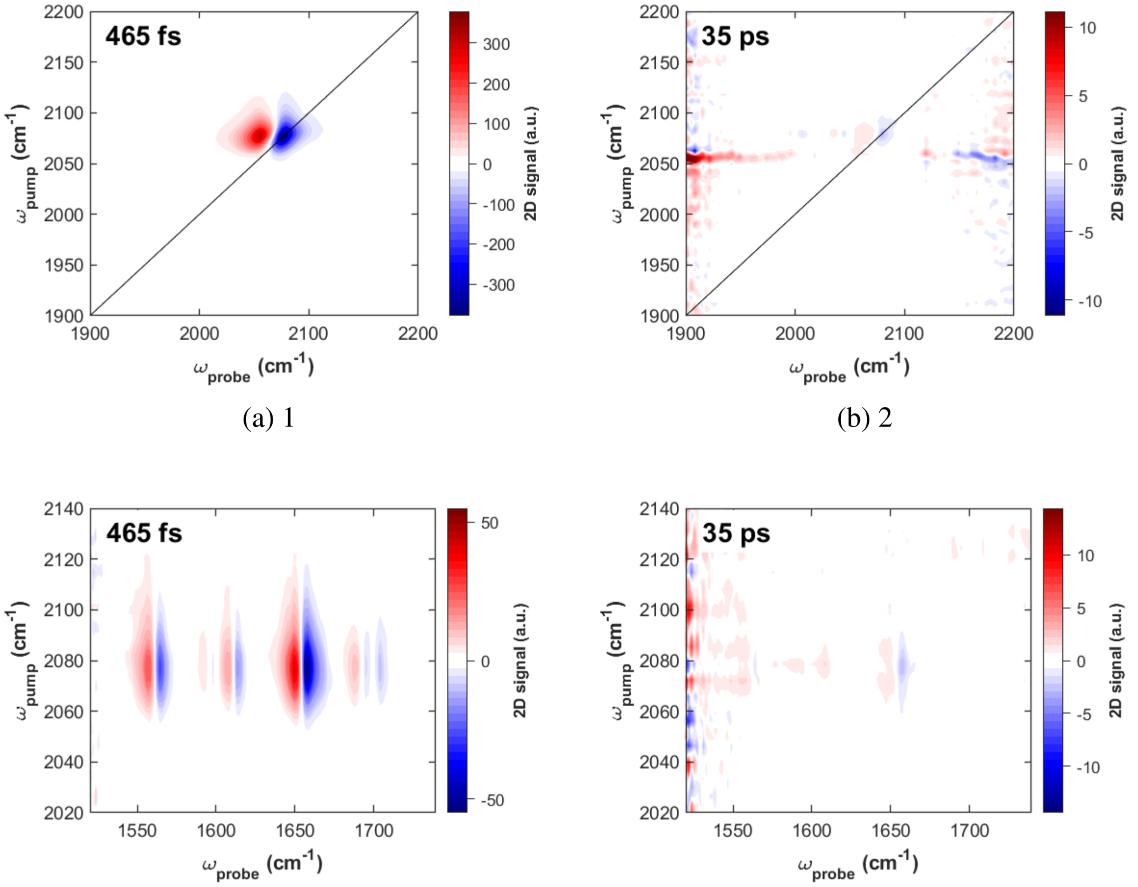

(a) 1

(b) 2

(c) 3

(d)

Figure 6.11: 2DIR of Complex 3.1 in DCM at 465 fs and 35 ps in both high (a and b) and low (c and d) frequency probe regions with pump excitation centred at 2090 cm^{-1}.

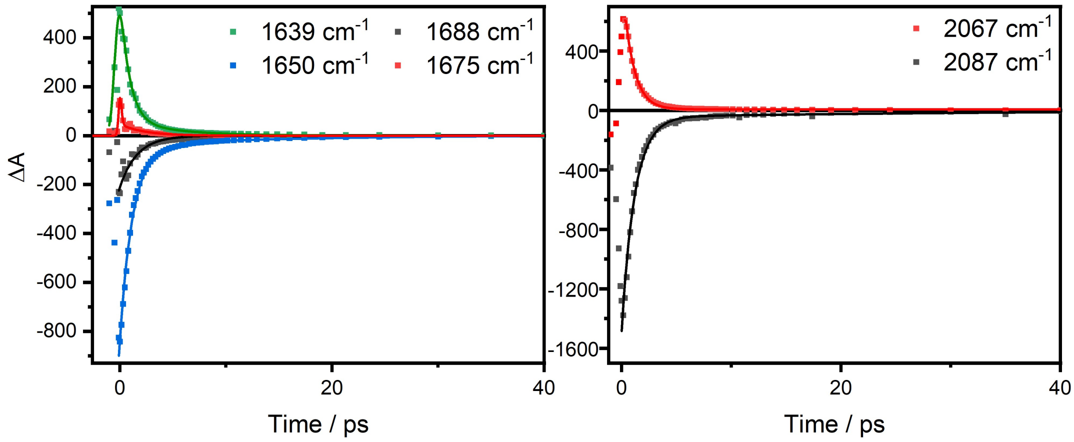

Figure 6.10: Kinetics at various wavenumbers (given as insets) in both low (left) and high (right) frequency regions for pump excitation centred at 2090 cm^{-1} for Complex 2.1.

6.3.2 2DIR spectroscopy of NDI-Pt-3-PTZ (Complex 3.1)

Vibrational energy transfer in the ground state, following perturbation of the acetylide modes in the Pt(II)-bridge has been studied in Complex 3.1. Using two broadband IR pumps and a broadband probe, the coupling between the asymmetric acetlyide mode and the ν(CO) and ν(Ar) modes has been investigated and the results are shown in Figure 6.11. Figure 6.11 shows the ground state 2DIR spectra for high and low frequency probe regions. Panel (a) and (b) show the self response signals of the asymmetric ν(CC) mode at 2090 cm^{-1} in Complex 3.1 at pump-probe delays of 465 fs and 35 ps. The blue peak positioned at 2090 cm^{-1}, representing the bleaching of the $0 \rightarrow 1$ vibrational transition, is due to two contributions, ground state depopulation and stimulated emission from the $1 \rightarrow 0$ transition. The red peak at 2070 cm^{-1} at 465 fs is the accompanying transient and results from the $1 \rightarrow 2$ transition. The transient is blue shifted relative to the bleach by 20 cm^{-1}, due to the anharmonic nature of the transition. This anharmonic shift is consistent with previously reported Pt(II) acetylide molecules. The two lifetimes associated with biexponential decay of ν(CC) transient are 0.89 and 7.2 ps. The shorter 0.89 ps lifetime correspond to the ultrafast IVR of the excited ν(CC) mode, followed by slower cooling of the molecule with the surrounding solvent (7.2 ps). The two lifetimes associated with biexponential decay of ν(CC) bleach 0.08 and 1.72 ps. The cross peaks at 1564, 1615, 1658, 1695 and 1704 cm^{-1} are present at zero time, which indicates that these lower frequency modes are anharmonically coupled with the initially excited acetlyide transition at 2090 cm^{-1}. The bleaches at 1564, 1598, 1615 cm^{-1} assigned to the ν(Ar) vibration on the NDI acceptor, with accompanying transients at 1556, 1592 and 1607 cm^{-1}. The bleaches at 1658, 1695 and 1705 are assigned to the symmetric and asymmetric ν(CO) vibrations on the NDI, which have accompanying transients at 1650 and 1688 cm^{-1}. The cross peaks reach maximum signal at 1 ps, whereas the ν(CC) modes reach maximum signal at roughly 0.35 ps. This could indicate population transfer from the acetylide mode to the lower frequency modes. The kinetics shown in Figure 6.10, show that both the recovery of the ν(CC) and the ν(CO) bleaches are biexponential. The two lifetimes associated with the ν(CO) bleaches are 0.04 and 10.5 ps (symmetric) and 0.01 ps and 12.4

ps (asymmetric). The sub ps lifetime is assigned to the initial anharmonic population, the second 12 ps is assigned to their population via IVR from the ν(CC) mode. The transient of the ν(CO) symmetric mode is also bi-exponential, the first lifetime is 1 ps and the second is 9 ps. The transient of the ν(CO) asymmetric mode is also bi-exponential, the first lifetime is 0.7 and the second is 10 ps. An averaged 11 ps lifetime for decay of symmetric and asymmetric ν(CO) modes in 3-PTZ-Pt-NDI has been calculated, this is the same as that reported in Complex 1 (11 ps). The attachment of the donor has little affect on the depopulation of the carbonyl modes on the acceptor. However, a striking difference between Complex 3.1 and Complex 1 is the significantly shorter lifetime of the acetylide bleach/transient pairs in Complex 3.1. In Complex 3.1 the acetylide bleach reaches a maximum at 0.35 ps compared to 2.5 ps in Complex 1. The stronger conjugation of the donor in Complex 3.1 significantly shortens the VC lifetime.

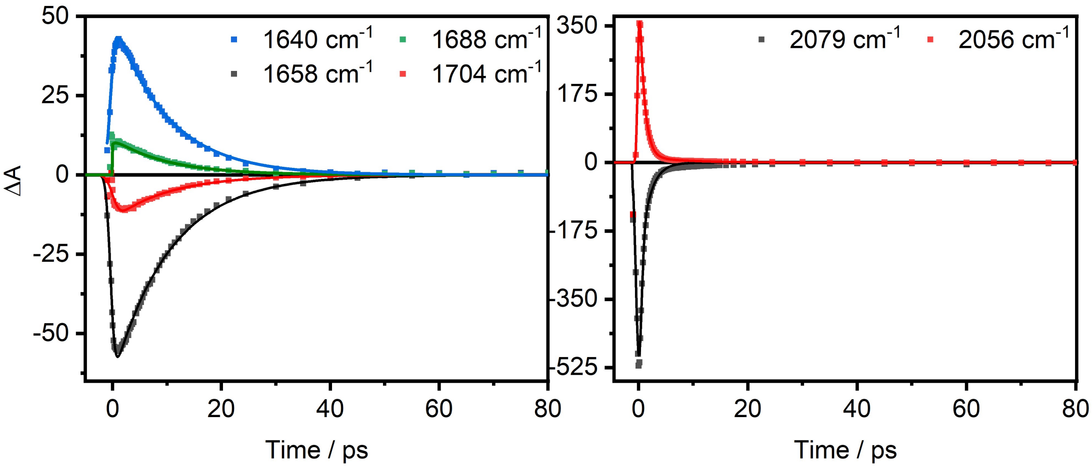

Figure 6.12: Kinetics for both low (left) and high (right) frequency regions at various wavelengths which are given as insets on the graphs, following excitation at 2079 cm^{-1} for Complex 3.1.

	Bleach		**Transient**	
Complex	carbonyl region	acetylide region	carbonyl region	acetylide region
1	11 ps	1.2, 12 ps	11 ps	1, 12 ps
2.1	9 ps (s), 10 ps (a)	1.2, 12 ps	11 ps	1, 11 ps
3.1	10.5 ps (s), 12 ps (a)	0.08, 1.7 ps	1, 9 ps (s) 1, 10 ps (a)	1, 7.2 ps

Table 6.1: A table of the carbonyl and acetylide vibrational lifetimes for the bleach/transient pairs for Complexes 1, 2.1 and 3.1

6.3.3 Vibrational control of NAP-Pt-3-PTZ (Complex 2.1)

The TRIR (top panels) and the vibrational control (bottom panels) experimental data for Complex 2.1 are shown in Figure 6.13. In Complex 2.1, the time delay between the UV_{pump}-IR_{pump}, τ, is 2 ps. The black trace in the high frequency region at 4 ps relative to the UV pump shows the self response peaks due to IR excitation at 1907 cm^{-1}. The IR pump is tuned to the ^{3}CT excited state. The red trace in the high frequency region at 150 ps relative to the UV pump shows the changes in yield of excited states state solely due to IR excitation. The black trace in the IR Pump ON - OFF data at T = 3 ps, shows a negative peak at 1583 cm^{-1} which corresponds to the transient of the carbonyl peak in the CT state in the TRIR. This could indicate a change in the yield or acceleration of the decay of the excited state. However, there are no peaks in the high frequency region or any positive peaks at the corresponding carbonyl bleach positions. This indicates that IR excitation has no long lasting manipulation of excited states. This is very different to Complex 2.3 (NAP-Pt-Ph-CH_2-PTZ), in which the excited state yield was manipulated significantly by IR excitation of the acetylide mode as previously discussed. There could be a few reasons why no vibrational control effect is observed in Complex 2.1. The strong-strong conjugation of the acceptor and donor significantly alters and accelerates the dynamics in both molecules. Therefore that it is difficult to pump initial excited state as it decays very quickly. The IR pump duration is 1 ps in duration, due to it being a narrowband pump, and so therefore the minimum time that the UV-IR pump delay can be set to is 2 ps. Also the fact that the initial excited state decays so quickly means that when probing at later time delays such as T = 150 ps, which are free from self response peaks, it is possible to only probe changes in yield relative to the ^{3}NAP state as the CT state has decayed by this point. Additionally the fact that no selective excitation of the acetylide and/or other vibrational modes was found to have an affect on the yield on any excited states in Complexes 2.1 and 3.1 is confirmed by theory calculations conducted by Heather Carson, in the Meijer group. It was found by conducting theoretical calculations that no vibrational modes exist that are highly similar to the gradient difference vector or the non-adiabatic coupling vector. This indicates that no sole pathway could be achieved by selective excitation, i.e only forming the ^{3}CT or ^{3}NAP state, however, acceleration of decay of states could have been observed.

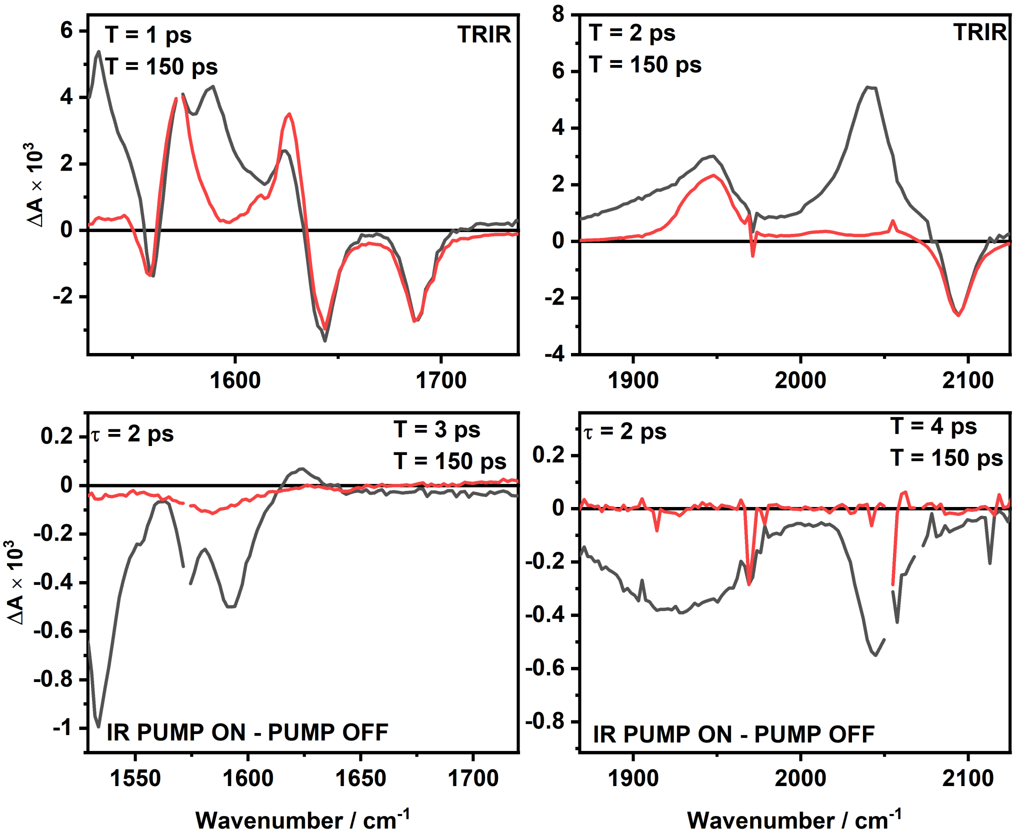

Figure 6.13: Complex 2.1, TRIR is shown in the top two panels, Vibrational control bottom UV excitation at 400 nm, IR excitation at around 1905 cm^{-1}. The black trace represents the earlier time trace, whereas the red trace represents the later time trace.

6.3.4 Vibrational control of NDI-Pt-3-PTZ (Complex 3.1)

The TRIR (top panels) and the vibrational control (bottom panels) experimental data for Complex 3.1 are shown in Figure 6.14. In Complex 3.1, the time delay between the UV_{pump}-IR_{pump}, τ, is 2 ps. The black trace in the high frequency region in the IR pump ON - OFF data at 4 ps relative to the UV pump shows the self response peaks due to IR excitation at 1907 cm^{-1}. The IR pump is tuned to the ^{3}IL excited state. The red trace in the high frequency region in the IR pump ON - OFF data at 150 ps relative to the UV pump shows the changes in yield of excited states state solely due to IR excitation. The red traces in both high and low frequency regions show some positive and negative signal, however, after analysing the signal relative to the negative time delays it appears that this is just noise and no vibrational control effect has been observed. This is the same effect observed in Complex 2.1, whereby no significant vibrational effect was observed. This indicates further that the conjugation of the donor plays a significant part in the excited state dynamics of the complex. For example, when there is strong acceptor weak donor conjugation, in Complex 1 (NDI-Pt-Ph-CH_2-PTZ), the vibrational control effect observed is very different, where a 7% yield decrease of the ^{3}IL excited state. was observed. Similar to Complex 2.1, the dynamics of Complex 3.1 are significantly accelerated compared to that in Complex 1, making the vibrational control experimental more difficult to carry out. This is because ideally the IR pump should excite the initially formed excited state at its maximum population, but as the dynamics are very accelerated the initial ^{3}IL state has decayed significantly. Also it would be ideal to excite the state that is the precursor to ^{3}CSS state, but as no ^{3}CSS state is not formed in Complex 3.1 this is also not possible.

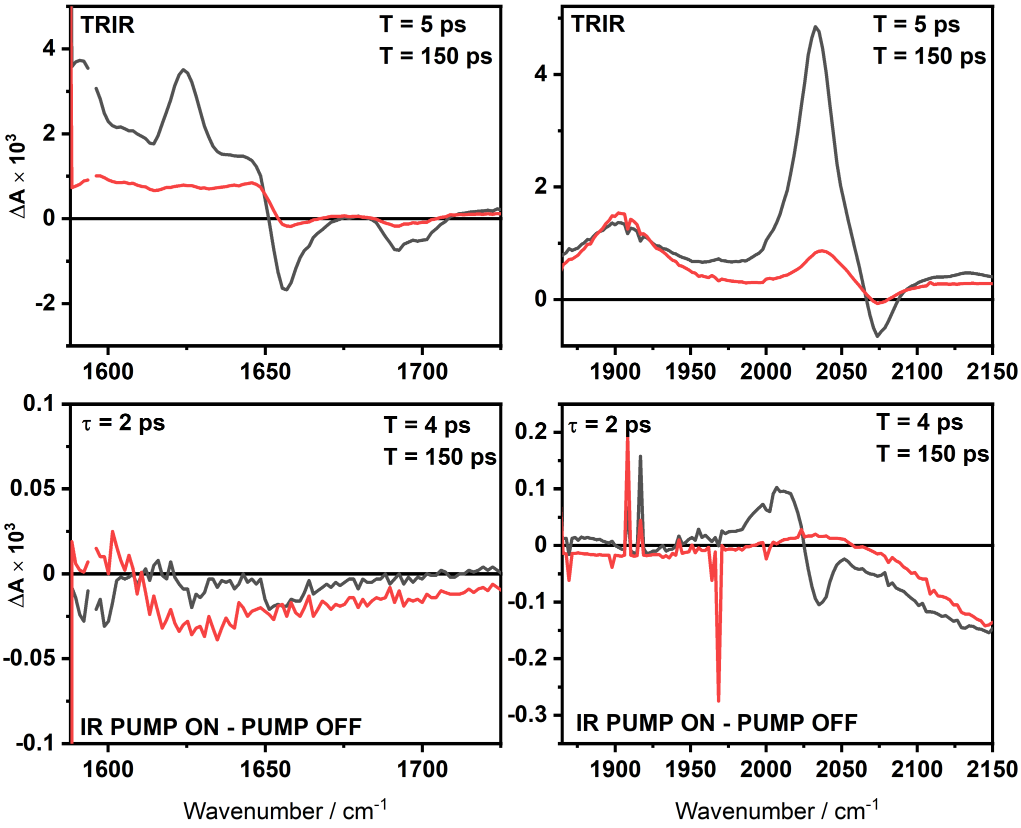

Figure 6.14: In Complex 3.1 the TRIR is shown in the top left and right panels, the vibrational control experiments are shown in the bottom left and right panels. UV excitation at 400 nm, IR excitation at 1974 cm^{-1}. The black trace represents the earlier time trace, whereas the red trace represents the later time trace.

6.4 Conclusions

Overall, the smaller the driving force the more likely that excitation of the acetylide vibration will have an affect on the yield of the ^{3}CSS. In Complexes 2 and 3 the addition of the methoxy groups to the PTZ donor increase the strength of the donor. The stronger the donor, the less effect the selective IR excitation has on the yield. The ^{3}CSS state in Complex 2 and 3 are the lowest out of all complexes and have the biggest energy gap between CT and ^{3}CSS, 1.26 and 1.16 eV respectively. Complex 1 exhibits a relative 7% change in yield and has a 0.84 eV energy gap between the CT and ^{3}CSS state. Complex 4 shows a relative 12% change in yield compared to negligible changes in yield in Complexes 2 and 3, and has a smaller energy gap between the CT and ^{3}CSS being 1.02 eV.

In previous complexes with a weaker acceptor (NAP) a similar trend was also observed whereby the smaller the driving force the greater the yield. The energy gap between the CT and ^{3}CSS vs the change in excited state yield is shown in Figure 6.15 to highlight the trend between driving force and yield. Complex 2.1 and 3.1 showed little difference in the coupling between the acetylide and carbonyl vibrations the ground state vibrational dynamics, indicating that the conjugation of the donor doesn't affect the coupling between the Pt(II) bridge moiety and the acceptor in the ground state, however, the conjugation of the donor clearly has a significant affect on the excited state dynamics. Complex 2.1 and 3.1 showed no change in excited state yield when the acetylide mode was excited with IR light, indicating that no vibrational control effect is observed when there is strong-strong conjugation of the acceptor and donor. It is hard to distinguish if this is due to experimental limitations and if a shorter IR pump could be used would the experiment yield a different affect. In the future, it would be interesting to see if a shorter duration of pulse for the IR pump could be used, with a broader bandwidth, in order to ascertain if any vibrational control affect could be yielded on Complexes 2.1 and 3.1.

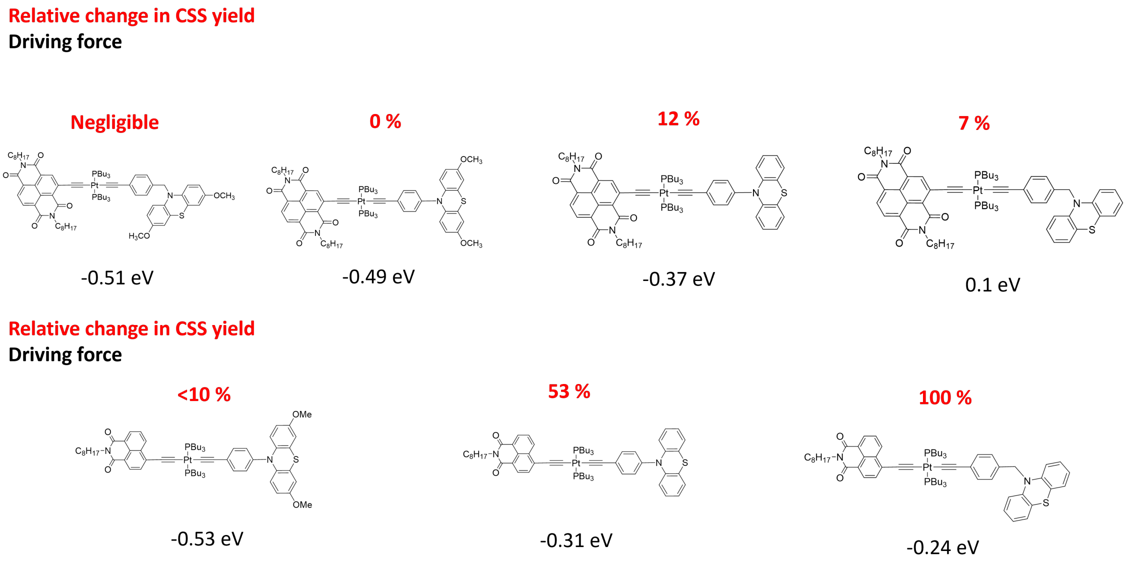

Figure 6.15: Schematic showing trend between driving force of the formation of the charge separated state (black) and percentage relative yield change of the ^{3}CSS due to IR perturbation of various Pt(II) trans-acetylide Donor-Bridge-Acceptor complexes.

Chapter 7

Conclusions and future work

In this thesis, several donor-bridge-acceptor complexes have been studied using a variety of experimental techniques, along with collaborative theory work conducted in the Meijer group. It was found making small changes to the structure of these molecules can have great affects on the dynamics and function of said molecules.

In Chapter three, a series of modified donor-bridge-acceptor complexes were studied using both steady state and ultrafast spectroscopy. It was found increasing the driving force of ET by alterations on the donor had a dramatic affect on the formation and decay of the ^{3}CSS state. In Complex 2, the appended MeO groups to the PTZ donor increased the rate of formation of the ^{3}CSS by a factor of 8 (TA) and 5 (TRIR), relative to the identical complex without the MeO groups (NDI-Pt-Ph-PTZ). This is due to the increased driving force for charge separation. In Complex 3, the removal of a CH_2 spacer and the addition of the MeO groups increases the rate of formation of the ^{3}CSS by factor of 16 (TA) and 18 (TRIR), relative to the unmodified complex,[73] while also decreasing the lifetime of the ^{3}CSS by a factor of 5 (TA) and 4 (TRIR). There is an increase in both the formation and decay rates of the ^{3}CSS due to the dual effect of the increased driving force and conjugation of the PTZ donor to the Pt(II)-bridge. In Complex 4, the removal of the CH_2 spacer group increases the rate of formation of the ^{3}CSS by a factor of 18 (TA) and 16 (TRIR) and decreases the lifetime of the ^{3}CSS by factor of 8 (TA) and 6 (TRIR), relative to the unmodified complex. The removal of the CH_2 spacer group accelerates both charge separation and charge recombination, due to the increased conjugation between the PTZ donor and the Pt(II)-bridge, meaning easier reduction of the oxidised bridge following the charge transfer. When comparing these DBA complexes to similar complexes (NDI-Pt-Ph-CH_2-PTZ, NDI-Pt-Cl, NDI-Pt-Ph and NAP-Pt-Ph-CH_2-PTZ) found in the literature[73] it is clear that the ^{3}CSS states are not as long lived and the rate of formation has significantly been increased. Therefore, there still remains a gap in the research to make DBA complexes with long lived ^{3}CSS states whose yield could potentially be increased via IR perturbation.

In Chapter four, two donor-bridge-acceptor complexes, 3-PTZ-Pt-NAP and OMe-PTZ-PTZ-Pt-Ph-NAP were studied to investigate the effect of having a strongly coupled acceptor and donor and also the effect of having an additional donor and how these modifications affect the excited state dynamics and vibrational energy flow through the system. The addition of a second PTZ donor extends the lifetime of the ^{3}CT by a factor of 9. When comparing these DBA complexes to similar complexes (NDI-Pt-Ph-CH_2-PTZ, NDI-Pt-Cl, NDI-Pt-Ph and NAP-Pt-Ph-CH_2-PTZ) found in the literature,[73,74] the striking difference is that the ^{3}CSS is no longer formed due to the modifications on the donor.

In Chapter five, two donor-bridge-acceptor complexes analogous to those in Chapter five but with an NDI acceptor instead of NAP, 3-PTZ-Pt-NDI and OMe-PTZ-PTZ-Pt-Ph-NDI were studied to investigate the effect of having a strongly coupled acceptor and donor and also the effect of having an additional donor and how these modifications affect the excited state dynamics and vibrational energy flow through the system. The increase in conjugation of the donor reduces the electron donating ability of the donor. The addition of a second PTZ donor extends the lifetime of the ^{3}CT by a factor of 5 with an 1,4,5,8-Napthalene diimde (NDI) acceptor. It would be very useful to have a calculated TRIR spectrum for Complexes 3.1-3.2 to see how the calculated spectra compares to the experimental spectra. This would help to ascertain if the ^{3}CSS looks different to what has been observed in previous complexes, where the acetylide band is usually similar to ground state geometry. When comparing these DBA complexes to complexes (NDI-Pt-Ph-CH_2-PTZ, NDI-Pt-Cl, NDI-Pt-Ph and NAP-Pt-Ph-CH_2-PTZ, Fc–Cu–NDI) to those found in literature with the same attachment of the NDI acceptor[79] a key distinguisment is that unlike in complexes found in the literature the ^{3}CSS is no longer formed due to the modifications on the donor.

In Chapter six, three-pulse experiments were conducted to analyse the affect on yield of various excited states compared to when there is no IR excitation and solely UV excitation. Overall, a trend was observed whereby the larger the driving force the less change in yield due to IR excitation was observed. No change in yield was observed in the strongly conjugated donor and acceptor complexes 3-PTZ-Pt-NAP and 3-PTZ-Pt-NDI. Future work could include using a wider bandwidth IR pump to allow for a shorter temporal pulse. Given that the charge transfer/interligand states are broad, but very short lived in several complexes this could allow for better control of excited states, by exciting them at their maximum signal. In future projects, appending dimethylamine groups, which are stronger electron donating group than methoxy groups, to the donor moeity. This could aid in providing further clarification on the affect of the driving force on the change in yield with IR excitation and UV/Visible excitation. When comparing these DBA complexes to similar complexes found in the literature[45,75] appending the methoxy groups and removal of the CH_2 spacer also increased the precursor state - ^{3}CSS state energy gap, which resulted in a hindering of the vibrational control effect. The complex PTZ-Pt-Ph-NDI also had a similar result, a relative 12% decrease in ^{3}CSS yield compared to 7% decrease witnessed in a similar previously studied complex found in the literature.[73]

Chapter 8

Appendix

8.1 Documentation and data

8.1.1 What data will you collect or create?

I will collect spectroscopic data from TA, TRIR, UV-Vis, FTIR and fluoresence measurements. Furthermore scanned digital copies of my laboratory notebooks will be made containing experimental details.

8.1.2 How will the data be collected or created?

Surface Xplorer will be used to process transient absorption data. I will use UltraView to process TRIR data. I will perform data analysis using OriginPro and Glotaran of all compounds. The raw TA, TRIR, UV-Vis, FTIR and fluoresence data will be in csv file format. The processed data will be stored in Origin and Glotaran project format and the spectra will be stored in jpeg format. Digital scanned copies of laboratory notebooks will be recorded in pdf format on a monthly basis. The files will include date of experiment and or experiment number and the name of the compound. This will amount to around 20 GB of data.

8.2 Ethics and legal compliance

8.2.1 How will you manage any ethical issues?

There no ethical issues surrounding the acquisition of the spectroscopic results for my project as there is no involvement with animals or humans.

8.2.2 How will you manage copyright and Intellectual Property Rights (IPR) issues?

Any work including but not limited to images, graphs and schematics taken directly from papers will be correctly referenced.

8.3 Data Storage and Archiving

8.3.1 How will the data be stored?

Data that has been collected in all formats such as csv, pdf, word and excel will be backed up by a personal external hard drive and on the CiCS server.

8.3.2 How will you manage data security?

Data that has been collected will be stored on the hardrive of the computer which is protected with a password and on the CiCS server which has restricted access.

8.3.3 How will the data be archived?

Data such as scanned copies of laboratory notebooks and spectroscopic data will be kept on the CiCS server in the Professor Weinstein group folder for a minimum of 10 years.

8.3.4 How will the data be shared?

Data will be published in research journals.

8.4 Implementing your plan

I will be responsible for the implementation of my data management plan including the organisation and storage of the data. My supervisor will be responsible for ensuring that the data is stored securely for 10 years on the CiCs server.

Bibliography

(1) I. Dincer, “On thermal energy storage systems and applications in buildings”, *Energy and Buildings*, 2002, DOI: `10.1016/S0378-7788(01)00126-8`.

(2) İ. Dinçer and C. Zamfirescu, *Sustainable energy systems and applications*, Publication Title: Sustainable Energy Systems and Applications, 2012.

(3) I. Dinçer and M. A. Rosen, *Thermal Energy Storage: Systems and Applications, Second Edition*, Publication Title: Thermal Energy Storage: Systems and Applications, Second Edition, 2010.

(4) GOV UK, *Energy Innovation - GOV.UK*, `https://www.gov.uk/guidance/energy-innovation` (visited on 01/07/2020).

(5) HM Government, *The Clean Growth Strategy Leading the way to a low carbon future*, 2017, p. 167.

(6) B. Parida, S. Iniyan and R. Goic, “A review of solar photovoltaic technologies”, *Renewable and Sustainable Energy Reviews*, 2011, **15**, 1625–1636.

(7) F. Wang, C. Li, H. Chen, R. Jiang, L. D. Sun, Q. Li, J. Wang, J. C. Yu and C. H. Yan, “Plasmonic harvesting of light energy for suzuki coupling reactions”, *Journal of the American Chemical Society*, 2013, **135**, 5588–5601.

(8) M. P. Johnson, “Photosynthesis”, *Essays in Biochemistry*, 2016, **60**, Publisher: Portland Press Ltd, 255–273.

(9) I. McConnell, G. Li and G. W. Brudvig, “Energy Conversion in Natural and Artificial Photosynthesis”, *Chemistry & Biology*, 2010, **17**, 434–447.

(10) B. Zhang and L. Sun, “Artificial photosynthesis: opportunities and challenges of molecular catalysts”, *Chemical Society Reviews*, 2019, **48**, 2216–2264.

(11) A. C. Benniston and A. Harriman, “Artificial photosynthesis”, *Materials Today*, 2008, **11**, 26–34.

(12) J. H. Alstrum-Acevedo, M. K. Brennaman and T. J. Meyer, “Chemical Approaches to Artificial Photosynthesis. 2”, *Inorganic Chemistry*, 2005, **44**, 6802–6827.

(13) A. Melis, “Solar energy conversion efficiencies in photosynthesis: Minimizing the chlorophyll antennae to maximize efficiency”, *Plant Science*, 2009, **177**, Publisher: Elsevier, 272–280.

(14) J. R. Bolton and D. O. Hall, “The maximum efficiency of photosynthesis”, *Photochemistry and Photobiology*, 1991, **53**, Publisher: John Wiley & Sons, Ltd, 545–548.

(15) D. Simionato, S. Basso, G. M. Giacometti and T. Morosinotto, “Optimization of light use efficiency for biofuel production in algae”, *Biophysical Chemistry*, 2013, DOI: `10.1016/j.bpc.2013.06.017`.

(16) A. Currao, “Photoelectrochemical water splitting”, *Chimia*, 2007, **61**, 815–819.

(17) R. Amadelli, R. Argazzi, C. A. Bignozzi and F. Scandola, “Design of Antenna-Sensitizer Polynuclear Complexes. Sensitization of Titanium Dioxide with [Ru(bpy)2(CN)2]2Ru(bpy
”, *Journal of the American Chemical Society*, 1990, DOI: `10.1021/ja00176a003`.

(18) M. Grätzel, “Dye-sensitized solar cells”, *Journal of Photochemistry and Photobiology C: Photochemistry Reviews*, 2003, DOI: `10.1016/S1389-5567(03)00026-1`.

(19) B. O’Regan and M. Grätzel, “A low-cost, high-efficiency solar cell based on dye-sensitized colloidal TiO2 films”, *Nature*, 1991, DOI: `10.1038/353737a0`.

(20) M. Grätzel, “Photoelectrochemical cells”, *Nature*, 2001, DOI: `10.1038/35104607`.

(21) M. Grätzel, “Solar energy conversion by dye-sensitized photovoltaic cells”, *Inorganic Chemistry*, 2005, DOI: `10.1021/ic0508371`.

(22) S. Zhang, J. Jin, D. Li, Z. Fu, S. Gao, S. Cheng, X. Yu and Y. Xiong, "Increased power conversion efficiency of dye-sensitized solar cells with counter electrodes based on carbon materials", *RSC Advances*, 2019, DOI: `10.1039/c9ra03344k`.

(23) M. Born and R. Oppenheimer, "Zur Quantentheorie der Molekeln", *Annalen der Physik*, 1927, **389**, 457–484.

(24) J. M. Standard and B. K. Clark, "The Franck-Condon principle and Condon parabolas in a physical chemistry or quantum physics course", *Journal of Chemical Education*, 1999, **76**.

(25) C. X. Sheng, S. Singh, A. Gambetta, T. Drori, M. Tong, S. Tretiak and Z. V. Vardeny, "Ultrafast intersystem-crossing in platinum containing -conjugated polymers with tunable spin-orbit coupling", *Scientific Reports*, 2013, DOI: `10.1038/srep02653`.

(26) P. W. Atkins and J. d. Paula, *Atkins' Physical Chemistry*, Google-Books-ID: sWTYAwAAQBAJ, OUP Oxford, 2014, 1035 pp.

(27) A. M. Kelley, *Condensed-Phase Molecular Spectroscopy and Photophysics*, 2012.

(28) G. W. Robinson and R. P. Frosch, "Electronic excitation transfer and relaxation", *The Journal of Chemical Physics*, 1963, DOI: `10.1063/1.1733823`.

(29) M. Maiuri, M. Garavelli and G. Cerullo, "Ultrafast Spectroscopy: State of the Art and Open Challenges", *Journal of the American Chemical Society*, 2020, DOI: `10.1021/jacs.9b10533`.

(30) R. Berera, R. van Grondelle and J. T. Kennis, "Ultrafast transient absorption spectroscopy: Principles and application to photosynthetic systems", *Photosynthesis Research*, 2009, **101**, Publisher: Springer, 105–118.

(31) R. Marcus, "NOBEL LECTURES, CHEMISTRY 1992, ELECTRON TRANSFER REACTIONS IN CHEMISTRY: THEORY AND EXPERIMENT, DECEMBER 8, 1992", *Nobel Lectures*, 2009.

(32) R. A. Marcus, "On the theory of oxidation-reduction reactions involving electron transfer. I", *The Journal of Chemical Physics*, 1956, **24**, 966–978.

(33) R. A. Marcus, “Electron Transfer Reactions in Chemistry: Theory and Experiment (Nobel Lecture) - Marcus - 2003 - Angewandte Chemie International Edition in English - Wiley Online Library”, *Angewandte Chemie International Edition*, 1993.

(34) T. Van Voorhis, T. Kowalczyk, B. Kaduk, L.-P. Wang, C.-L. Cheng and Q. Wu, “The Diabatic Picture of Electron Transfer, Reaction Barriers, and Molecular Dynamics”, *Annual Review of Physical Chemistry*, 2010, DOI: `10.1146/annurev.physchem.012809.103324`.

(35) E. J. Piechota and G. J. Meyer, “Introduction to Electron Transfer: Theoretical Foundations and Pedagogical Examples”, *Journal of Chemical Education*, 2019, **96**, Publisher: American Chemical Society, 2450–2466.

(36) P. F. Barbara, T. J. Meyer and M. A. Ratner, “Contemporary issues in electron transfer research”, *Journal of Physical Chemistry*, 1996, DOI: `10.1021/jp9605663`.

(37) M. Kuss-Petermann and O. S. Wenger, “Unusual distance dependences of electron transfer rates”, *Physical Chemistry Chemical Physics*, 2016, **18**, Publisher: Royal Society of Chemistry, 18657–18664.

(38) M. Kuss-Petermann and O. S. Wenger, “Unusual distance dependences of electron transfer rates”, *Physical Chemistry Chemical Physics*, 2016, **18**, Publisher: Royal Society of Chemistry, 18657–18664.

(39) M. Sykora, K. A. Maxwell, J. M. DeSimone and T. J. Meyer, “Mimicking the antenna-electron transfer properties of photosynthesis”, *Proceedings of the National Academy of Sciences of the United States of America*, 2000, **97**, Publisher: National Academy of Sciences, 7687–7691.

(40) M. Chergui, “On the interplay between charge, spin and structural dynamics in transition metal complexes”, *Dalton Transactions*, 2012, **41**, Publisher: Royal Society of Chemistry, 13022–13029.

(41) A. Vlček, “The life and times of excited states of organometallic and coordination compounds”, *Coordination Chemistry Reviews*, 2000, **200-202**, 933–978.

(42) P. S. Wagenknecht and P. C. Ford, “Metal centered ligand field excited states: Their roles in the design and performance of transition metal based photochemical molecular devices”, *Coordination Chemistry Reviews*, 2011, **255**, 591–616.

(43) S. A. Archer, T. Keane, M. Delor, A. J. H. M. Meijer and J. A. Weinstein, “C or Not 13 C: Selective Synthesis of Asymmetric Carbon-13-Labeled Platinum(II) cis-Acetylides”, 2012, **12**, Publisher: UTC ISBN: 1153311542, 32.

(44) J. Zhao, S. Ji, W. Wu, W. Wu, H. Guo, J. Sun, H. Sun, Y. Liu, Q. Li and L. Huang, “Transition metal complexes with strong absorption of visible light and long-lived triplet excited states: From molecular design to applications”, *RSC Advances*, 2012, **2**, Publisher: The Royal Society of Chemistry, 1712–1728.

(45) P. A. Scattergood, M. Delor, I. V. Sazanovich, M. Towrie and J. A. Weinstein, “Ultrafast charge transfer dynamics in supramolecular Pt(II) donor-bridge-acceptor assemblies: The effect of vibronic coupling”, *Faraday Discussions*, 2015, **185**, Publisher: Royal Society of Chemistry, 69–86.

(46) I. V. Sazanovich, J. Best, P. A. Scattergood, M. Towrie, S. A. Tikhomirov, O. V. Bouganov, A. J. Meijer and J. A. Weinstein, “Ultrafast photoinduced charge transport in Pt(ii) donor-acceptor assembly bearing naphthalimide electron acceptor and phenothiazine electron donor”, *Physical Chemistry Chemical Physics*, 2014, **16**, Publisher: The Royal Society of Chemistry, 25775–25788.

(47) M. Delor, I. V. Sazanovich, M. Towrie, S. J. Spall, T. Keane, A. J. Blake, C. Wilson, A. J. Meijer and J. A. Weinstein, “Dynamics of ground and excited state vibrational relaxation and energy transfer in transition metal carbonyls”, *Journal of Physical Chemistry B*, 2014, **118**, Publisher: American Chemical Society, 11781–11791.

(48) P. Antoniou, Z. Ma, P. Zhang, D. N. Beratan and S. S. Skourtis, “Vibrational control of electron-transfer reactions: A feasibility study for the fast coherent transfer regime”, *Physical Chemistry Chemical Physics*, 2015, DOI: `10.1039/c5cp00610d`.

(49) D. N. Beratan, S. S. Skourtis, I. A. Balabin, A. Balaeff, S. Keinan, R. Venkatramani and D. Xiao, “Steering electrons on moving pathways.”, *Accounts of chemical research*, 2009, DOI: `10.1021/ar900123t`.

(50) Z. Lin, C. M. Lawrence, D. Xiao, V. V. Kireev, S. S. Skourtis, J. L. Sessler, D. N. Beratan and I. V. Rubtsov, “Modulating unimolecular charge transfer by exciting bridge vibrations”, *Journal of the American Chemical Society*, 2009, DOI: `10.1021/ja907041t`.

(51) T. X. Leong, B. K. Collins, S. Dey Baksi, R. T. Mackin, A. Sribnyi, A. L. Burin, J. A. Gladysz and I. V. Rubtsov, “Tracking Energy Transfer across a Platinum Center”, *Journal of Physical Chemistry A*, 2022, DOI: `10.1021/acs.jpca.2c02017`.

(52) C. E. Mccusker, A. Chakraborty and F. N. Castellano, “Excited State Equilibrium Induced Lifetime Extension in a Dinuclear Platinum(II) Complex”, *J. Phys. Chem. A*, 2014, **118**, Publisher: UTC, 15.

(53) J. B, “Symmetry and spectroscopy; an introduction to vibrational and electronic spectroscopy”, *Journal of Molecular Structure*, 1980, DOI: `10.1016/0022-2860(80)85247-1`.

(54) C. Berthomieu and R. Hienerwadel, “Fourier transform infrared (FTIR) spectroscopy”, *Photosynthesis Research*, 2009, DOI: `10.1007/s11120-009-9439-x`.

(55) J. R. Lakowicz, *Principles of fluorescence spectroscopy*, Publication Title: Principles of Fluorescence Spectroscopy, Springer, 2006, 1-954.

(56) H. Abraham and L. J, “Disparition instantanée du phénomène de Kerr”, *CR Acad. Sci. Hebd Seances Acad. Sci.*, 1899, 206–208.

(57) R. G. Norrish and G. Porter, “The application of flash techniques to the study of fast reactions”, *Discussions of the Faraday Society*, 1954, DOI: `10.1039/DF9541700040`.

(58) R. G. Norrish and G. Porter, “Chemical reactions produced by very high light intensities [1]”, *Nature*, 1949, DOI: `10.1038/164658a0`.

(59) M. Dantus, M. J. Rosker and A. H. Zewail, “Real-time femtosecond probing of ”transition states” in chemical reactions [3]”, *The Journal of Chemical Physics*, 1987, DOI: `10.1063/1.453122`.

(60) C. Manzoni and G. Cerullo, “Design criteria for ultrafast optical parametric amplifiers”, *Journal of Optics (United Kingdom)*, 2016, DOI: `10.1088/2040-8978/18/10/103501`.

(61) R. A. Baumgartner and R. K. Byer, “Optical Parametric Amplification”, *IEEE Journal of Quantum Electronics*, 1979, **15**, 432–444.

(62) J. A. Giordmaine and R. C. Miller, *ir ˜Ael Wg gl 4e eel s TUNABLE COHERENT PARAMETRIC OSCILLATION IN LiNbO˜AT OPTICAL FREQUENCIES*, 1965.

(63) P. Hamm and M. Zanni, *Concepts and methods of 2D infrared spectroscopy*, Publication Title: Concepts and Methods of 2D Infrared Spectroscopy, 2011.

(64) C. T. Kuhs, B. M. Luther and A. T. Krummel, “Recent Advances in 2D IR Spectroscopy Driven by Advances in Ultrafast Technology”, *IEEE Journal of Selected Topics in Quantum Electronics*, 2019, DOI: `10.1109/JSTQE.2019.2900597`.

(65) J. Bredenbeck, J. Helbing, C. Kolano and P. Hamm, “Ultrafast 2D–IR Spectroscopy of Transient Species”, *ChemPhysChem*, 2007, **8**, _eprint: https://onlinelibrary.wiley.com/doi/pdf/10.1
1747–1756.

(66) I. V. Rubtsov and R. M. Hochstrasser, “Vibrational Dynamics, Mode Coupling, and Structural Constraints for Acetylproline-NH2”, *The Journal of Physical Chemistry B*, 2002, **106**, Publisher: American Chemical Society, 9165–9171.

(67) N. N. Elgrishi, K. J. Rountree, B. D. Mccarthy, E. S. Rountree, T. T. Eisenhart and J. L. Dempsey, “A Practical Beginner’s Guide to Cyclic Voltammetry”, 2017, DOI: `10.1021/acs.jchemed.7b00361`.

(68) G. M. Greetham, P. Burgos, Q. Cao, I. P. Clark, P. S. Codd, R. C. Farrow, M. W. George, M. Kogimtzis, P. Matousek, A. W. Parker, M. R. Pollard, D. A. Robinson, Z.-J. Xin and M. Towrie, “ULTRA: A Unique Instrument for Time-Resolved Spec-

troscopy", *Applied Spectroscopy*, 2010, **64**, Publisher: Society for Applied Spectroscopy, 1311–1319.

(69) P. Dedecker, "Software review: Glotaran", *Journal of Chemometrics*, 2014, **28**, ISBN: 9781627036481, 137–138.

(70) J. J. Snellenburg, S. P. Laptenok, R. Seger, K. M. Mullen and I. H. M. v. Stokkum, "**Glotaran** : A *Java* -Based Graphical User Interface for the *R* Package **TIMP**", *Journal of Statistical Software*, 2012, **49**, ISBN: 9781439811870, –.

(71) T. MathWorks, "MATLAB (R2022a)", *The MathWorks Inc.*, 2022.

(72) I. V. Sazanovich, M. A. Alamiry, J. Best, R. D. Bennett, O. V. Bouganov, E. S. Davies, V. P. Grivin, A. J. Meijer, V. F. Plyusnin, K. L. Ronayne, A. H. Shelton, S. A. Tikhomirov, M. Towrie and J. A. Weinstein, "Excited state dynamics of a PtII diimine complex bearing a naphthalene-diimide electron acceptor", *Inorganic Chemistry*, 2008, **47**, Publisher: American Chemical Society, 10432–10445.

(73) A. J. Auty, P. A. Scattergood, T. Keane, T. Cheng, G. Wu, H. Carson, J. Shipp, A. Sadler, T. Roseveare, I. V. Sazanovich, A. J. Meijer, D. Chekulaev, P. I. Elliot, M. Towrie and J. A. Weinstein, "A stronger acceptor decreases the rates of charge transfer: ultrafast dynamics and on/off switching of charge separation in organometallic donor–bridge–acceptor systems", *Chemical Science*, 2023, **14**, Publisher: Royal Society of Chemistry, 11417–11428.

(74) P. A. Scattergood, M. Delor, I. V. Sazanovich, O. V. Bouganov, S. A. Tikhomirov, A. S. Stasheuski, A. W. Parker, G. M. Greetham, M. Towrie, E. S. Davies, A. J. Meijer and J. A. Weinstein, "Electron transfer dynamics and excited state branching in a charge-transfer platinum(II) donor-bridge-acceptor assembly", *Dalton Transactions*, 2014, **43**, Publisher: Royal Society of Chemistry, 17677–17693.

(75) M. Delor, T. Keane, P. A. Scattergood, I. V. Sazanovich, G. M. Greetham, M. Towrie, A. J. H. M. Meijer and J. A. Weinstein, "On the mechanism of vibrational control of light-induced charge transfer in donor-bridge-acceptor assemblies", *Nature Chemistry*, 2015, **7**, 689–695.

(76) J. A. Christensen, B. T. Phelan, S. Chaudhuri, A. Acharya, V. S. Batista and M. R. Wasielewski, “Phenothiazine Radical Cation Excited States as Super-oxidants for Energy-Demanding Reactions”, *Journal of the American Chemical Society*, 2018, DOI: `10.1021/jacs.8b01778`.

(77) K. Kawai, T. Takada, S. Tojo and T. Majima, “Hole transfer through DNA monitored by transient absorption of phenothiazine radical cation”, *Tetrahedron Letters*, 2002, DOI: `10.1016/S0040-4039(01)02064-0`.

(78) M. Pan, X. M. Lin, G. B. Li and C. Y. Su, “Progress in the study of metal-organic materials applying naphthalene diimide (NDI) ligands”, *Coordination Chemistry Reviews*, 2011, DOI: `10.1016/j.ccr.2011.03.013`.

(79) M. Sandroni, A. Maufroy, M. Rebarz, Y. Pellegrin, E. Blart, C. Ruckebusch, O. Poizat, M. Sliwa and F. Odobel, “Design of efficient photoinduced charge separation in donor-copper(i)-acceptor triad”, *Journal of Physical Chemistry C*, 2014, DOI: `10.1021/jp507984s`.

(80) M. Delor, S. A. Archer, T. Keane, A. J. Meijer, I. V. Sazanovich, G. M. Greetham, M. Towrie and J. A. Weinstein, “Directing the path of light-induced electron transfer at a molecular fork using vibrational excitation”, *Nature Chemistry*, 2017, **9**, Publisher: Nature Publishing Group, 1099–1104.